ASSESSMENT OF CRACKING POTENTIAL OF HIGH-PERFORMANCE CONCRETE DUE TO RESTRAINED SHRINKAGE

by

KAGAN AKTAS

A Thesis submitted to the

Graduate School – New Brunswick

Rutgers, The State University of New Jersey

in partial fulfillment of the requirements

for the degree of

Master of Science

Graduate Program in Civil and Environmental Engineering

written under the direction of

Dr. Hani H. Nassif

and approved by

_____

_____

_____

New Brunswick, New Jersey

October 2007

ABSTRACT OF THE THESIS

Assessment of Cracking Potential of High-Performance Concrete due to Restrained Shrinkage

by KAGAN AKTAS

Thesis Director:

Dr. Hani H. Nassif

Many State Engineers have observed that a number of high-performance concrete (HPC) bridge decks exhibited cracking and sometimes soon after being poured. Although deck cracking can be attributed to various causes, in many cases, concrete shrinkage is considered the main contributor. Additionally, concrete in bridge decks is considered restrained and there is a need to examine the behavior of HPC mixes under those conditions.

The AASHTO test (PP 34-06, The Passive or Restrained Ring Test) is employed to measure the cracking potential and restrained shrinkage behavior of various HPC mixes used in bridge deck projects contracted by the New Jersey Department of Transportation (NJDOT). This thesis presents the results of a study which utilized a

method for directly measuring the strain development in the concrete ring using Vibrating Wire Strain Gages (VWSG). For each mix, additional tests were performed to determine the corresponding mechanical properties (e.g., elastic modulus, tensile splitting strength, compressive strength, etc.). The effect of total amount of cementitious materials and the potential of cracking for various mixes are also reported. The results of the study are used to correlate strains from restrained shrinkage tests with those from free shrinkage tests. Results show that the coarse aggregate (CA) content, the coarse/fine aggregate ratio, and cementitious content have the greatest effect on both free and restrained shrinkage. Mixes with higher cementitious content were observed to crack earlier. In general, to minimize HPC cracking potential, it is suggested that a limit on free shrinkage (450 micro strain at 56 days) be specified in bridge decks to indirectly reflect restrained shrinkage conditions. Additional limits for the total amount of coarse aggregate (1800 lb/cu yd.) and Coarse/Fine aggregate ratio (1.48) should also be considered.

ACKNOWLEDGEMENTS

I would like to thank Dr. Hani H. Nassif for his continuous support throughout my years in Rutgers. It was a great honor to have him as an adviser, and a friend, who was always there for me in any way imaginable.

I would also like to thank Dr. Husam S. Najm and Dr. Kaan Ozbay for being in my committee and for their valuable advices.

I would like to thank my father and my mother who always supported my decisions and inspired me in my life with their success, care, and loving. In particular I would like to thank my sister for sharing her life experiences, for listening to my complaints and frustrations, and for believing in me.

I would like to thank Bahar Demirdirek with all my heart for being with me to the end with her unconditional support and love.

I would like to thank Chris, Boxer, Eric, Kyle, Shane, John, and all my friends in the lab that worked with me and eased my burden of tasks. This wouldn't have been possible without you guys.

I would like to thank Dr. Nakin Suksawang for helping me to get started in the lab and for being available whenever I needed him.

Special thanks and gratitude is for Joseph C. Davis who has been a great friend and colleague throughout my studies here. His creative mind always figured out ways to take the most fun out of every situation. I will never forget him.

Special thanks also are for Neba who has been like a second sister to me. Her support and love was invaluable.

I would like to thank my friends Anil, Erman, Umut, Evren, Ozlem, Oncel, Zafer, Basar, Erhan, Layla and all that I other friends in my life who made it worthwhile to live here.

Finally, I would like to thank Bekir Bartin and Oguz Ertekin for their support early in my career here.

TABLE OF CONTENTS

LIST OF TABLES

LIST OF FIGURES

CHAPTER I

INTRODUCTION

1.1 PROBLEM STATEMENT

Concrete cracking is one of the most critical issues that lead to deterioration of bridge decks, increasing maintenance costs, and shortening the overall service life. Cracks allow water and chemicals to penetrate into the concrete which increases the damage from freeze and thaw cycles, and also leave the reinforcing steel susceptible to corrosion. Cracks that extend through full depth of the deck lead to other problems such as deterioration of joints or even steel girders that may be supporting the deck. Cracking in a deck takes place due to a combination of events. These include but are not limited to concrete deck pouring sequence, negative moment regions in continuous bridges, improper curing and/or construction practices, magnitude of loads on the bridge, environmental effects, concrete mix design and its properties.

Concrete, by its nature, undergoes volume changes during the course of its life time. These changes are a result of its chemical and physical composition, curing history, and environmental conditions under drying. If concrete is not restrained, these volume changes do not create any stress in the concrete and simply lead to length change in concrete. If, however, concrete is restrained from shrinking freely, internal tensile

stresses will develop. When the level of restraint is high enough, it will induce stresses that exceed the tensile capacity of concrete which will lead to cracking. In a bridge deck, there are several restraining factors that prevent the free shrinkage of concrete. Reinforcing steel bars and closely spaced studs are the major causes of restraints in a deck. Steel girders themselves can be a major source of restraint if the bridge superstructure is composed of concrete deck over steel girders. Areas such as negative moment regions and sections close to the abutments are the areas with highest restraint in a deck.

Minimizing the factors that lead to cracking of concrete is one of the easiest ways of extending service life of bridges. Since control over loading, temperatures cycles due to environmental conditions and restraints in a deck are not easily controllable, choosing concrete mixes that have less potential to crack under restrained conditions remains to be one of the best alternatives in reducing cracking. Amount of cement and cementitious materials, type and amount of aggregates used, water to binder ratio, and various chemicals used all have effects on properties of concrete that affect its behavior under restrained conditions. Therefore, identifying these effects and defining potential of cracking of concrete mixes accurately are vital in controlling cracking.

1.2 RESEARCH OBJECTIVES AND SCOPE

The primary purpose of this research is to define and compare the cracking potential of common high performance concrete (HPC) mixes used in bridge decks by New Jersey Department of Transportation (NJDOT). This study will be used as a guide

to selecting HPC mixes with lower cracking potentials. Basic properties to be investigated include compressive strength, splitting tensile strength, modulus of elasticity, unrestrained drying shrinkage and restrained shrinkage. Total of 16 mixes are provided by NJDOT. The water to binder ratio ranges between 0.34 – 0.40 and majority of the mixes have slag as a replacement for cement. Mixes are grouped according to the cement replacement percentages. Two main groups are 30% and 40% slag replacement. Remaining mixes have varying percentages of slag, silica fume and fly ash as cementitious replacements. Also, source of coarse and fine aggregates, as well as type and manufacturer of admixture chemicals are varied within groups of mixes. This forms a complex matrix of variables by which the effects of most sensitive parameters can be determined.

1.3 THESIS ORGANIZATION

This thesis consists of six chapters as the following:

Chapter I covers the introduction consisting of problem statement, research objective and scope, and thesis organization.

Chapter II covers general background and literature review on shrinkage types, factors affecting shrinkage of high-performance concrete, and the restrained shrinkage test.

Chapter III covers the experimental program, including all material properties, mixing procedures, and testing procedures.

Chapter IV covers all test results, including mechanical properties, comparison of free and restrained shrinkage rates for all mixes, correlation of cracking potential with

major mix design parameters, and also the correlation of free and restrained shrinkage test results

Chapter V covers the conclusions, recommendations, and scope for future research.

CHAPTER II

LITERATURE REVIEW

2.1 INTRODUCTION

Concrete changes volume during its lifetime due to various reasons. If concrete were free of any restraints to deform, these volume changes would be of no importance; but since concrete in service is mostly restrained by many elements, significant stresses might develop that could lead to cracking of concrete. In order to study the behavior of concrete under restrained conditions, one has to understand the reasons behind volume changes of concrete.

Volume change is defined simply as an increase or decrease in volume. The volume changes in concrete are generally expressed in a linear direction. This is due to the fact that in majority of exposed concrete elements one or two dimensions are much smaller than the third, and the effect of volume change is greatest in the third dimension. Most commonly, volume change in concrete is contraction as a result of temperature and moisture changes and this is called shrinkage of concrete. Shrinkage in concrete begins shortly after it is cast and could continue for a number of years. Chronologically, types of shrinkage can be listed as plastic shrinkage, thermal shrinkage, autogenous shrinkage, and drying shrinkage.

2.2 TYPES OF SHRINKAGE

Shrinkage of concrete begins shortly after it is cast. Depending on the characteristics and proportions of the mix design, different types of shrinkage will have varying effects. The types of shrinkage and their effects are discussed below.

2.2.1 Plastic Shrinkage

Plastic shrinkage refers to change in length that occurs while the concrete is still fresh, before hardening. The driving force behind this is rapid evaporation of water form the exposed surface of concrete due to environmental agents, such as wind, relative humidity and temperature. The critical condition is when the rate of evaporation is greater than the rate of bleeding. Wind speeds in excess on 5 mph, low relative humidity and high ambient temperatures increase the rate of evaporation and therefore the probability of having plastic shrinkage cracks.

Concrete mixtures with a reduced rate of bleeding, like HPC, are more susceptible to plastic shrinkage than regular concrete mixes. Any factor that delays the setting of concrete also increases the possibility of shrinkage cracking. Fogging and wet burlap curing (protected by plastic sheets) eliminates plastic shrinkage.

2.2.2 Thermal Shrinkage

Hydration of cement is accompanied by a generation of heat which results in an increase in the temperature of concrete. Soon after setting, when final dimensions of a concrete element or mass become fixed, this temperature starts to decrease causing an overall shrinkage in the concrete element. The amount of shrinkage depends on many factors such as, size and volume of concrete, type of cement, thermal properties of the

aggregates used, ambient temperature and the placement temperature of concrete. For elements that are relatively thin in one dimension, such as bridge decks, the generated heat is dissipated easily and the rise in concrete temperature is negligible. Therefore, the shrinkage resulting form this temperature change is also negligible.

2.2.3 Autogenous Shrinkage

Visible dimensional change of cement paste, mortar, or concrete caused by hydration of cement is called autogenous shrinkage. As cement hydrates a very fine pore network is formed within the hydrated cement as a result of an absolute volume change. This network starts to drain water from the coarse capillaries created during mixing of concrete. If there is no external water supply, from curing or bleeding, the drying outer capillaries are emptied as if the concrete were drying. This is referred to as self-desiccation. This is different from drying in the sense that all the water actually remains in the concrete, but it migrates to the very fine pores created as a result of hydration.

In case of high-performance concrete (HPC) with low water to binder ratios (w/b), there is significantly more cement and less water. As a result the pore network is composed of very fine capillaries (Aitcin 1998). As soon as hydration begins self-desiccation starts and the menisci rapidly develops within the fine capillary system in the absence of external water supply. When most of the cement particles start to hydrate simultaneously, the drying of the capillaries result in high tensile stresses which in turn results in shrinkage of the cement paste. This is basically the driving force behind autogenous shrinkage. If an external water source is present during significant portion of the hydration process, the external capillaries will not dry out which means that no menisci will develop. As a result the tensile stresses that result in shrinkage will not

exist, eliminating autogenous shrinkage. This is true as long as the pores are interconnected to the external water source. Autogenous shrinkage continues as long as the cement hydrates. Autogenous shrinkage increases with a decrease in w/b and an increase in cement content. It is mostly observed in concrete with w/b ratios less than 0.42 (Holt 2001)

2.2.4 Drying Shrinkage

Hardened concrete will change volume due to the moisture changes within its capillary pore system. The driving source of drying shrinkage is the evaporation of free water from this capillary pore system. Drying takes place from the surface that is exposed to the air and it only continues if the relative humidity of air is less than the humidity within the capillary pores. The loss of water due to evaporation is progressive, from outside to inside, and proceeds at a decreasing rate depending on the properties of the concrete considered. Some of these properties include porosity of the concrete, size and shape of the pores and their continuity, surface to volume ratio of the element considered, and ambient relative humidity. Drying shrinkage may continue for a number of years depending on these properties. Large volume elements will experience lower shrinkage over a longer period of time where as elements with large surface areas will tend to shrink more in a shorter period of time. This is particularly important for bridges since the surface exposed to drying is much larger and this can cause significant drying shrinkage.

Drying shrinkage alone would not be of any concern if the concrete was allowed to shrink freely. However, restraints imposed on elements subject to drying shrinkage will cause internal tensile stresses to be developed. The magnitude of these stresses

increases with the amount of restraint and if the stresses exceed the tensile capacity of a particular mix cracks will develop. When no cracking is present, stresses that are developed are locked inside the element and this will reduce the effectiveness of the element under service loads. Therefore, it is very important to select and design mixes that are less likely to shrink.

2.3 Factors Affecting Shrinkage

Major parameters that influence the shrinkage of concrete are aggregate type and volume, cement content and type, and water to binder ratio. Other parameters that can affect shrinkage include types of cementitious materials, various admixtures, environmental conditions, and curing history of concrete.

Aggregate type and volume in a concrete mix greatly affect the shrinkage behavior. Coarse aggregate physically restrains the shrinkage of hydrating cement paste. Hard, rigid aggregates are difficult to compress and provide more restraint to shrinkage than softer, less rigid aggregates. Avoiding aggregates that have high drying shrinkage properties and aggregates that contain excessive amounts of clay can also reduce the shrinkage of concrete. Quartz, granite, feldspar, limestone, and dolomite aggregates generally produce concretes with low drying shrinkage (ACI Committee 224). Volume of coarse aggregate in a mix also effects shrinkage significantly. As the amount of coarse aggregate is increased the restraint on the shrinking cement paste is also increased. This reduces the overall shrinkage of a given concrete mix. In a study by Hansen and Almudaiheem (1987) an increase of aggregate volume from 65% to 70% resulted in a decrease of 18% in drying shrinkage. Pickett (1956) also reported a 20% decrease in

drying shrinkage (for mixes with the same water to binder ratio) caused by an increase in aggregate volume from 71% to 74%.

The other major factor affecting the shrinkage behavior of concrete is the cement paste itself. Controlling the cement and water content, thus the water to binder ratio, can have a significant effect on early and total shrinkage. Increasing the cement content while keeping the water to binder ratio constant will increase the shrinkage since amount of paste that hydrates, which causes shrinkage is increased. Increase in water content also increases drying shrinkage since amount of evaporable water in unit volume increases. Therefore, lowering the water to binder ratio, while keeping the amount of cement low, can help lower total shrinkage.

Cement type and fineness also have an effect on shrinkage. Over the past years chemistry and fineness of cements has changed. Due to improved techniques and competition within the industry cements are blended finer (Krauss and Rogalla 1996). Finer cement particles react much more quickly and therefore can increase autogeneous shrinkage considerably. Also, finer cement particles mean a finer pore structure in the concrete, which causes higher capillary stresses that increases the shrinkage (Chariton and Weiss 2002). On the other hand, larger cement particles do not undergo full hydration and the reaction takes place much more slowly. This reduces the hydration temperatures as well as the autogeneous shrinkage. Unhydrated cement particles act as restraints to the shrinking paste, just like coarse aggregates, which reduces shrinkage even more. Krauss and Rogalla (1996) point out that many researches have found coarse ground Type II cement to reduce shrinkage.

Modern concrete mixes, especially high-performance concrete (HPC), does not only contain cement as a binder. Cementitious materials such as fly ash, slag, and silica fume are commonly used to replace a portion of cement to increase cost efficiency and to achieve standards that are related to durability such as permeability. The addition of these materials has effects on early and total shrinkage of concrete. Silica fume, which is a highly reactive pozzolan, increases the rate of hydration, temperatures during hydration, and also the autogeneous shrinkage of concrete. Paillere et. al. (1989) report that concrete with silica fume does not swell during hydration and shrinkage is immediate on the contrary to regular concrete. This greatly increases the susceptibility of concrete to plastic shrinkage if curing is not adequate. McDonald (1992) also claimed that silica fume increases early age shrinkage and shrinkage related cracking.

Another supplementary cementitious material is fly ash. Fly ash reacts much more slowly compared to cement, which reduces the hydration temperatures as well as the strength gain of concrete. There are conflicting results in literature about the performance of fly ash concretes under shrinkage. Gebler and Klieger (1986) compare the drying shrinkage of class C and F type fly ashes to a control mix and conclude that within normal dosages fly ash has no significant effect on drying shrinkage. The dosage used in the study was 25% of the total cementing material. Nasser and Al-Manaseer (1986) studied the shrinkage and creep of concrete containing 50 percent fly ash. The shrinkage results show about 11 percent increase compared to ordinary portland cement concrete. Sivasundaram, Carette, and Malhotra (1989) study the properties of concrete with high volume Class F fly ash and low w/b ratios (0.31). The properties in this study are characterized by strength, modulus of elasticity, drying shrinkage, freezing and

thawing durability, carbonation, and permeability to chloride ions. The drying shrinkage performance of the fly ash mixes were equally well and in some cases better than control specimens.

Ground granulated blast furnace slag, also called cement slag, is the third most common supplementary material available. Average blaine fineness of slag particles is around 45 microns and compared to fly ash slag is slightly more reactive. Three grades, namely Grade 80, 100, 120, are classified by their reactivity. Shrinkage behavior of concrete that constitutes slag changes depending on the amount of cement replacement. Just as in the case of fly ash, there are conflicting reports about the effects of slag on total shrinkage in literature. However, there is an agreement that slag significantly increases early age autogenous shrinkage. Saric-Coric and Aitcin (2003) studied the effects of curing conditions on shrinkage for concrete specimens containing 20, 30, 50, and 80% slag replacements. They reported that when under sealed conditions, concrete containing slag presented a much higher autogeneous shrinkage than pure Portland Cement concretes; the magnitude increasing with increasing slag percentages. At the same time they found out that 7 day moist cured samples containing slag presented a smaller total shrinkage (autogeneous and drying) than samples from pure portland cement. Another study conducted by Collins and Sanjayan (2000) on the other hand reported that concrete containing slag has 1.6 to 2.1 times greater drying shrinkage than regular concrete. Study was composed of four mixes each having a w/b ratio of 0.5. A control mix which had only ordinary Portland cement was used to compare the unrestrained and restrained shrinkage behavior of slag concretes.

The amount and type of curing can affect the rate and ultimate amount of shrinkage. HPC must be cured quite differently from regular concrete. If HPC is not water cured immediately after placement it can be subject to severe plastic shrinkage, and later it also develops excessive autogeneous shrinkage due to its rapid hydration reaction (Aitcin 1997). The critical curing period to prevent or minimize autogeneous shrinkage is between 12 to 36 hours after casting. If there is continuous water supply during this period autogeneous shrinkage can be eliminated. In cases of very fine pore structure within the concrete surface water can not reach the inner parts of the element and some autogeneous shrinkage may develop. Saric-Coric and Aitcin (2003) studied the effect of curing conditions on shrinkage of concrete containing various amounts of slag. They report that total shrinkage of all mixes was reduced when 7 days moist curing was applied. The difference was due to the elimination of autogeneous shrinkage in the presence of constant water supply. Although curing does not affect the magnitude of drying shrinkage, it slows the rate at which it takes place. After several days of moist curing most of the cement particles at the surface reaches full hydration. Therefore, the concrete develops its compact microstructure which slows down the process of evaporation of water.

Most chemical admixtures have little effect on shrinkage. Air entrainment has little or no effect on drying shrinkage (Neville 1996). Water reducing admixtures can increase shrinkage; especially the ones that contain an accelerator to counteract the retarding behavior of the admixture. Superlasticizers also have little effect on shrinkage. A study conducted by Whiting and Dziedzic (1992) compared three different concrete mixtures with different superplasticizers against a control mix with no admixtures. All

four mixes had very close drying shrinkage amounts at the end of 32 weeks. However, the dosage of these admixtures can have an effect. A study conducted by Bisonnette et al. (2002) showed that melamine and naphthalene-base superplasticizers had an effect on early volume changes of concrete as their addition rate was increased. This also increased the shrinkage rate and ultimate shrinkage that was observed.

Although ambient relative humidity and temperature do not affect the ultimate shrinkage of a member, they play an important role on the rate at which evaporation takes place and thus on the rate of drying shrinkage. As relative humidity decreases it is common knowledge that is increases the rate of drying. Higher temperatures have the same effect. The importance of ambient conditions is realized during casting and curing period of concrete. If adequate curing is not provided, high temperatures coupled with low relative humidity and wind can cause excessive plastic shrinkage.

2.4 Ring Test

Many methods have been developed to test the performance of cement mortar and concrete under restrained conditions. These include flat panel test, linear restrained shrinkage test, and restrained shrinkage ring test. Restrained shrinkage ring test has been the most popular out of these tests due to its simplicity and relatively low cost.

2.4.1 Ring Test Back Ground

In the restrained shrinkage test, concrete is cast around an inner steel ring. The concrete is cast around the steel ring, such that as the concrete shrinks, a compressive stress is developed in the steel ring which is balanced by a tensile stress in the concrete ring. If this tensile stress is greater than the allowable tensile stress of the concrete, it

cracks. The steel ring can be instrumented with strain gages to signal the time of cracking accurately and to monitor the strain development in the steel ring.

First ring tests were performed by Carlson and Reading (1988) between 1939 and 1942. For many years no standardized testing procedure existed to test for restrained shrinkage behavior of concrete mixes. Starting early 90s extensive research projects were undertaken to assess and identify the causes of transverse bridge deck cracking. One of most important factors was identified as shrinkage of concrete and cracking under restrained conditions. There was a need to evaluate the cracking tendency of different concrete mixes to choose the concrete design that was least likely to crack under these conditions. As a result, restrained shrinkage ring test, which was utilized as a part of NCHRP Project C12-37, was proposed for adoption by American Association of State Highway and Transportation Officials (AASHTO) in NCHRP Report 380. In this report, Krauss and Rogalla (1996) discussed the usefulness of the proposed test. The major advantage of the ring test is that it accounts for all of the material factors that influence shrinkage cracking from the time of casting. It simultaneously considers stress development, dimensional changes, and creep at early ages therefore it does not require complex calculations or assumptions of early concrete behavior. Also, the test is simple to execute and the apparatus is inexpensive. Most importantly, stresses developed in the restrained test samples closely simulate those developed by real structures. The amount of restraint can be modified by changing the dimensions of the test to simulate effects of different degrees of restraint depending on the structures under consideration. For bridge deck applications Weiss and Shah (2002) stated that the concrete ring simulates an infinitely long deck which is partially restrained from shrinking.

In 1998 AASHTO accepted the ring test as a provisional standard as "AASHTO PP34-98: Standard Practice for Estimating the Cracking Tendency of Concrete", but it has not been approved yet. In 2004, American Society for Testing and Materials (ASTM) approved "C 1581 – 04: Standard Test Method for Determining the Age at Cracking and Induced Tensile Stress characteristics of Mortar and Concrete under Restrained Shrinkage"

2.4.2 AASHTO Ring Test

This test covers the determination of the cracking tendency of restrained concrete specimens. It is used to determine the effects of variations in the properties of concrete as related to the time-of-cracking of concrete when restrained. These variations might include aggregate type and gradation, cement type, cement content, water content, mineral and chemical admixtures. Actual cracking in service depends on many factors and therefore this method is only used for comparative analysis of concrete mixtures and to aid in the selection of mixes that are less likely to crack. The test can be modified to evaluate other factors such as curing time and methods, evaporation rate and temperature.

The procedure consists of casting a 76 mm (3 in.) thick concrete annulus around a steel ring with a wall thickness of 12.7 mm ± 0.4 mm (1/2 in. ± 1/64 in.), an outside diameter of 305 mm (12 in.), and a height of 152 mm (6 in.). The inner and outer surfaces of the ring should be machined smooth, round and true, and polished. The outer mold has a 457 mm (18 in.) diameter which produces the required 3 in. wall thickness. Four foil strain gages (FSG) are instrumented at mid-height of the inner surface of the steel ring so that abrupt changes in the steel strain can signal the age of cracking. The strain readings are recorded by using a data acquisition system (DAS) which is capable of

recording strains every 30 minutes. The outer mold is removed from the concrete ring at 24 ± 1 h and after curing period the top and bottom surfaces of the concrete ring is sealed to allow for drying to take place from the circumferential surface. The specimens are stored and monitored in a controlled-environment room with a constant air temperature of 23 ^{0}C ± 1.7 ^{0}C (73.4 ^{0}F ± 3 ^{0}F) and a relative humidity of 50 ± 4 percent. The strain measurements are started in the rings as soon after casting as possible. Every 2 to 3 days, the strain profile is reviewed and the rings are visually inspected for cracking. Concrete is considered cracked when a strain decrease of 30 microstrains or more is observed. After cracking, time to cracking is recorded and the rings are monitored for two more weeks. Within this period crack widths are recorded and cracking pattern is characterized.

2.4.3 ASTM Ring Test

This test is very similar to the AASHTO test. However, it has some differences in size and geometry of the setup. The steel ring used has a wall thickness of 13 ± 0.12 mm (0.5 ± 0.05 in), an outside diameter of 330 ± 3.3 mm (13.0 ± 0.12 in), and a height of 152 ± 6 mm (6.0 ± 0.25 in). The inner and outer surfaces of the ring are machined to produce a smooth surface with a texture of 1.6 micrometers (63 microinches). The outer mold should have a diameter of 406 ± 3 mm (16.0 ± 0.12 in) to produce a concrete ring with a wall thickness of 38 mm (1.5 in). The size of the steel ring was increased and the thickness of the concrete was decreased to produce higher restraint in a thinner element to reduce to time to cracking. This way the results can be obtained much more quickly compared to the AASHTO setup. One drawback of this change in dimensions is that it limits the maximum coarse aggregate size that can be used to 13 mm (0.5 in). The test

covers the laboratory determination of the age at cracking and induced tensile stress characteristics of mortar and concrete specimens under restrained shrinkage. The procedure can be used to determine the effects of variations in the proportions and material properties of mortar or concrete on cracking due to both drying and deformations caused by autogeneous shrinkage and heat of hydration. These variations can include aggregate source, aggregate gradation, cement type and content, water content, supplementary cementitious materials and mineral admixtures. The test is carried out by casting at least three concrete rings with the given dimensions. The inner steel ring should have at minimum 2 strain gages to record the strain development. The strain should be measured by a DAS that is capable of recording at every 30 minutes or less. After samples are cast they are moved into the testing environment within 10 minutes. The testing environment should have a constant air temperature of 23.0 ^{0}C ± 2.0 ^{0}C (73.5 ^{0}F ± 3.5 ^{0}F) and a relative humidity of 50 ± 4%. The specimens are cured with burlap and covered with polyethylene sheets for the first 24 h, after which the molds are removed and the top and bottom of the ring is sealed to allow circumferential drying only. The rings are monitored for at least 28 days under drying, unless cracking is observed earlier. The strain is plotted against time and monitored every 2 to 3 days to check for cracking. If the rings do not crack within 28 days, the test can be stopped and the rate of shrinkage at the termination of the test can be used to determine the cracking potential of the sample.

2.5 PREVIOUS WORK

First ring tests were performed by R. W. Carlson and T.J. Reading from 1939 to 1942. They discussed these tests in a study that investigated the cracking of concrete

building walls (Carlson and Reading 1998). The tests were used to explain the influence of resistance of concrete mixtures to cracking on shrinkage cracking in walls. Restrained ring specimens consisted of concrete rings with a radial thickness of 25 mm (1 in.) and a width of 38 mm (1.5 in) cast around steel rings which had an internal diameter of 125 mm (5 in.) and an external diameter of 175 mm (7 in.). The steel was coated with an incompressible paraffin wax layer to eliminate friction between concrete and the steel ring. After casting and initial moist curing, bottom and top surfaces of the rings were sealed to permit drying from the outer circumference. Specimens were subjected to drying in environments with relative humidities of 25, 50, and 75 percent. Time of cracking was obtained by periodical visual observation. Companion free shrinkage bars of 300 mm (12 in.) length and 1 x 1.5 in. cross section were also cast to determine the strain at the time of cracking. To simulate the same drying condition as the rings, these bars were allowed to dry from one face only; either the top or the bottom of the specimen. They found that the specimens which were exposed to lowest relative humidity developed the highest stresses and the time to cracking was observed to be much faster than at higher humidities. They also found that the type of coarse aggregate had an important effect on cracking resistance.

Until the development of standardized ring tests many studies incorporated the use of restrained ring specimens. Grzybowski and Shah (1990), while studying the effects of fiber reinforcement on shrinkage cracking, made use of a restrained ring test setup. They chose this setup since it was difficult to provide sufficient restraint with linear specimens. They modified the setup used by Carlson and Reading to achieve uniform tensile stresses at the inner and outer surfaces of the concrete ring. The inner

and outer diameters of the steel ring they used were 254 and 305 mm (10 and 12 in.), respectively. The concrete that was cast around the steel ring had a thickness of 35 mm (1.38 in.) and a width of 140 mm (5.5 in). They pointed out that for their setup the difference in stress between outer and inner concrete surfaces was 10% and the radial stress in the ring was only 20% of the hoop stresses. With these values in mind they assumed that the concrete is subject to uniform uniaxial tensile stress. Also, they assumed that shrinkage was uniform along the width of the specimen since the width to thickness ratio of the specimen was four. The mix proportions were 1:2:2:0.5 by weight of cement, sand, coarse aggregate and water, respectively. The maximum aggregate size was limited to 9 mm (3/8 in.). Steel and polypropylene fibers were also used to test their effects. The concrete was cast around the steel ring using a cardboard tube as an outer mold. The mold was stripped off after 24 hours for regular specimens and 2.5 hours later for early age specimens. Regular specimens were cured for 4 days at 20 ^{0}C and 100% relative humidity and than they were kept in a controlled environment with the rest of the specimens at 20 ^{0}C and 40% relative humidity. The top and bottom of the specimens were sealed using a silicon rubber sealer to allow circumferential drying only. In addition to the restrained ring specimens, free ring specimens and two companion free shrinkage blocks measuring 225 x 75 x 25 mm (9 x 3 x 1 in.) were cast for comparison purposes. For manufacturing free ring specimens, a steel inner ring with four removable pieces was used and after de-molding inner surface of the concrete ring was sealed using the same sealer. The authors used a specially designed microscope setup to check for cracking and also for measuring crack widths. Also, they mounted three equally spaced strain gages on mid-height of the concrete ring to monitor strain development. As a

result of the study, they found out that addition of fibers did not affect restrained shrinkage cracking but helped in reducing crack widths. They also concluded that free-shrinkage test results of ring specimens were independent of specimen geometry.

Wiegrink, Marikunte, and Shah (1996) studied the behavior of high-strength concrete under restrained shrinkage. The restrained shrinkage test setup was the same as the one used by Grzybowski and Shah (1990). For this experiment, however, the specimens were demolded at 6 hours and monitored in an environment with 20 ^{0}C temperature and 50% relative humidity. The free shrinkage specimens were also different with a length of 400 mm (15.75 in.) and a 100-mm square (0.15 in. square) cross section. The authors tested concrete mixtures consisting of Type I Portland cement, sand, and pea gravel with a maximum aggregate size of 9 mm (3/8 in.). Silica fume was also used in various percentages as a replacement for cement. 6 hours after casting, the molds were removed and samples were exposed to the drying environment. Compressive strength, splitting tensile strength, modulus of elasticity, creep and free shrinkage measurements were also made as well as monitoring the rings. As a result of the study, authors found a correlation between free shrinkage and restrained shrinkage behavior of concrete. They found that as the percentage of silica fume increased drying shrinkage increased which lead to earlier cracking of ring specimens. The crack widths for high silica fume percentage mixes were also larger.

Krauss and Rogalla (1996) performed an extensive study on transverse bridge deck cracking. One of the parameters that were investigated included the cracking tendency of typical concrete mixes used in bridge decks subject to restrained shrinkage. The effects of concrete mix design factors such as cement content, water to binder ratio,

aggregate type, silica fume addition, fly ash addition, superplasticizers, certain chemical admixtures, and entrained air were studied to determine their effects on cracking. In addition, effects of evaporation rate, temperature, curing period, casting time and insulation were also taken into account. The geometry of the ring was selected after a finite element analysis that examined the theoretical shrinkage stresses in the inner steel ring and the restrained concrete ring. Various steel and concrete radii were tested to find the most suitable geometry which would be cheap, practical, and yield reliable results. Their analyses revealed that for steel ring wall thicknesses between 13 and 25 mm (1/2 and 1 in.), concrete shrinkage stresses and cracking-tendency are not significantly different, but the stresses in the steel are much greater with decreasing thicknesses. Also, they showed that concrete experiences more stresses as the diameter of the steel ring increases. As a result, they used steel rings with 305 mm (12 in.) outside diameter, 19 mm (3/4 in.) wall thickness, and a 152 mm (6 in.) height. The rings were custom machined for the project and were more expensive than regular steel pipe sections. The procedure followed in sample preparation and mixing was very similar to previously discussed ring test setups. Two rings, five 100 x 200 mm (4 x 8 in.) cylinders, and two 75 x 75 x 280 mm (3 x 3 x 11 in.) companion free shrinkage samples were cast for each concrete mixture. All specimens were removed from their forms at 24 hours and placed in a 22 ^{0}C and 50% relative humidity room. The evaporation rate in the controlled environment was approximately 0.15 kg/m^3/hr (0.03 lb/ft^2/hr). The ring specimens were left on the forms and sealed on top with double layer of polyethylene or rubber to allow circumferential drying only. Strain development in the steel rings was monitored using a data acquisition system that collected measurements hourly. The strains were

periodically analyzed and the concrete rings were checked for cracks in the event of a sudden change in the strain profile. When a ring cracked the initial crack width was measured and it was monitored for at least one more week. The authors found that the mixes that performed the best under restrained shrinkage were the ones with low cement and water contents. However, these mixes had essentially no slump, and therefore, were not practical. For the remaining mixes cracking tendency decreased as the cement content decreased and water-cement ratio increased. Although free shrinkage of mixes was directly proportional to the cement paste volume, cracking tendency was not. Krauss and Rogalla associated this fact to the complexity of the restrained shrinkage behavior, which is governed by an interaction of shrinkage, strength and moduli development, and early creep. Also, they found out that the type of aggregate has a significant effect on cracking tendency. Out of the four types of aggregates types investigated, No. 56 crushed limestone performed the best. The rings cast with this material did not exhibit a single distinct crack, but instead minor surface cracks that extended 1 in. towards the steel ring were discovered. Also, a sudden decrease was not experienced in these rings. The authors also experienced earlier cracking in samples that were not cured versus samples that were wet cured, and the higher rates of evaporation decreased the time to cracking. As a result of the study, the authors proposed the ring test to AASHTO as a standard method for testing the cracking tendency of concrete.

As discussed before, the proposed test was accepted as a provisional test in 1998. Although it was an affective method in measuring relative likelihood of cracking of different mixes, it did not provide any information on concrete mixes that did not crack. There was a need to quantify the stress development within the concrete. Also, the long

times before a visual crack would occur made it a time consuming experiment. The stress development and the time to cracking can all be associated with the geometry of the ring test which determines the amount of restraint on the concrete ring. The geometry also has a profound effect on drying of concrete and the humidity gradient within the concrete ring.

Weiss and Shah (2002) investigated the effect of moisture gradients and specimen geometry on maximum strain development and cracking. They used various ring test arrangements while studying the effects of shrinkage reducing admixtures (SRA) on restrained shrinkage cracking. The authors performed two series of experiments, which both incorporated ring specimens of different geometries and drying conditions cast around a solid cylindrical plate with a radius of 150 mm (6 in.). Three different concrete wall thicknesses were selected for the experiment, namely 25, 75, and 150 mm (1, 3, and 6 in.). In the first series of experiments, called short ring series, 30 mm (1.2 in.) high samples were cast and drying was permitted through the top and bottom of the ring by sealing the outer circumference. By doing this a uniform moisture gradient was achieved along the radial direction which would result in uniform shrinkage. Also, free shrinkage specimens of 100 x 100 x 400 mm (4 x 4 x 16 in) dimensions were cast to compare the drying shrinkage of the mixes under investigation. All samples were stored in a controlled environment with 30 ^{0}C and 40% for the duration of the tests. The authors found out that for a given mix the potential for cracking was reduced as the wall thickness of the concrete ring was increased. The difference in cracking potential was related to the geometry since surface to volume ratio and drying shrinkage was same for all samples under consideration. Taking these factors into account and assuming uniform

moisture gradient and no radial displacement between the steel and concrete ring, Weiss and Shah outlined a procedure to quantify the stresses in the concrete ring. The second phase of the study concentrated on effect of geometry considering moisture profiles using tall ring specimens. The concrete rings had 150 mm (6 in.) height and they were cast with varying thicknesses to simulate slabs of different thicknesses. For this set of experiments the top and bottom of the specimens were sealed and drying was permitted form the outer circumference. This resulted in a moisture gradient which decreased from outside surface to the inner surface in contact with the steel ring. The increasing concrete wall thickness was again shown to delay the age of cracking even in the presence of a moisture gradient. The authors also measured higher change in radius for the specimens with uniform shrinkage (short rings) than the tall specimens. They explained that this was due to the fact that the taller specimens experience most of the shrinkage on the outer radius where as the short rings shrink uniformly throughout the radius. Even though the authors outlined a procedure to determine the stresses in the concrete, they stated that the closed form solution for non-uniform drying would be much more difficult.

See et al. (2003) performed also performed a study to determine the effects of geometry and to identify the shrinkage cracking characteristics of concrete. The test setup included an inner steel ring with a 13 mm (1/2 in.) wall thickness, 305 mm (12 in.) inner diameter, and 330 mm (13 in.) outside diameter. Also, a 405 mm (16 in.) inside diameter PVC pipe was cut to a height of 152 mm (6 in.) to be used as the outer mold. The rings were allowed to dry from the outer circumference only. The authors calculated the degree of restraint R, by comparing stiffness of the steel ring to the combined stiffness of steel and concrete ring,

$$R = \frac{A_{st}E_{st}}{A_{st}E_{st} + A_cE_C} \tag{1.1}$$

where A_{st} and A_c are the cross-sectional areas of the steel and concrete rings, respectively, and E_{st} and E_c are the modulii of elasticity of the steel and concrete, respectively. For their setup, the authors calculated the degree of restraint to be from 70 to 75% depending on the modulus of elasticity of concrete. Also, the average radial compressive stress was 10% of the hoop stresses. In contrast, AASHTO setup would only yield 55 to 60% restraint, which explains the longer times for a visual crack to take place. Also, the average radial compressive stresses were 25% of the hoop stresses which made analysis of this setup more difficult.

See et al. (2003) also proposed the following equation to evaluate the average tensile stress in the concrete at time t,

$$\sigma_t(t) = \frac{E_{st}r_{ic}h_{st}}{r_{is}h_c}\varepsilon_{st}(t) \tag{1.2}$$

Where E_{st} is the modulus of elasticity of steel, h_{st} and h_c are the thicknesses of the steel and concrete ring, respectively, and r_{is} and r_{ic} are the internal radii of steel and concrete, respectively. By using this equation they compared theoretical time to cracking, to observed time of cracking. They observed that the actual observed time to cracking was much later than the theoretical time to cracking. They concluded that tensile creep relaxation is the most likely reason for this difference. However, they also mentioned that other factors, such as shrinkage rate might play a significant role in cracking.

Hossain and Weiss (2003) performed a study to assess the residual stress development and come up with an analytical stress formulation to quantify this stress.

All ring specimens had a concrete wall thickness of 75 mm (3 in.) but many different steel ring thicknesses were utilized to study the effects of the degree of restraint. The steel ring thicknesses used were 3.1 mm (1/8 in.), 9.5 mm (3/8 in.), and 19.0 mm (3/4 in.). Each steel ring was instrumented at mid-height by 4 strain gages. The data was monitored every 10 minutes by the use of a data acquisition system. The ring test setup in the study was very similar to the AASHTO Provisional Test with two exceptions. First, the outer circumference of the concrete ring was sealed using aluminum tape to allow drying from top and bottom only. This was done to eliminate the moisture gradient that occurs when circumferential drying is permitted. As a consequence, uniform moisture loss along the radial thickness was achieved, simplifying modeling of stress development. Another difference from AASHTO test was that the height of the specimens was reduced to 75 mm (3 in.). This was done to increase the shrinkage rate and to allow a direct comparison to free shrinkage prism tests with 75 x 75 x 250 mm (3 x 3 x 10 in.) dimensions. The free shrinkage samples were modified in this study to simulate identical drying conditions with the ring specimens. This was achieved by sealing two sides and the ends of the specimens. This way the authors hoped to compare or correlate the results from restrained shrinkage test to the free shrinkage test. In addition to shrinkage specimens, cylindrical specimens were cast to determine various other properties such as splitting tensile strength, modulus of elasticity, and compressional wave velocity at different ages. The specimens used for the splitting tensile strength had a height of 75 mm (3 in.) which was equal to ring height, but the rest of the testing procedure was carried out as it is specified in the ASTM. The authors developed analytical models to predict the actual maximum tensile stress in the concrete

rings. To do this they separated the ring test setup into a steel ring pressurized at the outer circumference and a concrete ring pressurized with an equal but opposite force at the inner circumference (Figure 2.1).

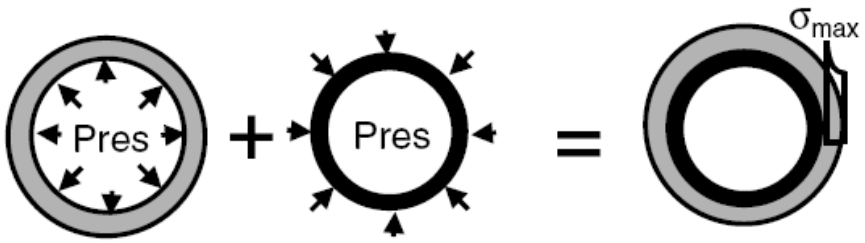

Figure 2.1 Idealization for computing the actual stress in concrete (Hossain and Weiss, 2003)

The authors came up with the following equation to predict the actual maximum circumferential tensile stress at a given time, t,

$$\sigma_{actual-\max} = -\varepsilon_{steel}(t) \cdot E_s \cdot C_{3R} \cdot C_{4R} \tag{1.3}$$

Where C_{3R} and C_{4R} are ring constants which can be calculated using,

$$C_{3R} = \frac{R_{OS}^2 + R_{OC}^2}{R_{OC}^2 - R_{OS}^2} \tag{1.4}$$

$$C_{4R} = \frac{R_{OS}^2 - R_{IS}^2}{2R_{OS}^2} \tag{1.5}$$

where R_{IS} and R_{OS} are inner and outer radii of the steel ring respectively, and R_{OC} is the outer radius of the concrete ring. As a result of the study, the authors concluded that using thicker steel rings would lead to higher stresses in the concrete ring which would shorten the time to cracking. They also defined a ratio of the actual stress to the tensile strength to define a potential of cracking for mixes that did not crack. However, they

realized that this ratio was not constant at failure and more parameters should be taken into account in defining the cracking potential of a concrete mix. It should be noted that the derived formulas are only applicable to cases were the concrete rings are allowed to dry from top and bottom.

See, Attiogbe, and Miltenberger (2004) improved their formulation of average residual stress that they derived in 2003 by including the effects of tensile creep and rate of stress development. The experimental setup was exactly the same as the setup used by See et al. (2003). The test program included the testing of 16 concrete and 4 mortar mixtures under restrained shrinkage. The effect of curing was also studied by using a variety of curing times. The authors' main argument was that the elastic strain rate and tensile creep play a significant role on the net time to cracking. Following the analysis in 2003 they defined the average residual stress in the concrete at time t after initiation of drying as,

$$\sigma_t(t) = G\left|\varepsilon_{st}(t)\right| = G\left|\varepsilon_{sh}(t) - \varepsilon_e(t) - \varepsilon_{cp}(t)\right| \tag{1.6}$$

Where $\varepsilon_{st}(t)$ is the average absolute strain in the steel ring, and $\varepsilon_{sh}(t)$, $\varepsilon_e(t)$, and $\varepsilon_{cp}(t)$ are the free drying shrinkage strain, elastic strain, and tensile creep strain, respectively. Elastic strain is dependent on the modulus of elasticity of the concrete used in the test, and G is a constant for the ring test setup which can be calculate using the following formula.

$$G = \frac{E_{st} r_{ic} h_{st}}{r_{is} h_c} \tag{1.7}$$

Where E_{st} is the modulus of elasticity of steel, h_{st} and h_c are the thicknesses of the steel and concrete ring, respectively, and r_{is} and r_{ic} are the internal radii of steel and concrete, respectively. The authors also developed a method to assess the potential for cracking of the mixes based on the stress rate at cracking or at the time of termination of the test. They introduced an equation which defined the stress rate at time, t, after initiation of drying as,

$$S(t) = \frac{G|\alpha|}{2\sqrt{t}} \tag{1.8}$$

where the value of α is determined from the strain readings obtained form the ring test. To do this, See et al. plotted the strains against the square root of time to obtain linear relationships in which the slope of the equation, which defines this relationship, would yield α. As a result of their experiments they concluded that lower stress rates generally meant that the mix would crack at a later age, which means that it would have a lower potential for cracking. They suggested four zones of performance which were 1) a zone of "High" potential for cracking with stress rates exceeding 0.34 MPa/day (50 psi/day) and cracking occurring within 7 days after drying starts; 2) a zone of "Moderate-High" potential for cracking with stress rates between 0.17 and 0.34 MPa/day (25 and 50 psi/day) and cracking occurring between 7 and 14 days; 3) a zone of "Moderate-Low" potential for cracking with stress rates between 0.10 and 0.17 MPa/day (15 and 25 psi/day) and cracking occurring between 14 and 28 days; and 4) a zone of "Low" potential for cracking with stress rates lower than 0.10 MPa/day (15 psi/day) and cracking occurring beyond 28 days or no cracking occurring at all. For mixes that did not

crack they suggested that the comparison should be made based on the stress rate at the termination time of the test.

In 2004, ASTM adopted the restrained shrinkage setup used by See et al. (2004) as a standard test to measure the cracking potential of concrete and mortar. The test setup was identical to the one used by See et al. (2003 and 2004), and used the same criteria to define the potential for cracking of mixes. Since a 28 day limit for maximum test duration was specified it became a quick and reliable method to measure the cracking potential of mixes with aggregate sizes less than 0.5 in. However, concrete mixes used in bridge decks commonly incorporate 0.75 in (or larger) aggregates, which means that ASTM ring test can not be used for these mixes. AASHTO setup is still being used for that purpose. Recently, several studies focused on the cracking behavior and residual stress build up in the AASHTO ring test.

Hossain and Weiss (2006) studied the effects of boundary conditions and geometry on stress development in the concrete ring. The study compared the effects of curing from top and bottom to drying from the outer circumference. Also, effects of using different steel and concrete ring thicknesses were investigated. The authors used three different test methods to compare the effects of geometry and drying conditions. First they used two different free shrinkage tests in which they measured the free shrinkage of unrestrained rings specimens and standard linear free shrinkage specimens that are used by ASTM C-157 test. Restrained shrinkage test samples were separated into three different groups to study the various effects under consideration. In the first group, where the degree of restraint was studied, concrete outer diameter was fixed to 450 mm (18 in), and the steel ring thicknesses were varied by using rings with 3.1 mm

(1/8 in.), 9.5 mm (3/8 in.), and 19 mm (3/4 in.) wall thicknesses. In the second group, the steel ring thickness was fixed 9.5 mm (3/8 in.), however, the concrete ring thicknesses were varied to include rings with wall thicknesses of 37.5 mm (1.5 in.), 75 mm (3.0 in), 112.5 mm (4.5 in.), and 150 mm (6.0 in). Finally, in the last group rings similar to the first two groups were used but the drying conditions were changed. The rings were sealed with aluminum tape to obtain two different boundary conditions, such as drying from the outer circumference, and drying from top and bottom. In all groups the height of the ring specimens were limited to 75 mm (3.0 in), and the inner diameter of the concrete rings were 300 mm (12 in.). All steel rings were instrumented with four strain gages at mid-height and they were monitored continuously for the duration of the test. The authors also used acoustic emission sensors to detect crack development, and compare the cracking behavior of rings with different boundary conditions. One of the important conclusions of the study was the significant difference in cracking behavior of rings which had different boundary conditions. On the specimens which had circumferential drying (top and bottom sealed) visual cracks were observed earlier even though the interface pressures on the steel rings were lower. On the other hand, the rings which were allowed to dry from top and bottom (sides sealed) experienced higher ring pressures, but cracked at a later age. The authors explained this by comparing the moisture profiles of the two boundary conditions. When concrete is allowed to dry from the outer circumference, the outer surface looses moisture much more quickly due to the larger surface area that is exposed to drying. This creates a moisture gradient in the ring, which results in cracking starting from the outer circumference moving towards the inner steel ring. In the case where the top and bottom drying is allowed moisture is lost more

uniformly along the radius and therefore a more uniform moisture profile is attained. They supported this theory by comparing the acoustic emission measurements from both setups. The acoustic sensors showed that the cracks developed on the outside surface and moved inwards for the samples that dried from the circumference. The cracking for the top and bottom drying was exactly the opposite. The effects of using various steel and concrete thicknesses were as expected. Thicker steel rings would lead to higher restraints and therefore earlier cracking. Where as thicker concrete rings would lead to higher resistance to cracking, which would delay the age of cracking.

Moon and Weiss (2006) developed an analytical solution for the residual stress development of restrained ring specimens under circumferential drying. They argued that the stresses that develop in the restrained ring specimen are due to a combination of two components. The first component results from the effect of non-uniform drying in which the outer circumference of the concrete, which shrinks very rapidly, is restrained by the inner concrete itself. This restraint exists until the moisture profile is closer to uniform, which the authors estimate to be around 50 days. The second component of restraint is the external restraint, which is provided by the inner steel ring. By combining the effects of these two components overall stress profile can be identified. In their analyses, Moon and Weiss considered the moisture diffusion to be linear, in contrast to Bazant and Najjar (1971) who define the moisture diffusion in concrete as a non-linear function. This was done to enable a closed form solution to the problem. The authors also assumed that the relationship between shrinkage and relative humidity is linearly proportional. As a result they expressed the drying shrinkage strain by a constant free shrinkage coefficient

($\varepsilon_{SH-const}$). In the end, they came up with the following formulation which enabled the determination of stress at any point in the concrete ring at a time, t.

$$\sigma_{\theta\theta}(r,\gamma) = -\varepsilon_{steel}(t)\cdot E_S \cdot \frac{R_{OS}^2 - R_{IS}^2}{2\cdot\left(R_{OC}^2 - R_{OS}^2\right)}\left(1+\frac{R_{OC}^2}{r^2}\right) + \frac{\varepsilon_{SH-const}\cdot E_{con}}{r^2}\left[\frac{r^2+R_{IC}^2}{R_{OC}^2-R_{IC}^2}\cdot\left(f(R_{OC})-f(R_{IC})\right)+f(r)-f(R_{IC})-erfc(A)\cdot r^2\right] \quad (1.9)$$

The first part of the equation is the stress caused by the external restraint (steel ring) as discussed earlier by Hossain and Weiss (2003). The second part of the equation defines the stress caused by internal restraint from concrete as a result of the moisture gradient. The variables used in the equation are explained below:

γ : a parameter which depends on diffusion coefficient of concrete and time ,t.

r : radial distance in cylindrical coordinates system

E_{con} : effective elastic modulus of the test sample

erfc : complimentary error function

$A = (R_{OC} - r)/\gamma$

Details of the authors' stress formulation can be found in Ref. [31]. To verify the validity of the equation the authors compared the analytical approach to a series of finite element simulations and obtained good agreement resulting in minor differences. They also explained how the formula could be applied to experiments with varying properties, such as diffusion coefficient and drying shrinkage coefficient.

2.6 SUMMARY OF PREVIOUS WORK

Restrained ring test is being used widely due to its simplicity, relatively low cost, and the ease with which the data can be analyzed and interpreted. Currently one standard ASTM test and a provisional AASHTO test are being used to test restrained shrinkage behavior of concrete and mortar of various proportions. Although much work has been done on quantifying the stresses that are developed in the ring test due to effects of drying conditions and ring geometry, there is still room for improvement. Currently the only standard test, which is the ASTM C-1581, has some limitations due to the maximum coarse aggregate size that can be used in the test. This is a major limitation for many common and realistic mixes that are being used in the industry. Most of the mixes used in bridge decks, pavements or other structures use aggregate sizes greater than 0.5 in. In consequence, AASHTO restrained shrinkage test is being used to evaluate such mixes. Recent studies that focus on quantifying the stress profiles in the AASHTO test all face the same challenge, which is the non-uniform stress development due to the moisture gradients that are present in thicker rings which are subjected to drying from the outer circumference. Although analytical solutions have been proposed for this case, they have not been fully tested or confirmed by other researchers. It should also be noted that all of the studies drive the stress profile in the concrete ring based on the strains that are experienced in the inner steel ring, using certain assumptions, and applying basic laws of engineering mechanics. Although these formulas are useful in interpreting the results of restrained shrinkage ring tests, they should be verified and tested thoroughly before they can be used confidently.

CHAPTER III

EXPERIMENTAL SETUP

3.1 INTRODUCTION

The experimental setup consists of mixing and testing the restrained shrinkage performance of 16 HPC mixes using the designs that are given by NJDOT, which are common bridge deck mixes used in The State of New Jersey. The materials used in the study are from local sources throughout the state (except for fly ash, which is supplied from Pennsylvania). The mixes are grouped into four according to the percentage of supplementary materials utilized in their design. Group 1 mixes consist of four 40% slag replacement mixes, Group 2 mixes are 30% slag replacement with 4% silica fume, Group 3 mixes are silica fume only mixes, and Group 4 mixes consist of four mixes with varying proportions of slag and silica fume. Fly ash is utilized in only one of the mixes in Group 4. Although the majority of the mixes use a w/b ratio of 0.40, there are few mixes with 0.34 and 0.37 w/b ratios.

A broad range of tests are performed on each mix to determine their mechanical properties to assist in determining the cracking potential. Furthermore, gradation of coarse and fine aggregates is tested, and the specific gravities for those materials are determined to better understand the differences caused by various sources and quarries.

3.2 MATERIAL PROPERTIES

The raw materials are supplied by NJDOT from various sources in New Jersey with the exception of fly ash. Fly ash is obtained from Pennsylvania since it is the only source in this region. Raw materials used to produce the mixes include cement, slag, silica fume, fly ash, water, coarse and fine aggregates, and chemical admixtures.

The mixes involve the use of two different cement types (Type I and II) from four suppliers, silica fume from three suppliers, slag from three suppliers, and fly ash from a single source as far as the cementitious materials are concerned. Cementitious materials and their suppliers can be seen in Table 3.1.

Table 3.1 Cementitious Materials and Suppliers

	Material	Supplier
Portland Cement	Portland Type I/II	Essroc
		LaFarge
		Lehigh
		Riverside Cement
Slag	Slag Grade 120	Essroc
	Newcem	Lafarge
	Grancem	St. Lawrence
Silica Fume	Euclide MSA	Euclide Chemical
	Rheomac SF100	Master Builder
	Sikacrete 950DP	Sika
Fly Ash	Type F Fly Ash	Separation Tech

Coarse aggregate utilized is No. 57 Crushed Stone with a nominal maximum diameter of 3/4 inches, and nine different local quarries supply the needed amount of material. Types of coarse aggregates obtained from the nine quarries include quartz, granite, and limestone which are low shrinkage producing aggregates. Other types

include trap rock and argillites which have high shrinkage characteristics. Fine aggregate is C33 sand and it is from seven sources. With the exception of sand from Amboy Aggregates all other six types have the same properties and are classified as concrete sand. Sand supplied by Amboy Aggregates is obtained by drenching and may contain deposits of chloride ions. However, this does not have any effect on shrinkage properties of the concrete made by this type of sand. Table 3.2 illustrates the aggregates used and their respective quarries.

Table 3.2. Aggregates and Suppliers

	Material	Supplier
Coarse Aggregate	No. 57 Coarse Aggregate	Tilcon Quarries
		Trap Rock Industries
		Plumstead Material
		Fanwood Crushed Stone
		Independence Materials #57 Devault
		Better Materials Penns Park
		Stavola Construction Materials
		Mt. Hope Rock Products
		Oxford Quarry
Fine Aggregate	C33 Fine Aggregate	Sahara Sand
		Clayton Sand
		Tuckahoe Sand &Gravel
		RE Pierson
		Dunrite Sand
		Amboy Aggregates
		County Concrete

The admixtures used in mixing the sixteen HPC mixes include air entraining agent (AEA), water reducer (WR), high range water reducer (HRWR), and retarder. The suppliers of these chemicals are shown in Table 3.3.

Table 3.3. Chemical Admixtures and Suppliers

	Material	Supplier
AEA	Daravair 1000	W.R. Grace
	Euclid Air	Euclide Chemical
	Euclide AEA-92	Euclide Chemical
	MB AE-90	Master Builder
	MB VR	Master Builder
	Setcon 6A	Great Eastern
	Sika AEA-15	Sika
Water Reducer	Chemstrong A	Great Eastern
	Euclide WR 89	Euclide Chemical
	WRDA/HYCOL	W.R. Grace
HRWR	Chemstrong SP	Great Eastern
	Daracem 19	W.R. Grace
	Eucon 37	Euclide Chemical
	MB Glenium 3030	Master Builder
	MB Rheobuild 1000	Master Builder
	Sika Sikament 86	Sika
Retarder	Eucon 75	Euclide Chemical
	MB Pozz 100xr	Master Builder
	Sika Plastimen	Sika

3.3 MIX PROPORTIONS

Mix design proportions are obtained from NJDOT and most of them are common bridge deck mixes used within the state. The original designations for the mixes were kept, but new designations were also given according to comparison parameters to make the process of analysis easier. The majority of the mixes include slag as a cementitious replacement in high percentages (such as 30 or 40%). There are two mixes which have only silica fume in their composition, which is currently not allowed in NJDOT specifications due to problems encountered with cracking on bridge projects. There is only one mix with fly ash replacement. All mix proportions are shown in Table 3.6

through Table 3.9. NJDOT designations are followed by Rutgers designations. Mixes have been grouped into 4 groups and the group properties are defined in Table 3.4.

Table 3.4. Mix Group Definitons

Group	Definition
1	40% Slag replacement
2	4% Silica fume and 30% Slag replacement
3	Only Silica fume replacement
4	Various percentages of silica fume, slag, and fly ash

Abbreviations were also used to identify properties of each mix and they are summarized in Table 3.5.

Table 3.5. Abbreviations

Abbreviation	Definition
SF	Silica Fume
SL	Slag
F.Ash	Fly Ash
CA	Coarse Aggregate
FA	Fine Aggregate

Mix design proportions for Group 1 mixes are illustrated in Table 3.6. All mixes have 40% slag as a cementitious replacement and for all mixes the w/b ratio is 0.4. Total cementitious content is the same except for mix G1M1 which has 800 lbs/cu.yd of total cementitious content. Coarse aggregate content varies between 1650 – 1850 lbs/cu.yd and fine aggregate content is between 1195 and 1250 lbs/cu.yd. Mix G1M4 was not mixed since the coarse aggregate received was not a #57 crushed stone and it failed the gradation tests.

Table 3.6. Group 1 Mix Design Proportions

(lb/cyd)	R311266	R408847	R200578S	R309494*
Mix Designation	G1M1	G1M2	G1M3	G1M4
Portland Cement	480	395	396	394
Type	I	I	I	I
Silica Fume	0	0	0	0
Fly Ash Class F	0	0	0	0
Slag	320	263	264	263
	40%	40%	40%	40%
Total Cementitious Content	800	658	660	657
Course Agg. No. 57	1650	1700	1875	1850
Fine Agg.	1240	1199	1195	1250
Course Agg./Fine Agg.	1.33	1.42	1.57	1.48
Water (gal)	38.3	31.2	31.7	31.5
W/(C+P)	0.4	0.4	0.4	0.4
Water Reducer (oz/cwt)	2.3	-	3.5	3
Retarder	-	-	-	-
Superplasticizer (oz/cwt)	19.9	8.4	13.4	12
AEA (oz/cwt)	1.0	0.7	1.0	0.8
Slump (in)	6	5.5	8	-
Air Content (%)	6.4	7.5	4.0	-

Table 3.7 illustrates the mix design proportions for Group 2 mixes. This group contains 6 mixes with 4% silica fume and 30% slag as a replacement for cement. Out of these 6 mixes 5 of them have a total cementitious content of approximately 660 lbs/cu.yd. The remaining mix has a slightly higher value of 683 lbs/cu.yd. If Table 3.7 is analyzed closely, it can be seen that the mixes can be grouped into three within each other based on their aggregate contents and also cement types. The first two mixes have the lowest coarse aggregate content and coarse to fine aggregate ratio (1800 lbs/cu.yd and 1.42, respectively), the third and fourth mixes have the highest coarse aggregate content of 1850 lbs/cu.yd, and the last two mixes use Type II cement while having slightly less coarse aggregate content than the previous two mixes.

Table 3.7. Group 2 Mix Design Proportions

(lb/cyd)	R408850	R409239	R309497	R310682	R200626S	R200633S
Mix Designation	G2M1	G2M2	G2M3	G2M4	G2M5	G2M6
Portland Cement	436	436	435	436	436	461
Type	I	I	I	I	II	II
Silica Fume	25	25	25	25	25	25
	4%	4%	4%	4%	4%	4%
Class F Fly Ash	0	0	0	0	0	0
Slag	197	197	197	197	200	197
	30%	30%	30%	30%	30%	30%
Total Cementitious Content	658	658	657	658	661	683
Course Agg. No. 57	1700	1700	1850	1850	1825	1811
Fine Agg.	1196	1196	1247	1230	1170	1156
Course Agg./Fine Agg.	1.42	1.42	1.48	1.50	1.56	1.57
Water (gal)	31.1	31.1	31.5	31.5	30.5	32.8
W/(C+P)	0.4	0.4	0.4	0.4	0.4	0.4
Water Reducer			3	3	3	
Retarder		1.0				2.0
Superplasticizer (oz/cwt)	7.6	8.0	12.0	12.0	8.0	4.0
AEA (oz/cwt)	0.7	0.9	0.6	1	1.3	0.36
Slump (in)	5.25	6	5.5	5.25	6.5	5
Air Content (%)	7.00%	7.75%	3.75%	5.70%	7.50%	4.50%

Group 3 mixes and their design proportions are illustrated in Table 3.8. It can be seen that both of the mixes have only silica fume as a supplementary cementitious material. Currently The NJDOT Specifications do not allow the use of such mixes due to the high shrinkage potential and cracking observed in bridge deck applications. However, testing these mixes under restrained shrinkage would be important to verify the observations and experiences from the field. Both mixes have relatively high total cementitious content and relatively low total coarse aggregate content. The two major differences between G3M1 and G3M2 are the type of cement and percentage of silica fume in their design.

Table 3.8. Group 3 Mix Design Proportions

(lb/cyd)	R308163	R308278
Mix Designation	G3M1	G3M2
Portland Cement	700	655
Type	1	2
Silica Fume	35	50
	5%	7%
Class F Fly Ash	0	0
Slag	0	0
Total Cementitious Content	735	705
Course Agg. No. 57	1725	1750
Fine Agg.	1190	1280
Course Agg./Fine Agg.	1.45	1.37
Water (gal)	35.2	33.8
W/(C+P)	0.4	0.4
Water Reducer (oz/cwt)		
Retarder (oz/cwt)	1.5	2.0
Superplasticizer (oz/cwt)	8.0	10.0
AEA (oz/cwt)	0.5	0.8
Slump (in)	5.5	5
Air Content (%)	6.5	6.0

Finally, the remaining four mixes are grouped into Group 4. Mix proportions for this group are illustrated in Table 3.9. This group consists of mixes with varying proportions of silica fume and slag. Furthermore, the only mix which contains fly ash is in this group. Water-to-binder ratio varies between 0.34 and 0.4. It can be seen that all mixes have a high silica fume content of 5% or more (up to 7.5%). Except mix G4M2, all mixes have high coarse aggregate amounts (1800 lbs/cu.yd or more). Although a direct comparison of these mixes is not possible within this group due to the number of variables, comparison could be made with similar mixes from other groups.

Table 3.9. Group 4 Mix Design Proportions

(lb/cyd)	R309495	R408844	R309496	R408694
Mix Designation	G4M1	G4M2	G4M3	G4M4
Portland Cement	435	411	394	571
Type	1	1	1	1
Silica Fume	35	50	50	50
	5%	7.5%	7%	7%
Class F Fly Ash	0	0	0	69
				10%
Slag	197	197	263	0
	30%	30%	37%	
Total Cementitious Content	667	658	707	690
Course Agg. No. 57	1850	1700	1850	1800
Fine Agg.	1247	1187	1250	1232
Course Agg./Fine Agg.	1.48	1.43	1.48	1.46
Water (gal)	29.5	31.1	31.5	28.4
W/(C+P)	0.37	0.4	0.37	0.34
Water Reducer (oz/cwt)	3		3	
Retarder (oz/cwt)				
Superplasticizer (oz/cwt)	12.0	7.3	12.0	18.0
AEA (oz/cwt)	1	0.7	0.6	1.7
Slump (in)	6.75	4	7	6.75
Air Content (%)	5.0	6.5	4.0	7.0

3.4 MIXING and FRESH SAMPLING of CONCRETE

Mixing is done in the structural laboratory of Rutgers University, Civil Engineering Department according to ASTM C-192. Fresh concrete testing such as slump (ASTM – C 143 – 05a), and air content (ASTM C – 231) are done immediately after mixing to ensure that the mixes are within NJDOT Specification limits. Samples are consolidated using a vibrating table and a 7 day wet cure is applied to all samples to conform to NJDOT Specifications. Mixing, fresh sampling, and curing procedures are explained in greater detail in the next four sections.

3.4.1 Mixing (ASTM C - 192)

The mixing starts with adding coarse and fine aggregates to the mixer. While the mixer is running, 1/3 of the water is added, followed by the air entraining agent. The mixer is allowed to run for 30 seconds and then the cement is added with the rest of the water, and the cementitious materials. The concrete is mixed with all ingredients in the mixer for at least three to four more minutes. After three or four minutes of mixing, the batch is allowed to hydrate by resting for three to four minutes. During the waiting period the concrete mixer is covered to avoid loss of moisture. Then the superplasticizer is added to the mix while the mixer is spinning. Finally the mixer is allowed to run for three more minutes or until the superplasticizer reacts with the concrete such that there is uniformity in the concrete. Figure 3.1 shows the concrete drum mixer that is used for mixing in the laboratory.

Figure 3.1. Concrete Mixer

3.4.2 Slump Test (ASTM C-143-05a)

The slump of each batch of concrete is measured immediately after mixing in accordance with ASTM C-143. The slump cone is filled in three layers, with each layer approximately one-third the volume of the mold. Each layer is rodded with 25 strokes using the tamping rod. The strokes are uniformly spread over the cross section of each layer. Each layer is rodded throughout its depth, so that the strokes just penetrate into the underlying layer. In filling and rodding the top layer, the concrete is heaped above the mold before rodding is started. If the concrete level falls below the top edge of the mold after rodding, additional concrete is added to keep an excess of concrete above the top of the mold. The surface of the concrete is struck off by rolling motion of the tamping rod. The mold is immediately removed from the concrete by raising it in a vertical direction avoiding lateral or tensional motion. The slump is immediately measured by determining the vertical difference between the top of the mold and the displaced original center of the top surface of the specimen. Illustration of the slump test can be seen in Figure 3.2.

Figure 3.2. Slump Test

3.4.3 Air Content (ASTM C – 231)

Concrete air content is measured using a Type – B Pressuremeter (Figure 3.3) according to ASTM C – 231. After dampening the insides of the meter bowl, it is filled in three layers of equal volume. Each layer is rodded with 25 strokes using the tamping rod. The bottom layer is rodded throughout its depth without the rod forcibly striking the bottom of the bowl. The second and top layers are rodded throughout their depth so that the strokes penetrate about 1in. into the underlying layer. The bowl is tapped smartly 10 to 15 times with a rubber mallet after each layer is rodded. The top surface struck is off with plate or bar and finished smooth after rodding and tapping the last layer. The flanges of the bowl and the cover assembly are thoroughly cleaned, and the air meter is assembled to obtain a pressure tight seal. The air valve between air chamber and the bowl is closed, and both petcocks are opened. Using a rubber syringe, water is injected through one petcock until it emerges from the opposite petcock. The meter is jarred gently until all air is expelled from the same petcock. The air bleeder valve on the air chamber is closed and air is then pumped into the air chamber until the gage hand is on the initial pressure line. A few seconds should be allowed for compressed air to cool after which the gage hand at the initial pressure line is stabilized by pumping or bleeding-off air as necessary while tapping the gage lightly. Both petcocks are then closed, and the air valve between air chamber and measuring bowl is opened. The sides of measuring bowl are tapped with mallet to relieve local restraints. The pressure gage is tapped lightly with hand to stabilize the reading while the air valve is open and percentage of air on the dial of pressure gage is read and recorded.

Figure 3.3. Type - B Pressuremeter for determining concrete air content

3.4.4 Sampling of Specimens and Consolidation

A total of 45 cylindrical specimens (4 x 8 in.) are taken for standard ASTM tests. In addition two ring specimens are cast for testing restrained shrinkage. Companion free shrinkage blocks are also cast to determine the free shrinkage of all mixes and correlate the results with restrained shrinkage tests. All specimens are cast using a vibrating table. Consolidation requirements of AASHTO are used while casting the test specimens. Figure 3.4 and Figure 3.5 show free shrinkage blocks, cylinder molds and the vibrating table.

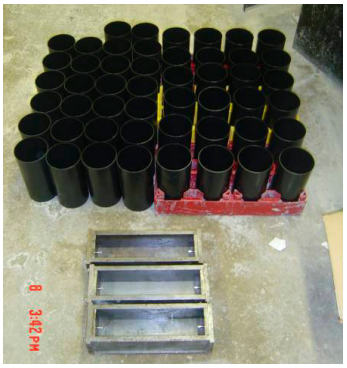

Figure 3.4. Shrinkage Blocks and Cylinder Molds

Figure 3.5. Vibrating Table

3.4.5 Curing

The NJDOT Specifications in the field require 7 day moist curing of concrete using wet burlap covered with polyethylene sheets. The same curing procedure is applied to all samples under study. After demolding at 18-24 hours, all samples are covered with wet burlap and polyethylene sheets and placed in an environmental chamber with a constant temperature of 74^0F. After the end of curing period, the burlap is removed and the specimens are left in the environmental chamber. The relative humidity in the chamber is kept constant at $50 \pm 4\%$. Curing procedure is illustrated in Figure 3.6 and Figure 3.7.

Figure 3.6. Restrained shrinkage specimen covered with wet burlap

Figure 3.7. All Specimens Under Burlap and Polyethylene Sheet

3.5 LABORATORY TESTING PROCEDURES

A broad range of tests are performed on each mix to determine their mechanical properties to assist in determining the cracking potential. Table 3.10 illustrates all the tests which are performed for each mix. In addition to the tests in Table 3.10, gradation

of coarse and fine aggregates is also tested. The specific gravities for those materials are also determined to better understand the differences caused by various sources and quarries.

Table 3.10. Summary of Laboratory Tests Performed on Each Mix

Test	Number of Specimens	Applicable ASTM Standard	Curing Conditions	Age of Concrete at Test, days
1. **Slump**	1 per batch	C143	None	0, fresh
2. **Fresh Air Content**	1 per batch	C231	None	0, fresh
3. **Free Shrinkage**	3 per mix	C157	7 day wet	1 to 91 days
4. **Restrained Shrinkage**	2 per mix	AASHTO PP34	7 day wet	1 to age of crack (max 91 days)
5. **Compressive Strength**	15 per mix (4 × 8 in)	C39	7 day wet	3, 7, 14, 28 days, and crack age
6. **Splitting Tensile Strength**	15 per mix (4 × 8 in)	C496	7 day wet	3, 7, 14, 28 days, and crack age
7. **Modulus of Elasticity**	15 per mix (4 × 8 in)	C469	7 day wet	3, 7, 14, 28 days, and crack age

3.5.1 Sieve Analysis of Fine and Coarse Aggregates (AASHTO T 27-06)

Gradation of sand and stone is important in evaluating shrinkage characteristics of a concrete mix. A more uniform gradation prevents formation of gaps between the aggregates and improves the pore structure of concrete. The sieve analysis determines the gradation (the distribution of aggregate particles, by size, within a given sample) in order to determine compliance with design, production control requirements, and verification specifications. The gradation data can be used to calculate relationships

between various aggregate or aggregate blends, to check compliance with such blends, and to predict trends during production by plotting gradation curves graphically.

To perform the test, a known amount weight of material (the amount being determined by the largest size of aggregate) is placed upon the top of a group of nested sieves (the top sieve has the largest screen openings and the screen opening sizes decrease with each sieve down to the bottom sieve which has the smallest opening size screen for the type of material specified) and shaken by mechanical means (Figure 3.8) for a period of time. After shaking the material through the nested sieves, the material retained on each of the sieves is weighed using one of two methods. The cumulative method requires that each sieve beginning at the top be placed in a previously weighed pan (known as the tare weight), weighed, the next sieve's contents added to the pan, and the total weighed. This is repeated until all sieves and the bottom pan have been added and weighed. The second method requires the contents of each sieve and the bottom pan to be weighed individually. Either method is satisfactory to use and should result in the same answer. The amount passing each sieve is then calculated. Second method was utilized for the aggregate sources in this study.

Figure 3.8. Mechanical Sieve Shaker

3.5.2 Specific Gravity and Absorption of Fine Aggregate (AASHTO T 84-04)

In concrete mix design, the specific gravity of the aggregate is used in calculating the percentage of voids and the solid volume of aggregates in computations of yield values. On the other hand, the absorption is important in determining the net w/b ratio in the concrete mix. The test requires the use of a scale, pycnometer (a flask or a container which the sand sample will be introduced), metal mold, and a tamper. After a sand sample is obtained by the procedures in AASHTO T 248, it is dried to constant mass. Immediately after it cools to handling temperature, the sand sample is soaked in water for 15 to 19 hours. Next, the excess water is removed and the sand is slowly dried to saturated surface dry (SSD) condition. Cone test is done by using the tamper and the metal mold to ensure that the sand has reached the SSD condition. Immediately after SSD is reached, the pycnometer is filled with water and the sand is introduced. After all air bubbles are removed by gently agitating the pycnometer total mass of the pycnometer is recorded. Than, the pycnometer is cleaned and weighed one more time with only water in it filled to its calibration capacity. The obtained measurements are used to calculate the absorption and bulk specific gravity of the sand sample.

3.5.3 Specific Gravity and Absorption of Coarse Aggregate (AASHTO T 85-04)

This test is very similar to the T 84 test and the determinations that may be made from this procedure are identical to those made from AASHTO T 84. To briefly summarize, an oven dried sample of coarse aggregate is submerged in water for approximately 15 hours. Next it is dried to SSD condition and weighed and than it is dried completely and weighed one last time. These measurements are used in determining of absorption and bulk specific gravity.

3.5.4 Compressive Strength of Cylindrical Concrete Specimens (ASTM C-39-05)

Two 4 x 8 in. cylinders are tested at 3, 7, 14, 28, and cracking day of restrained ring specimens using the Forney-1 million pound- compression machine (Figure 3.9) that complies with ASTM C-39. The loading rate of the Forney compression machine is kept constant throughout the test. The specimens are either capped with high strength sulfur capping compound or covered with steel caps. When steel caps are used, the rubber pads are replaced periodically according to the manufacturer recommendation. The maximum strength is recorded for each specimen.

Figure 3.9. Forney 1-Million Pound Compression Machine

3.5.5 Standard Test Method for Splitting Tensile Strength of Cylindrical Concrete Specimens (C – 496 –04ε1)

Splitting tensile strength is determined by splitting a 4 x 8 in. cylinder in accordance with ASTM C496 using the 400-kip Tinius Olsen Compression machine. The Tinius Olsen Compression machine is used because it has longer head extension than the Forney 1-million pound compression machine. Likewise in order to automate and to

minimize human error, a 250-kip digital load cell is also used in this test. Figure 3.10 shows the setup for the splitting tensile strength test.

Figure 3.10. Splitting Tensile Strength Test Setup

3.5.6 Modulus of Elasticity (ASTM C-469-02ε1)

The modulus of elasticity is measured according to ASTM C-469. At least two specimens are capped with sulfur compound to be tested in compression using a compressometer shown in Figure 3.11. The sulfur compound eliminates the creeping of the rubber pad in the steel cap. The specimens are loaded at least twice. During the first loading, which is primarily for the seating of the gages, the performance of the gage is observed. The load is applied at constant rate within the range of 30-40 psi/sec, and the load is applied up to approximately 40 percent of the ultimate compressive strength. The load and deformation are recorded manually at regular intervals. In order to determine the modulus of elasticity, the strains are plotted against the stresses where the slope represents the modulus of elasticity. Figure 3.12 shows the modulus of elasticity test setup.

Figure 3.11. Compressometer used for modulus tests

Figure 3.12. Modulus of Elasticity Test Setup

3.5.7 Free Shrinkage Test

The free shrinkage test is performed according to ASTM C157. Three 3x3x10 in. prism concrete specimens are cast with gage studs placed at each end. The gage studs are screwed into the plates at each end of the mold using a hex screw. The length between the two gage studs is measured as well as the length of the reference bar using a length comparator (Figure 3.13). When using the comparator, the specimen is slowly rotated such that the minimum reading is recorded. The length change at various ages is recorded, and it is calculated as follows (in percentage):

$$L = \frac{\left[\left(L_x - L_i\right) \times 100\right]}{G}$$

Where,

L_x = the difference between the length of the specimen and the reference bar at x number of days.

L_i = the difference between the length of the specimen and the reference bar at 1 day.

G = the total length of the specimen = 10 in.

In addition, embedded vibrating wire strain gages (VWSG) can be installed to capture autogenous shrinkage of concrete. This was done for several mixes to see the contribution of autogeneous shrinkage on total shrinkage using the setup shown in Figure 3.14.

Figure 3.13. Length Comparator

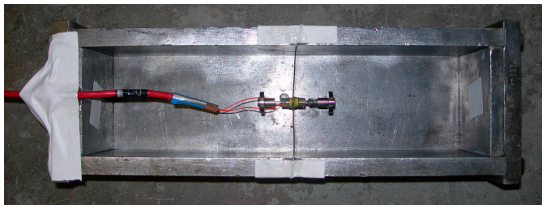

Figure 3.14. Shrinkage Molds with VWSG (Autogenous Shrinkage)

3.5.8 Restrained Shrinkage Ring Test

To measure restrained shrinkage, concrete is cast around a steel ring in accordance to the test method of AASHTO PP34. The concrete is cast around the steel ring, such that, as the concrete shrinks, a compressive stress is developed in the steel ring and balanced by a tensile stress in the concrete ring. If this tensile stress is greater than the allowable tensile stress of the concrete, it cracks. The cracks in the ring are

monitored daily using a crack microscope. The AASHTO setup also involves instrumenting the mid-height of the steel ring with four foil strain gages (FSG) so that abrupt changes (due to the release in concrete stress after cracking) in the steel strain can be observed indicating the exact age of cracking. Moreover, vibrating wire strain gages (VWSG) are installed at the top surface of the concrete ring using threaded bolts. The VWSG sensors are used to signal the crack location as well as to measure the exact strain in concrete. The advantage of using VWSG sensors is that the actual strain in the concrete is monitored and therefore, if the concrete does not crack the stress development can be quantified. This leads to better understanding of the test results and allows for a more refined comparison between mixes.

3.5.8.1 Sensors and Instrumentation

The VWSG is manufactured by Geokon Inc. and basically consists of a length of steel wire tensioned between two mounting blocks. The changing length of concrete due to shrinkage produces relative movement between the two mounting blocks causing a change in the wire tension and a corresponding change in its frequency of vibration. The resonant frequency is measured by plucking the wire using an electromagnetic coil connected through a signal cable to data acquisition system (DAS), which also measures the frequency and displays the strain in the wire directly in microstrain.

Figure 3.15. Geokon Model 4000 Vibrating Wire Gage

The FSG (Figure 3.16) is manufactured by Vishay Micro-Measurements and is a full bridge 120 ohm resistance gage with 0.6% tolerance. The procedure to install the gages includes sanding down the area to be instrumented, cleaning the surface using surface preparation compounds, and finally attaching the gage into position using adhesives. After the gage is fully bonded, all four sensors in the ring are coated with a water-proofing chemical and later they are connected to the DAS.

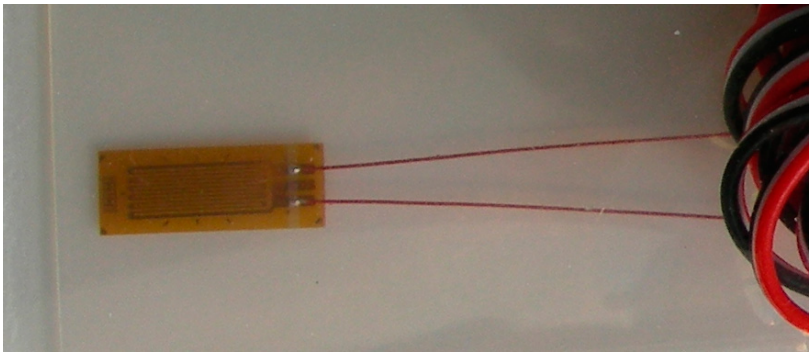

Figure 3.16. Vishay 120 Ohm Foil Strain Gage

3.5.8.2 Data Collection and Analysis

Data collection is done with the help of a data acquisition system manufactured by Campbell Scientific, Inc. The DAS (Figure 3.17) is installed permanently into the environmental chamber. It is equipped with strain gage modules that are capable of monitoring 12 rings simultaneously. For the purposes of this study DAS was programmed to collect data at an interval of five minutes and to download the data daily to a permanent computer.

The recorded data is monitored and plotted every three days to check for sudden jumps in strain readings (which may signal cracking). Also, gradual increase in strain is monitored and plotted against the cracking strain to quantify the cracking potential of

each mix. Cracking strain of each mix is obtained from the results of standard cylinder tests as follows,

$$\varepsilon_t = \frac{f_t}{E}$$

Where,

f_t : Tensile splitting strength

E : Modulus of elasticity

ε_t : Cracking strain

Figure 3.17. Data Acquisition System

After 91 days, an evaluation is made whether to continue collecting readings from the rings or not. If the strain values in the foil gages and VWSG have stabilized, this means that shrinkage has come to a plateau, and the test can be finalized. This can also be checked by examining the length comparator readings from the free shrinkage blocks. If the free shrinkage plot has reached a plateau and the concrete has not cracked after 91

days, it is concluded that it will not crack. However, if the readings are changing and increasing strains are observed in the rings, the tests are extended beyond 91 days.

Figure 3.18 below summarizes the restrained shrinkage test and data analysis procedure. Readings are obtained from DAS and graphed every 2 to 3 days. Any sensor which shows close to or higher than cracking strain signals a crack (In the case below VWSG 4 exceeds cracking strain first and the picture shows the observed crack). The first 7 days, which is the curing duration, no tensile strains are observed. Therefore, when analyzing the results strain measurements are assumed to start from initiation of drying.

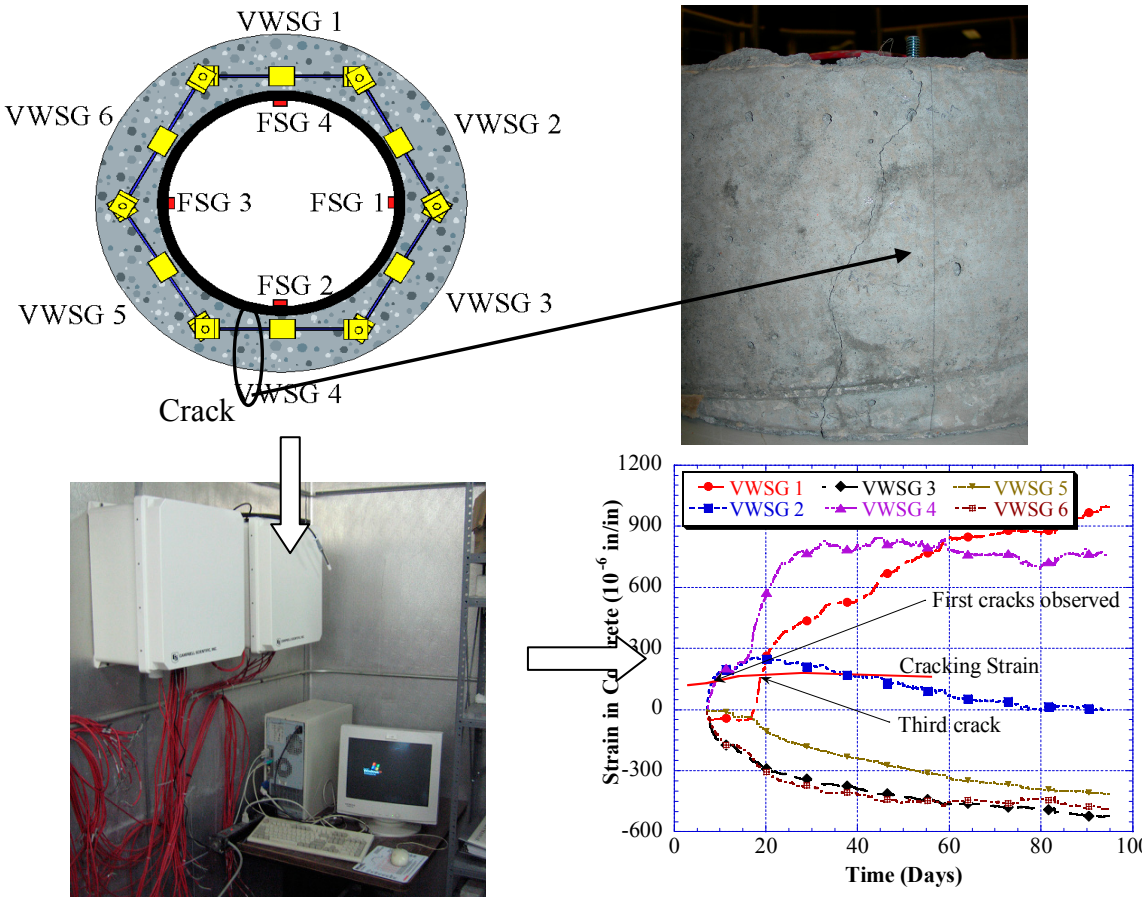

Figure 3.18. Schematic of the restrained shrinkage test setup, data collection schemes, and test results.

3.5.8.3 Environmental Chamber

Shrinkage is very sensitive to environmental conditions. Therefore, the shrinkage specimens need to be stored in an environmental chamber. The environmental chamber is a 24 × 16 × 8 ft room (Figure 3.19) that is made of insulated aluminum wall. The temperature and humidity of the room is controlled by a digital control unit located outside the chamber. The digital control unit acquires temperature and humidity readout from an environmental sensor inside the chamber. The sensor is positioned such that the overall temperature and humidity is at the set point. Inside the chamber, the temperature is adjusted through the heater and freezer units that are placed on one side of the wall. The unit is shielded with aluminum sheets with blowers to circulate the air in the chamber. The humidity is controlled by means of a steam generator that is located underneath the blowers. Dehumidification is done using an air conditioning unit to dry the air. For the purposes of this study the environmental chamber was set to a temperature of 74^0F and a relative humidity of 50 ± 4%.

Figure 3.19. Inside View of the Environmental Chamber

Figure 3.20. Close Up View of Rings in the Environmental Chamber

3.5.8.4 Restrained Shrinkage Test Setup with 4 Vibrating Wire Strain Gages

As explained previously, this test involves casting of a concrete ring around a steel ring, and than monitoring the ring until it cracks under the pressure that develops due to drying shrinkage. The dimensions of the steel and concrete ring are identical to those that are defined in AASHTO PP34. The inner steel ring is a 1/2 in. thick smooth A36 steel pipe, and the outer mold which is used to cast the concrete ring is an 18 in. inside diameter sonotube form. The only difference of the setup from AASHTO PP34 is the use of VWSG gages to monitor the strain development in the concrete directly. The gages have custom manufactured mounting pieces which enable the attachment of threaded bolts that are sunk into the concrete ring. The gages are positioned such that the middle of the gage coincides with the FSG on the steel ring. The threaded bolts are 3 in. long and have a diameter of 1/4 in. Special care is taken to position the studs exactly in the middle of the concrete ring. Figure 3.21 shows the schematic diagram and a picture of this setup.

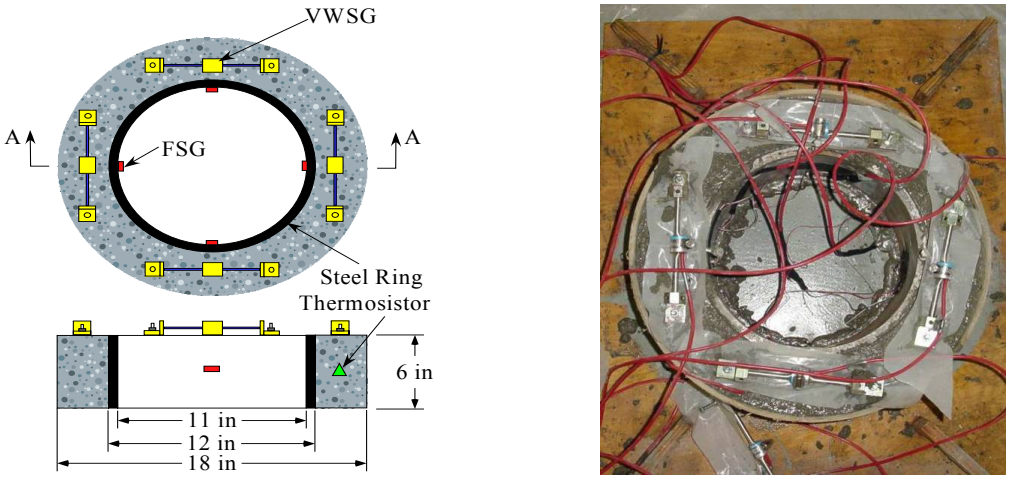

Figure 3.21. a) Schematic Diagram and b) Picture of the 4 VWSG Restrained Shrinkage Test Setup

Two specimens are cast per mix in an environmental chamber with constant ambient temperature and relative humidity of 74°F ± 3°F and 50% ± 4%, respectively. The concrete specimens are placed in the molds in three equal lifts and consolidated using a vibrating table. Immediately after casting the specimens, they are covered with wet burlap and polyethylene sheets. After 24 hours, each specimen is striped from its molds and covered with wet burlap for 7 days. Typical sample preparation is summarized in Figure 3.22. It consists of 3 stages.

1. Molds are prepared and placed on a plastic sheet inside the environmental chamber. Just before casting, outside face of the steel ring and the inside face of the sonotube is sprayed with a chemical release agent. This is done to assure that the friction on the contact surface between the steel and the concrete is minimal and it also makes the demolding procedure easier (Figure 3.22a).
2. Concrete is cast, consolidated, and sensors are embedded carefully in their positions (Figure 3.22b).
3. Samples are covered immediately with burlap and then sealed with plastic cover to prevent loss of moisture and the strain measurements are started (Figure 3.22c and Figure 3.22d).

After curing period is over, the plastic sheet and burlap is removed and the rings are moved to the permanent shelves in the environmental chamber and are monitored up to 91 days. During this period checks for cracks are made every two to three days both by naked eye and also with the help of microscopes. Data collected from the samples are examined to help determine possible crack locations. At the end of the 91 day test period

the ring specimens are carefully mapped for cracks and crack width measurements are taken.

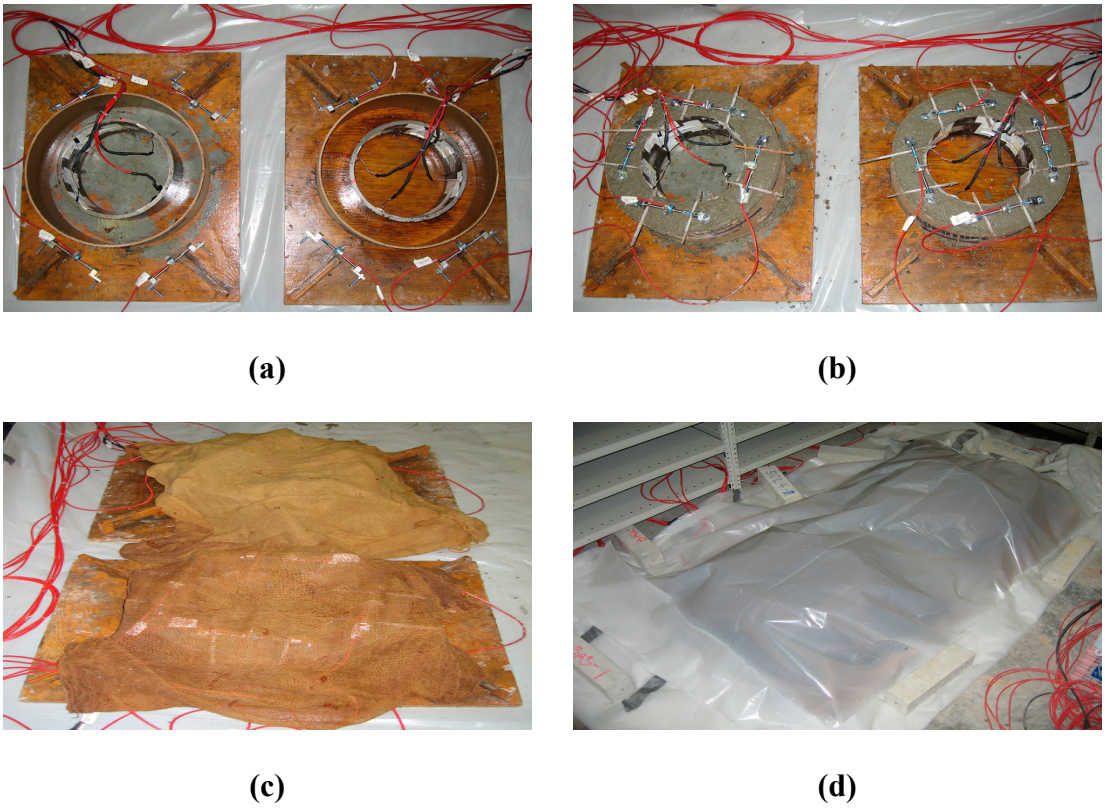

(a) **(b)**

(c) **(d)**

Figure 3.22. Preparation of Restrained Ring Specimens

3.5.8.5 Restrained Shrinkage Test Setup with 6 Vibrating Wire Strain Gages

After the very first few mixes were completed, another arrangement of strain gages were developed by the authors to better monitor the strain profile in the restrained rings for the duration of the test. The disadvantage of the four VWSG setup was that some portions of the concrete ring can not be monitored. When cracking takes place in between the sensors the strain development can not be quantified and a comparison of cracking potential with other mixes becomes very difficult. The six VWSG setup, however, solved this problem. In this setup sensors are connected to each other to form a

closed loop in the centerline of the concrete ring. This way, strain in any portion of the ring can be monitored and cracking locations can be identified much more easily. Other than the sensor arrangement, all other steps and analysis procedures are identical to the four VWSG setup. A schematic and picture of this setup can be seen in Figure 3.23a and Figure 3.23b, respectively.

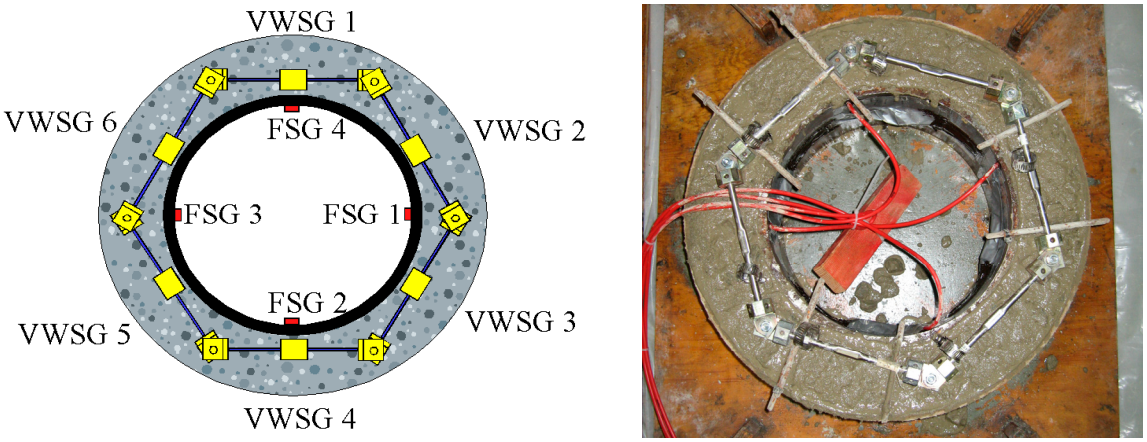

(a) **(b)**

Figure 3.23. a) Schematic Diagram of Six VWSGs, and b) picture of the Six VWSG Restrained Shrinkage Test Setup.

CHAPTER IV

TEST RESULTS

4.1 INTRODUCTION

This chapter presents the experimental results from the tests performed on the 16 HPC mixes. Mechanical properties such as compressive strength, splitting tensile strength, and modulus of elasticity are presented first. This is followed by the results from free and restrained shrinkage tests. Results from each group are presented separately to allow for better comparison and identification of the effects of certain parameters. Finally, correlation of restrained shrinkage strains with free shrinkage strains and mix design parameters (coarse aggregate content, CA/FA ratio, and total cementitious content) is presented.

4.2 FRESH CONCRETE TEST RESULTS

As described in Chapter III, the slump, and air content of concrete are measured for each mix. Since the mixes are common bridge deck mixes utilized in real projects, slump and air content values were provided from field production records. Special care was taken to obtain similar values to correctly reproduce the mixes. Table 4.1 illustrates the comparison of measured and given fresh concrete properties. It can be seen that the slump values were replicated within 1.5 in. and the maximum difference between

measured and given air content was 1%. This shows that the mixes were successfully replicated and the performance of the mixes done in the laboratory should closely resemble the field mixes.

Table 4.1. Comparison of Measured and Given Fresh Concrete Properties

	MEASURED		GIVEN	
MIX	**Slump (in)**	**Air Content (%)**	**Slump (in)**	**Air Content (%)**
G1M1	7	5.5	6	6.4
G1M2	5.5	7.5	6.5	7
G1M3	8	4	NA	NA
G2M1	5.25	7	5	6.7
G2M2	6	7.5	6	7.6
G2M3	5.5	3.75	7	4.5
G2M4	5.25	5.7	4.5	5.2
G2M5	6.5	7.5	NA	NA
G2M6	5	4.5	NA	NA
G3M1	5.5	6.5	5	6.8
G3M2	5	6	4.5	7
G4M1	6.75	5	6.25	5.2
G4M2	4	6.5	4.5	6.7
G4M3	7	4	6.5	5
G4M4	6.75	7	6.75	7.8

4.3 MECHANICAL PROPERTIES

4.3.1 Compressive Strength

Table 4.2 and Figure 4.1 show the variation of compressive strength with time for Group 1 mixes. Analyzing Table 3.6, it can be seen that mix G1M1 has the highest amount of cementitious materials. Mixes G1M2 and G1M3 have slightly less but equal

amount of cement content. The difference in their compressive strength is due to the higher aggregate content of G1M3. Strength of G1M1 is the highest as expected. It was observed that all the mixes attained 80% or more of their strength by day 14. After day 28, strength did not increase by more than 5%. This is typical for slag mixes since it is more reactive than ordinary cement at early ages.

Table 4.2. Compressive Strength of Group 1 (40% Slag) Mixes (ksi)

Day	G1M1	G1M2	G1M3
3	4.189	3.154	5.569
7	5.860	4.853	6.285
14	6.934	5.648	7.186
28	7.769	6.126	7.239
56	7.677	6.433	7.677
91	-	6.245	7.518

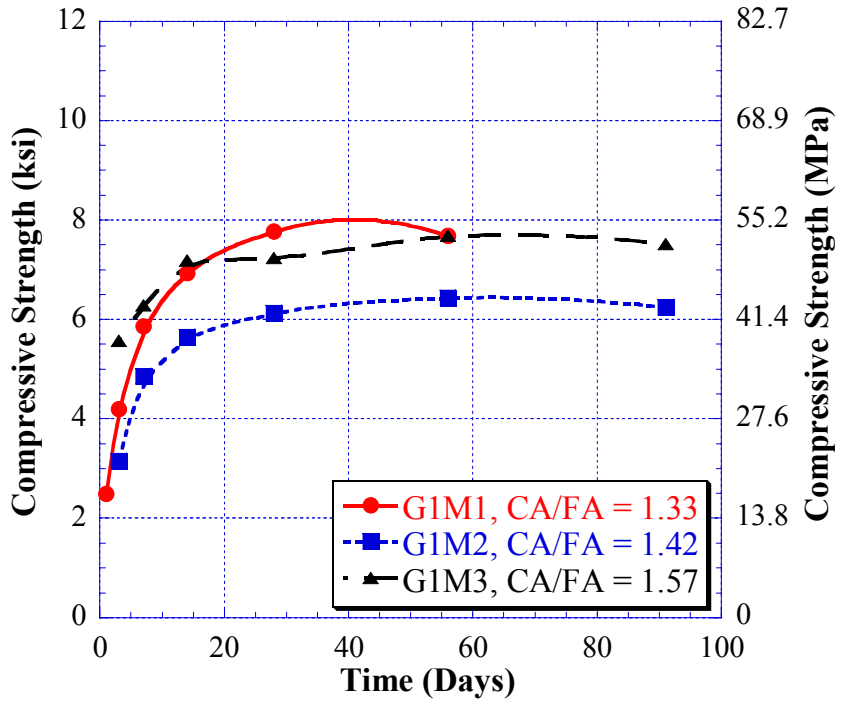

Figure 4.1. Compressive Strength of Group 1 (40% Slag) Mixes

Table 4.3 and Figure 4.2 show the variation of compressive strength with time for Group 2 mixes. Although total cementitious material is approximately same for all

Group 2 mixes, there is tremendous variance in terms of compressive strength. This difference can be attributed to the amount of coarse aggregate used in mix design and the CA/FA ratio. The mixes that attained the highest strengths have the highest coarse aggregate content (1825 lbs/cu.yd or higher). In comparison to Group 1 mixes with same proportions, higher strengths were achieved in Group 2.

Table 4.3. Compressive Strength of Group 2 (5% SF and 30% SL) Mixes (ksi)

Day	G2M1	G2M2	G2M3	G2M4	G2M5	G2M6
1	-	1.087	-	2.247	-	1.114
3	3.779	3.142	5.927	4.853	3.699	4.269
7	5.569	4.415	7.133	6.298	5.290	6.497
14	6.086	5.145	7.969	7.173	6.311	8.022
28	6.762	5.111	8.393	7.823	6.815	8.612
56	7.001	5.357	8.930	8.115	7.100	8.791
91	7.021	5.290	9.175	8.207	7.359	8.811

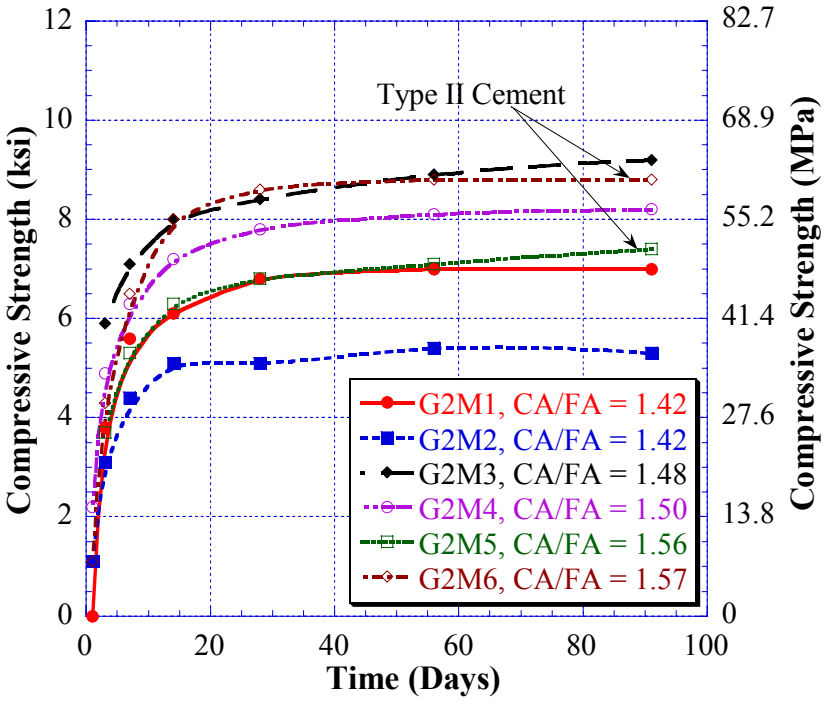

Figure 4.2. Compressive Strength of Group 2 (5% SF and 30% SL) Mixes

The results illustrated in Table 4.4 and Figure 4.3 show that the lower strength in Group 3 mixes was observed in mix G3M1 which is the 5% silica fume only mix. It should be noted that G3M2 uses Type II cement where as G3M1 uses Type I. Moreover, the total coarse aggregate content of mix G3M2 is slightly higher than mix G3M1. A portion of the difference in strength can be attributed to the difference in the percentages of silica fume and total coarse aggregate content. However, the main difference was due to the aggregate source that was used in G3M1 (Plumstead #57 Rock). The rock type from this source is argillite, which is a metamorphic rock. Shortly after testing period started it was realized that the aggregate source was contaminated with deposits of clay and mudstones. This explains the fluctuation in compressive strength values at different testing days. Other mechanical properties of G3M1 as well as the shrinkage behavior were also adversely affected by this contamination which will be discussed in greater detail in the later sections.

Table 4.4. Compressive Strength of Group 3 (Silica Fume Only) Mixes (ksi)

Day	G3M1	G3M2
1	-	2.586
3	3.660	5.914
7	4.322	7.120
14	4.912	8.731
28	5.449	8.930
56	5.065	9.308
91	4.972	-

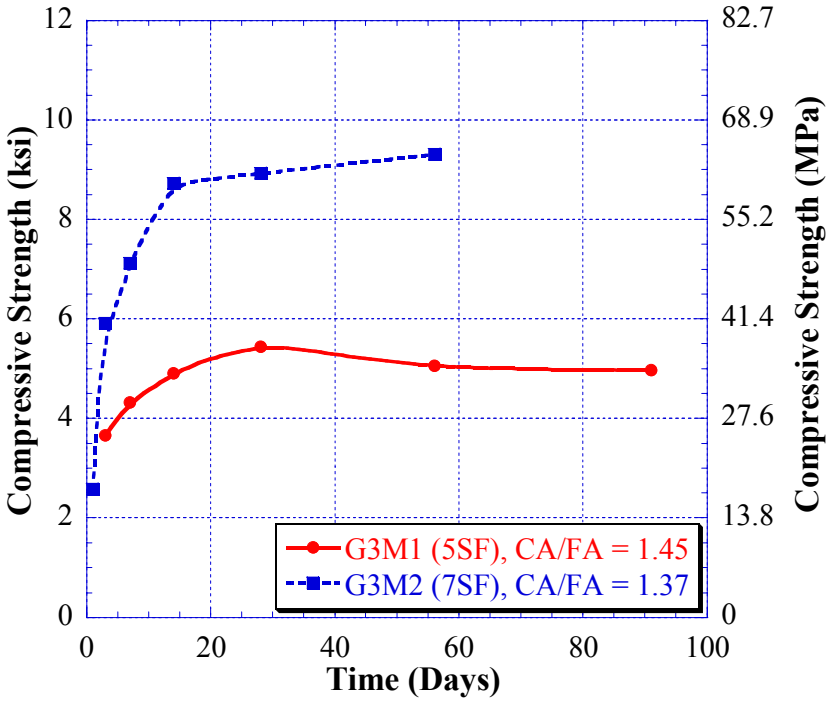

Figure 4.3. Compressive Strength of Group 3 Mixes

The variation of compressive strength of the various mixes in Group 4 versus time is illustrated in Table 4.5 and Figure 4.4. The highest strength was again achieved by mixes that have the highest CA/FA ratio and coarse aggregate content. It should be noted that all mixes, except G4M2 have coarse aggregate contents of 1800 lbs/cu.yd or more. Mix G4M2 has only 1700 lbs/cu.yd of coarse aggregate on top of the low CA/FA ratio. The effect of increasing the silica fume and slag amounts can also be analyzed when G4M1 and G4M3 are compared. Clearly increasing the percentages increased the ultimate strength of G4M3. It can also be seen that G4M4 which is a 10% fly ash and 7% silica fume mix has reached higher strengths compared to G4M2. Again, this is mostly due to the high coarse aggregate content of mix G4M4. Another factor in the difference could be the lower w/b ratio of mix G4M4.

Table 4.5. Compressive Strength of Group 4 Mixes (ksi)

Day	G4M1	G4M2	G4M3	G4M4
1	-	-	-	-
3	5.728	4.018	5.728	5.231
7	6.683	5.370	7.299	6.828
14	7.558	6.126	8.353	8.115
28	8.539	6.563	8.910	8.221
56	8.791	6.683	9.626	8.313
91	9.414	6.702	10.223	8.764

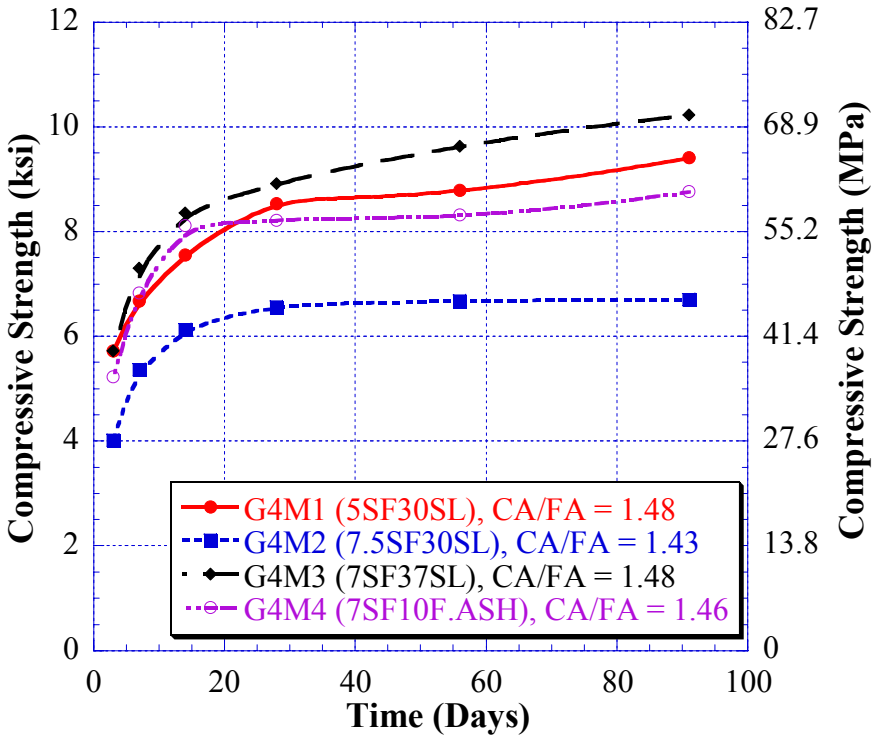

Figure 4.4. Compressive Strength of Group 4 Mixes

4.3.2 Splitting Tensile Strength

Tensile strength of all mixes closely resembled the trend obtained from compressive strength tests. Table 4.6 through Table 4.9 show the splitting tensile strengths with time for Group 1, 2, 3, and 4 mixes. Again, as in the case of compressive strengths, the mixes with high coarse aggregate contents (and CA/FA ratios) in every

Group showed higher splitting tensile strengths. Splitting tensile strength is known to depend primarily on the total amount of coarse aggregate in the mix and the lower values obtained from G1M1 are expected. The effects of coarse aggregate content, type, and the CA/FA ratio on tensile strength are shown graphically in Figure 4.5 through Figure 4.8 for Groups 1, 2, 3, and 4.

Table 4.6. Splitting Tensile Strength Group 1 (40% Slag) Mixes (ksi)

Day	G1M1	G1M2	G1M3
3	0.507	0.371	0.592
7	0.643	0.557	0.647
14	0.703	0.617	0.796
28	0.789	0.627	0.817
56	0.801	0.629	0.824
91	-	0.659	-

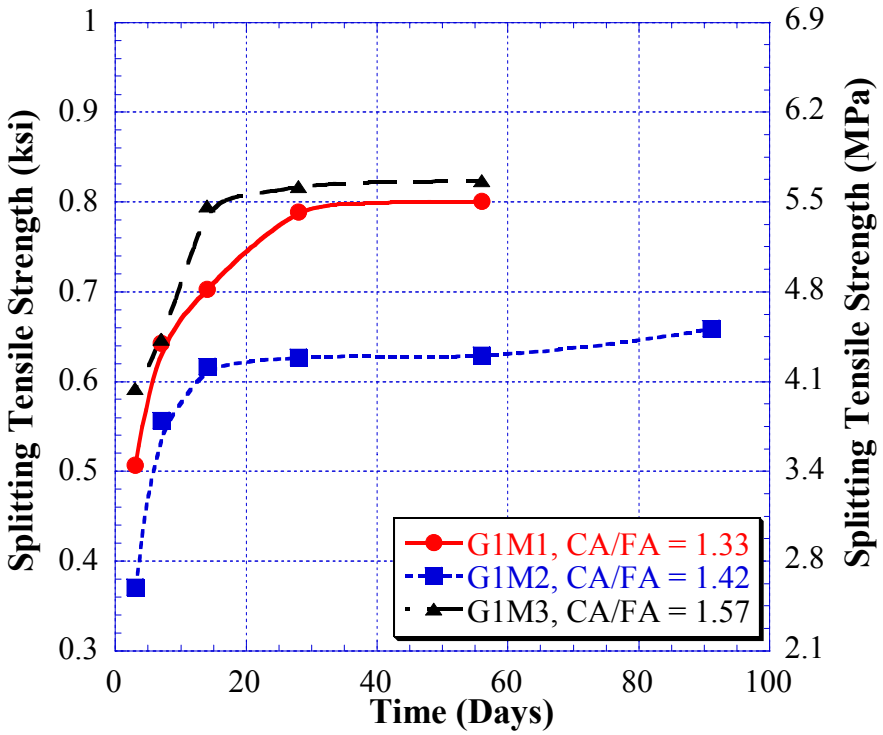

Figure 4.5. Splitting Tensile Strength of Group 1 (40% Slag) Mixes

The effect of coarse aggregate content and CA/FA ratio on the splitting tensile strength of Group 2 Mixes can be seen in Figure 4.6. The lowest values were obtained from mixes G2M1 and G2M2 which had the least amount of coarse aggregate content and the lowest CA/FA ratios. The highest tensile strengths were observed in mixes with the highest coarse aggregate content.

Table 4.7. Splitting Tensile Strength of Group 2 (5% SF and 30% SL) Mixes (ksi)

Day	G2M1	G2M2	G2M3	G2M4	G2M5	G2M6
3	0.453	0.329	0.656	0.521	0.446	0.478
7	0.517	0.405	0.713	0.643	0.473	0.625
14	0.555	0.527	0.766	0.770	0.621	0.691
28	0.574	0.576	0.882	0.770	0.674	0.795
56	0.594	0.598	0.891	0.781	0.731	0.876
91	0.629	0.571	0.901	0.782	0.741	0.872

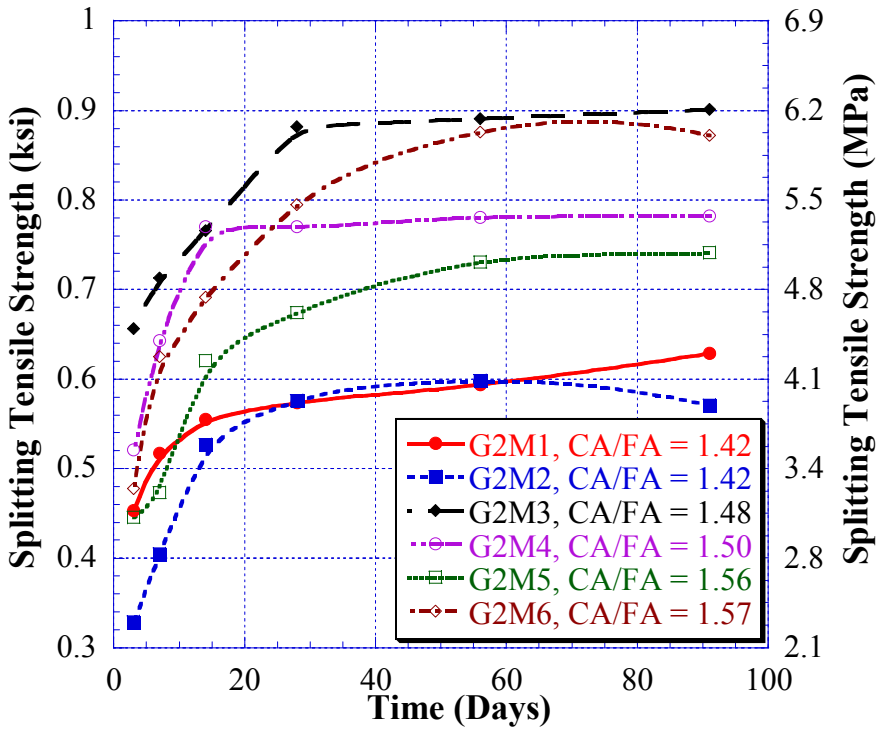

Figure 4.6. Splitting Tensile Strength of Group 2 (5% SF and 30% SL) Mixes

Figure 4.7 illustrates the tensile development of Group 3 mixes with time. Note that G3M1 has decreasing tensile strength after day 28. This is due to the contaminated argillite deposits as mentioned earlier. Test results had tremendous variation and the average of 3 samples was low on 56 and 91 day tests when compared to 28 day results. Although a slight decrease is also noticed in the other mix, the results are within the error tolerations of the ASTM C-496.

Table 4.8. Splitting Tensile Strength of Group 3 (Silica Fume Only) Mixes (ksi)

Day	G3M1	G3M2
3	0.384	0.508
7	0.428	0.686
14	0.553	0.730
28	0.639	0.848
56	0.603	0.838
91	0.534	-

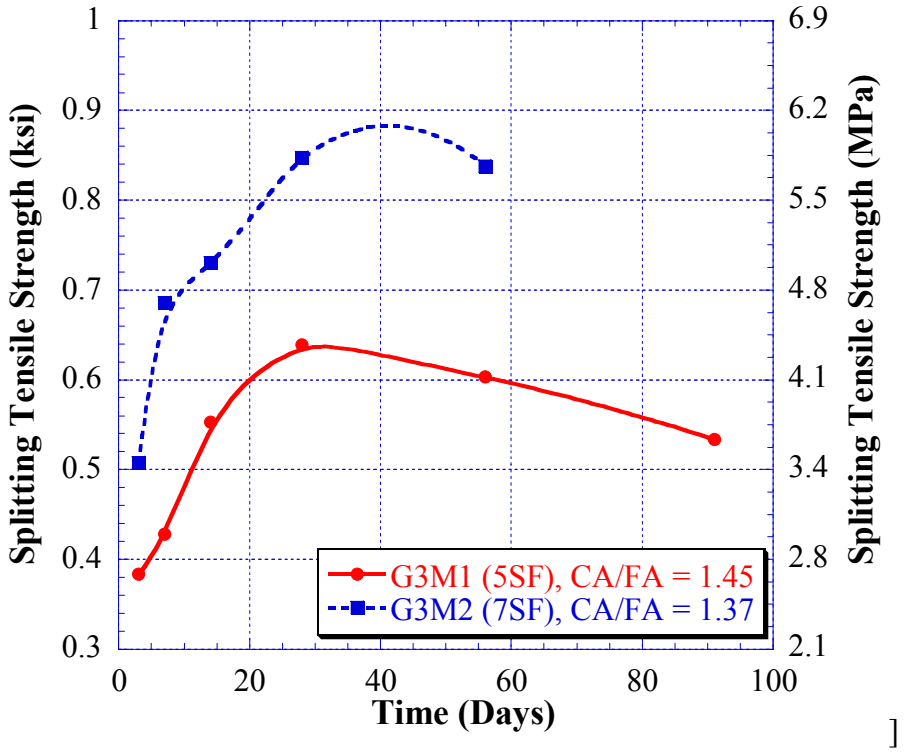

Figure 4.7. Splitting Tensile Strength of Group 3 (Silica Fume Only) Mixes

Figure 4.8 illustrates a similar trend in tensile strength development to the rest of the mixes. The lowest values were observed in mix G4M2 which had the lowest coarse aggregate content and CA/FA ratio. The strength gain of the remaining mixes increased with the increase in CA/FA ratio and the total coarse aggregate content.

Table 4.9. Splitting Tensile Strength of Group 4 Mixes (ksi)

Day	G4M1	G4M2	G4M3	G4M4
3	0.621	0.464	0.678	0.544
7	0.733	0.564	0.749	0.637
14	0.775	-	0.789	0.781
28	0.814	0.617	0.856	0.823
56	0.848	0.657	0.906	0.840
91	0.860	0.670	0.943	0.808

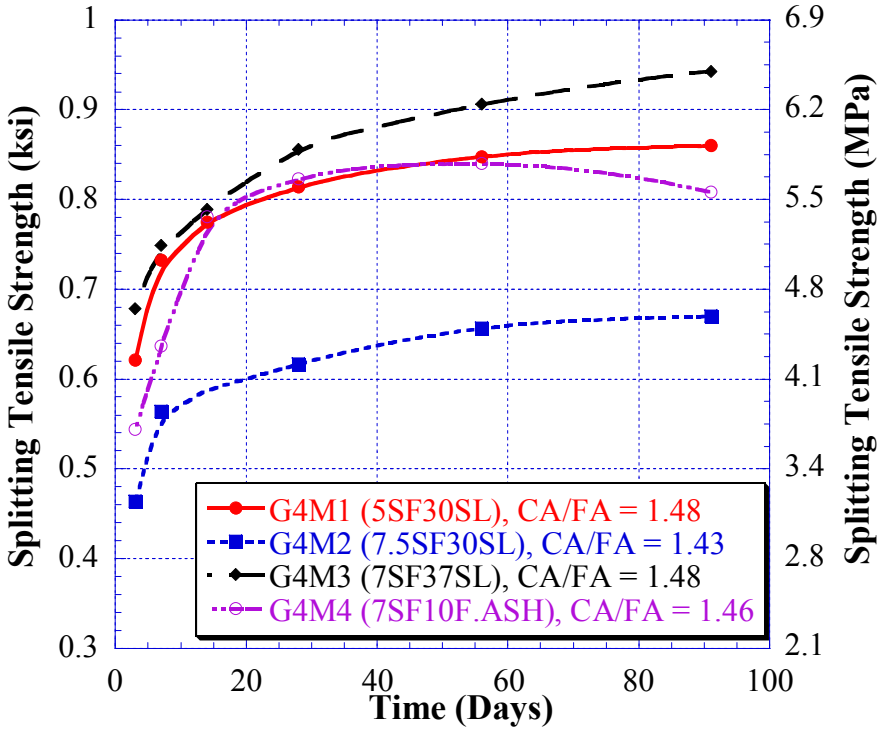

Figure 4.8. Splitting Tensile Strength of Group 4 Mixes

4.3.3 Modulus of Elasticity

All mixes have similar behavior in terms of elastic modulus development. During the first 7 day wet curing period, the elastic modulus is observed to increase rapidly. After the curing period modulus values peak at 14 days, and at later ages the elastic modulus remains constant or in some cases shows a slight decrease. This is due to the curing history of the test specimens. For the first seven days the samples are wet cured and the pore network within the concrete is filled with water. After removal of curing the specimens begin to dry and the water in the pores is replaced by air. As a result the modulus of elasticity does not increase much or even decreases in some cases.

Test results for Group 1 mixes are summarized in Table 4.10 and graphically represented in Figure 4.9. As with all mechanical properties the higher values are obtained in mixes with high coarse aggregate contents or high CA/FA ratios. Also, the increase of elastic modulus with time is not significant. This is most likely due to the reactive nature of slag. Since slag reacts much faster than cement at early age elastic modulus is high for all mixes.

Table 4.10. Modulus of Elasticity of Group 1 (40% Slag) Mixes (ksi)

Day	G1M1	G1M2	G1M3
3	4205	3577	4943
7	5087	3876	5156
14	5083	4052	5317
28	5128	4072	5341
56	5095	3851	5328
91	-	3672	5493

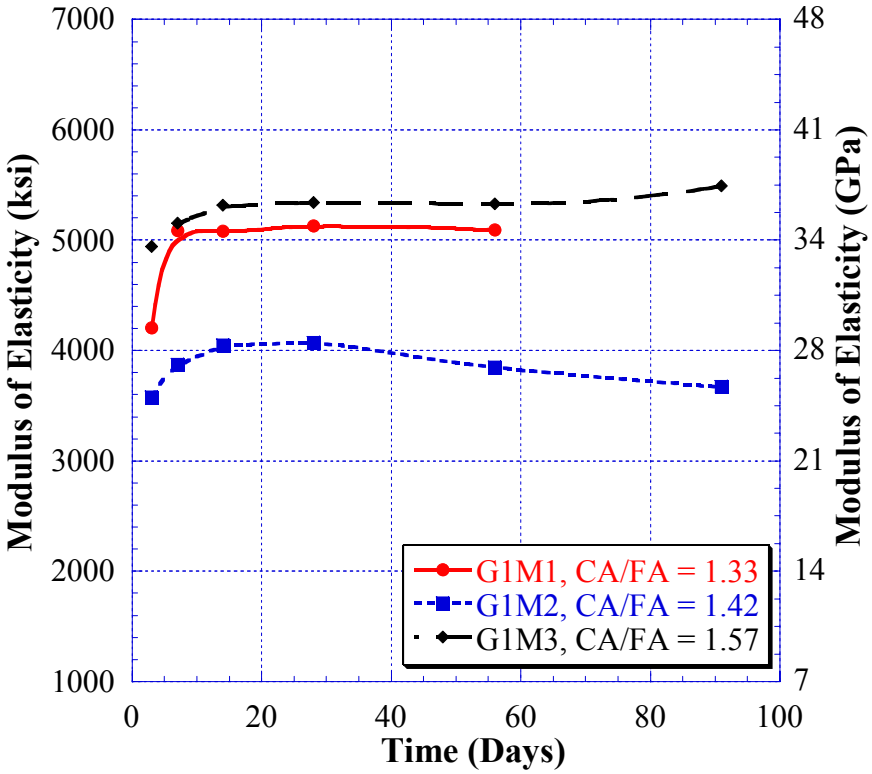

Figure 4.9. Modulus of Elasticity of Group 1 (40% Slag) Mixes

Table 4.11 and Figure 4.10 illustrate the modulus of elasticity of Group 2 mixes. The results are similar to Group 1 results with highest modulus observed in high CA/FA ratio mixes.

Table 4.11. Modulus of Elasticity of Group 2 (5% SF and 30% SL) Mixes (ksi)

Day	G2M1	G2M2	G2M3	G2M4	G2M5	G2M6
3	3501	3389	5522	4829	3800	3739
7	4289	3959	5838	5076	4026	4465
14	4094	3650	5898	5126	4093	4657
28	3991	3493	5820	4829	4181	4552
56	4019	3484	-	4710	4091	4727
91	3823	3344	5773	4387	3890	4600

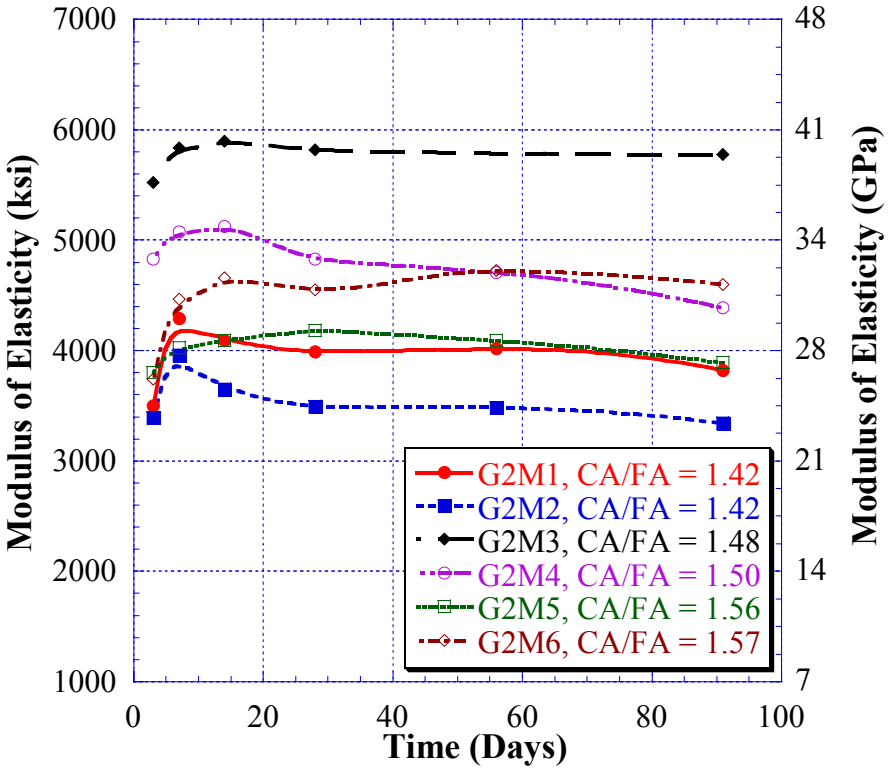

Figure 4.10. Modulus of Elasticity of Group 2 (5% SF and 30% SL) Mixes

Results for Group 3 and Group 4 are illustrated in Table 4.12, Table 4.13, Figure 4.11, and Figure 4.12.

Table 4.12. Modulus of Elasticity of Group 3 (Silica Fume only) Mixes (ksi)

Day	G3M1	G3M2
3	3168	4290
7	3276	4615
14	3376	4563
28	3533	4543
56	3712	4620
91	3416	-

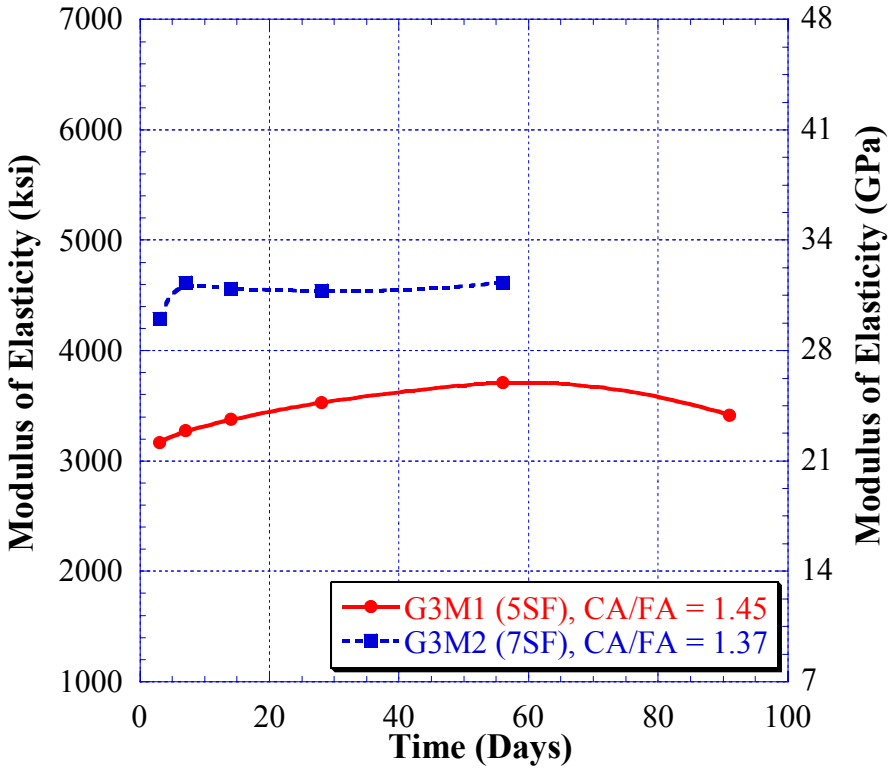

Figure 4.11. Modulus of Elasticity of Group 3 (Silica Fume only) Mixes

Table 4.13. Modulus of Elasticity of Group 4 Mixes (ksi)

Day	G4M1	G4M2	G4M3	G4M4
3	5189	3540	5449	4853
7	5348	4202	5572	5259
14	5463	4260	5578	5655
28	5783	4218	5596	5252
56	5885	-	5655	5278
91	5962	3977	5559	5133

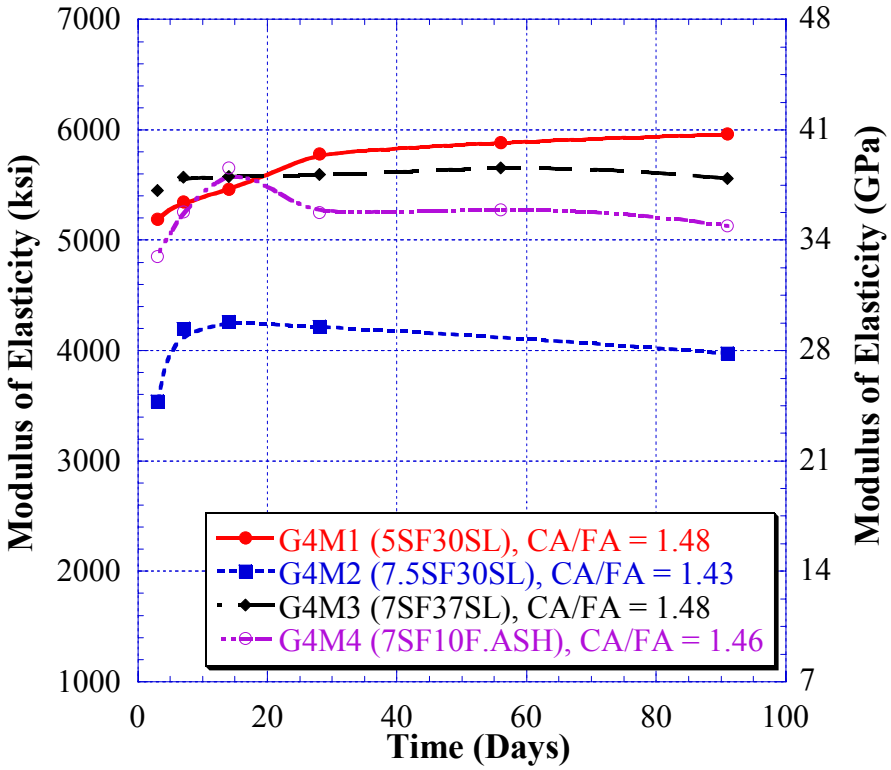

Figure 4.12. Modulus of Elasticity of Group 4 Mixes

4.3.4 Autogeneous Shrinkage

Autogeneous shrinkage is generally not significant if the initial water in a concrete mix design is enough to fully hydrate the cement particles. Therefore, this type of shrinkage is not expected to be significant for w/c ratios of 0.36 or higher. To test this, 3 mixes in Group 2 were tested using the setup in (Figure 3.14). The strains obtained are shown in Figure 4.13 and the temperature profile is illustrated in Figure 4.14. It can be seen that only mix G2M6 has experienced shrinkage, but this value is negligible compared to ultimate shrinkage. Remaining mixes showed expansion during hydration which is an indication that the initial water was enough to fully hydrate the cement particles. This is also supported by the temperature profile within the specimens. Strain values peak when the temperatures peak and later they start decreasing due to decreasing

temperature. It should also be noted that these samples were completely sealed and no curing water was available for the duration of the test. Autogeneous shrinkage is known to decrease or even eliminated in the presence of an outside water source. Since curing was started immediately following casting of specimens, effects of autogeneous shrinkage can be neglected for unrestrained and restrained shrinkage tests.

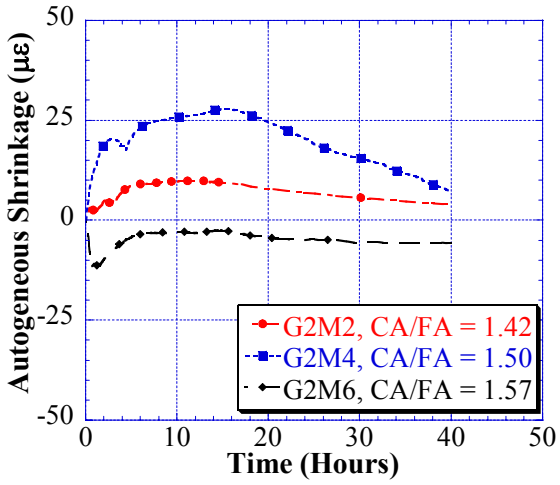

Figure 4.13. Autogeneous Shrinkage of Various Mixes in Group 2

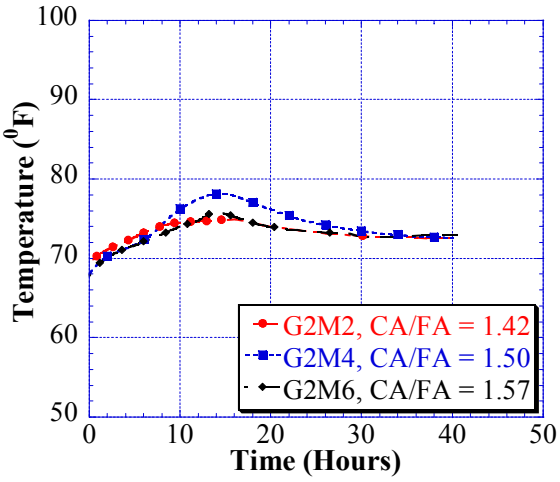

Figure 4.14. Temperature Profile of Autogeneous Shrinkage Specimens

4.3.5 Free Shrinkage

The major factors that were observed to affect shrinkage were cementitious content, percentage of cementitious materials, coarse aggregate content, and CA/FA ratio. Table 4.14 and Figure 4.15 illustrate the free shrinkage test results for Group 1 Mixes. Mix G1M1 and G1M2 were observed to experience the highest shrinkage. This is expected since both mixes have low total coarse aggregate contents. Note also that mix G1M1 has the highest cementitious content of 800lbs/cu.yd. On the other hand, mix G1M3 which

had the highest coarse aggregate content experienced less shrinkage and the shrinkage value at the end of 91 days was lower than 500 microstrains.

Table 4.14. Free Shrinkage of Group 1 (40% Slag) Mixes (με)

Day	G1M1	G1M2	G1M3
7	0	0	0
8	-112	-170	-90
10	-233	-249	-163
14	-323	-374	-237
21	-413	-471	-307
28	-483	-513	-367
42	-557	-577	-408
56	-597	-614	-440
91	-	-663	-477
154	-	-716	-509
187	-	-	-543

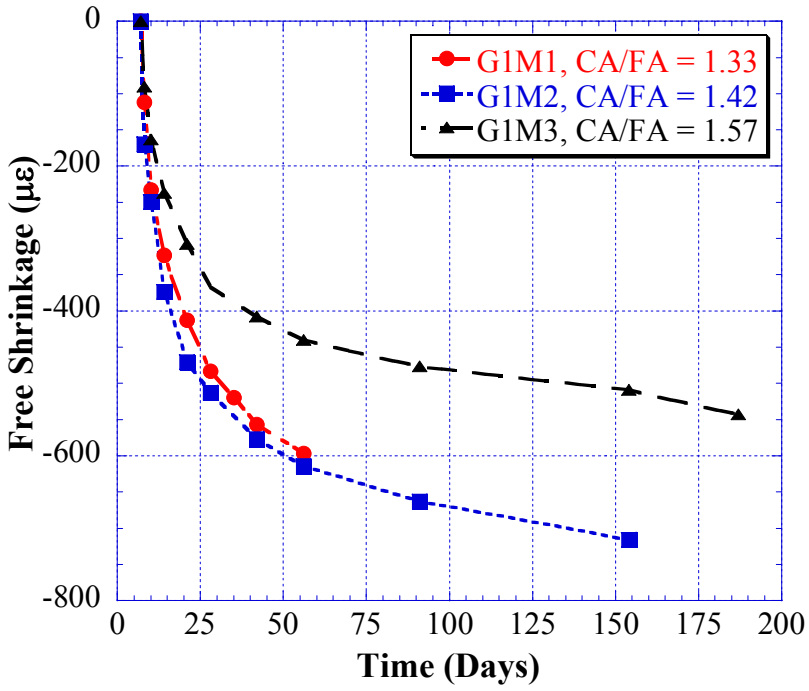

Figure 4.15. Free Shrinkage of Group 1 (40% Slag) Mixes

Table 4.15 and Figure 4.16 illustrate the free shrinkage results from Group 2 mixes. The highest shrinkage was observed in mixes with the lowest CA/FA ratios. The lowest

shrinkage was in mix G2M3 which has the highest aggregate content. Using Type II cement also reduced the free shrinkage considerably (G2M5 and G2M6). All mixes which had high CA/FA ratios and utilized type II cement had less than 500 microstains of shrinkage at the end of 91 days.

Table 4.15. Free Shrinkage of Group 2 (5% SF and 30% SL) Mixes (με)

Day	G2M1	G2M2	G2M3	G2M4	G2M5	G2M6
7	0	0	0	0	0	0
8	-123	-136	-63	-136	-83	-116
10	-216	-240	-129	-230	-156	-196
14	-323	-336	-176	-313	-213	-253
21	-397	-419	-217	-353	-266	-310
28	-493	-470	-250	-386	-306	-346
42	-536	-529	-298	-434	-343	-393
56	-563	-570	-340	-460	-366	-426
91	-605	-633	-360	-506	-406	-463
154	-660	-	-420	-	-	-
187	-660	-	-480	-	-	-

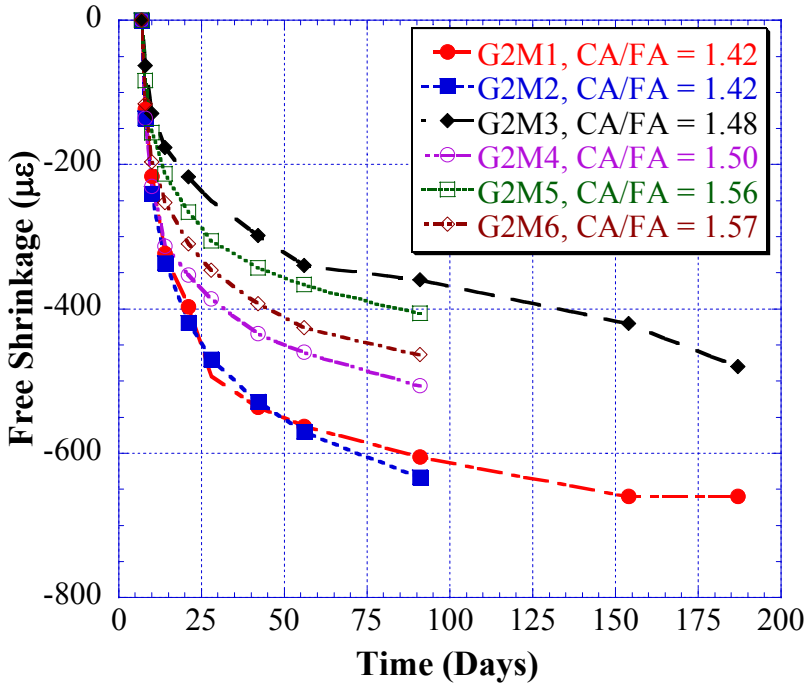

Figure 4.16. Free Shrinkage of Group 2 (5% SF and 30% SL) Mixes

Table 4.16 and Figure 4.17 illustrate the free shrinkage results for Group 3 mixes. Although the CA/FA ratio of G3M2 is lower than G3M1, the total amount of coarse aggregate is slightly higher. Also, G3M2 uses Type II cement. However, as mentioned earlier, the main reason for the difference between the two mixes is the source of the aggregate. G3M1 utilizes aggregates with argillites deposits which are known to have high shrinkage characteristics.

Table 4.16. Free Shrinkage of Group 3 (Silica Fume only) Mixes (με)

Day	G3M1	G3M2
7	0	0
8	-113	-80
10	-217	-147
14	-310	-213
21	-430	-286
28	-490	-323
42	-542	-358
56	-570	-383
91	-610	-426

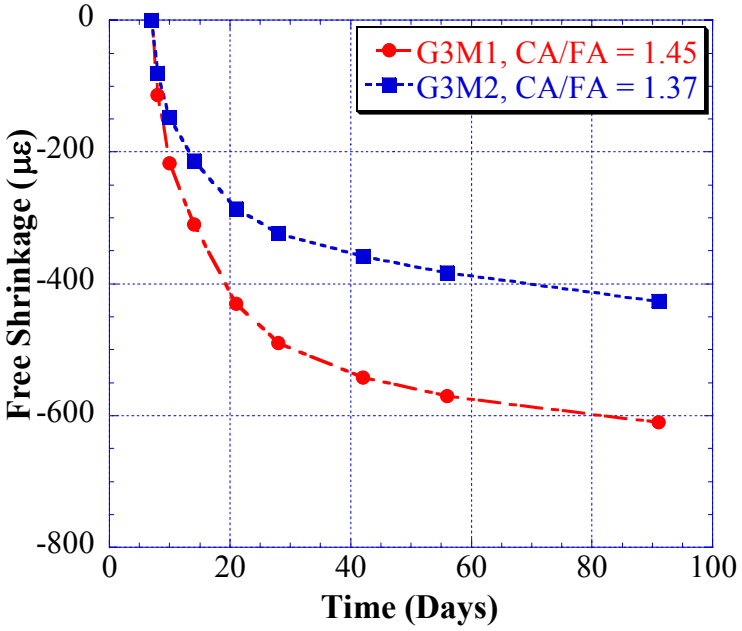

Figure 4.17. Free Shrinkage of Group 3 (Silica Fume only) Mixes

The free shrinkage results for Group 4 mixes are shown in Table 4.17 and Figure 4.18. Highest free shrinkage was observed in mix G4M2 which has the lowest CA/FA ratio and low aggregate content of 1700lbs/cu.yd. Remaining mixes have aggregate contents of 1800 lbs/cu.yd or more and they experienced considerably less free shrinkage.

Table 4.17. Free Shrinkage of Group 4 Mixes (με)

Day	G4M1	G4M2	G4M3	G4M4
7	0	0	0	0
8	-70	-75	-70	-73
10	-130	-174	-130	-120
14	-190	-310	-176	-193
21	-249	366	-220	-246
28	-290	-426	-226	-270
42	-334	-467	-265	-312
56	-365	-506	-303	-336
91	-410	-603	-340	-366
154	-	-663	-399	-
187	-		-426	-

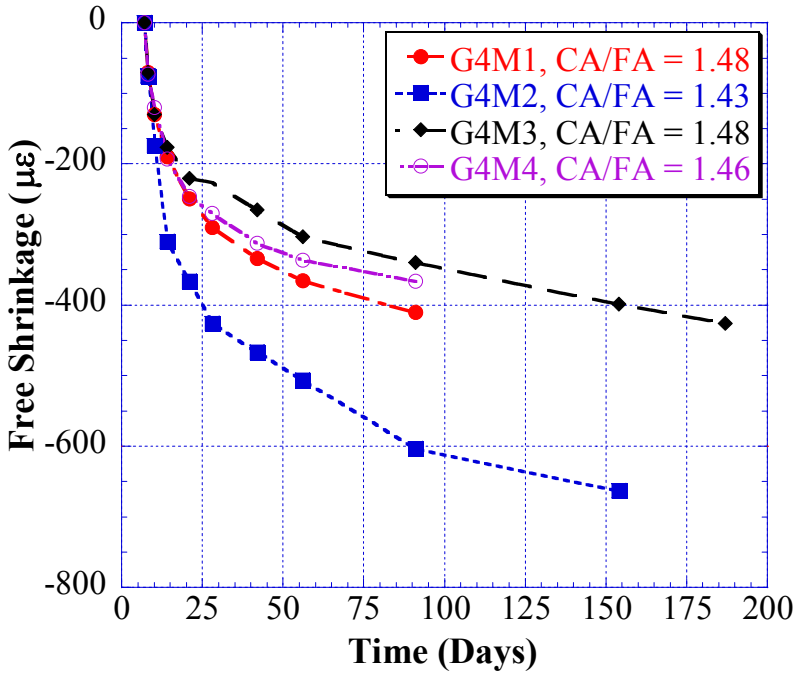

Figure 4.18. Free Shrinkage of Group 4 Mixes

4.4 RESTRAINED SHRINKAGE

Many parameters are investigated to compare the restrained shrinkage performance of the 16 mixes in this study. These parameters are (i) early age behavior, (ii) cracking behavior and patterns, (iii) effect of rate of shrinkage, (iv) effect of mix proportions, and (v) effect of mechanical properties. Moreover, the mixes are ranked based on the measured concrete strains and the days until cracking.

4.4.1 Early Age Behavior

The rings in this study were wet cured 7 days to conform to The NJDOT field curing requirements. Although, in most cases curing eliminates autogeneous shrinkage stresses, it is important to investigate the early age strain profile in the restrained shrinkage test. Figure 4.19 and Figure 4.20 illustrate the steel ring strains for the first 15 days of testing. During approximately the first 10 hours, when the concrete is setting, increasing strains are observed due to the increase in temperature. After 10 hours small amount of compressive strains are observed. This is most probably due to a combination of autogeneous shrinkage and the decrease in temperature. At 24 hours, after the rings are stripped of their molds the burlap is changed and slight expansion is observed in the ring as the concrete starts to absorb the curing water. During the later stages of the seven day wet curing period very minimal compressive strains are observed in the rings (In some cases no compressive strains are observed). This relationship was also observed in the remaining mixes. The highest compressive strain observed in all mixes was less than 10% of the total steel strain observed for the duration of the test. Graphical illustrations of the steel strains for the remaining mixes are provided in Appendix B.

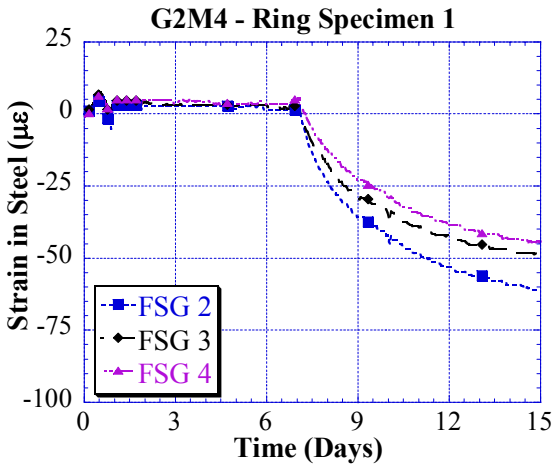

Figure 4.19. Early Age Steel Strains for G2M4 Ring Specimen 1

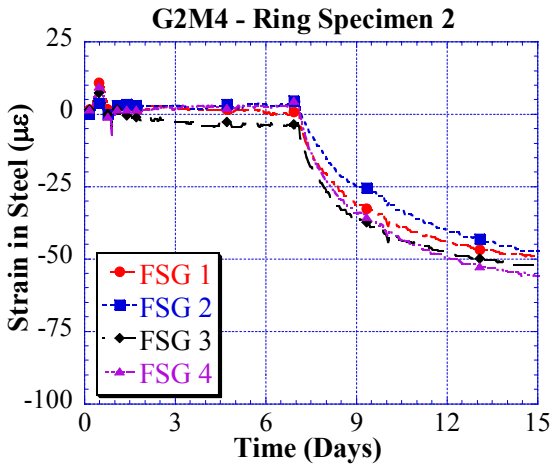

Figure 4.20. Early Age Steel Strains for G2M4 Ring Specimen 2

4.4.2 Cracking Behavior and Patterns

Defining the cracking behavior of the AASHTO PP34 restrained shrinkage test is important since the comparison of mixes is done based on the observed day of cracking from initiation of drying. Researchers have found that the time to cracking in this test setup was long (generally later than 56 days). However, the results obtained from the modified test utilized in this study show that most of the cracking takes place within 56 days of initiation of drying. When cracking takes place the crack initiates on the outer surface (generally close to the top or bottom of the ring) and slowly moves towards the inner steel ring (and towards the middle of the concrete outer surface). In cases where the crack does not reach the steel, no sudden jumps are experienced in the FSGs. If VWSG sensors were not installed those mixes would be considered not cracked and might have mislead the outcome of the tests.

Figure 4.21 and Figure 4.22 illustrate the measured steel strains and concrete strains for mix G3M1, respectively. It is observed that although VWSG sensors picked up the cracking at day 9, it took an additional 8 days for the crack to propagate to the steel ring.

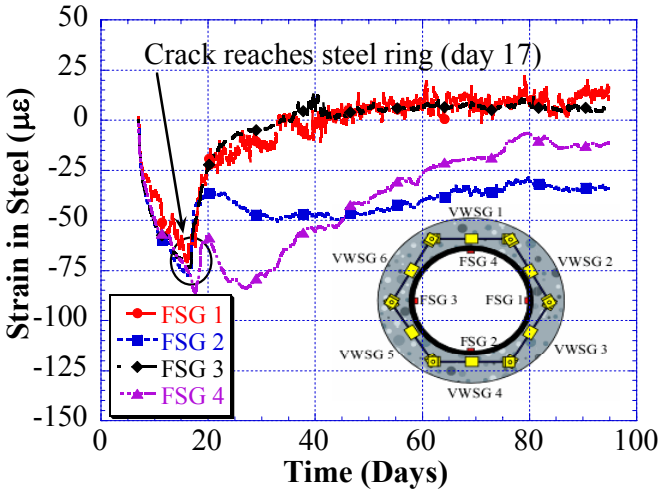

Figure 4.21. Steel Strains for G3M1 Ring Specimen 2

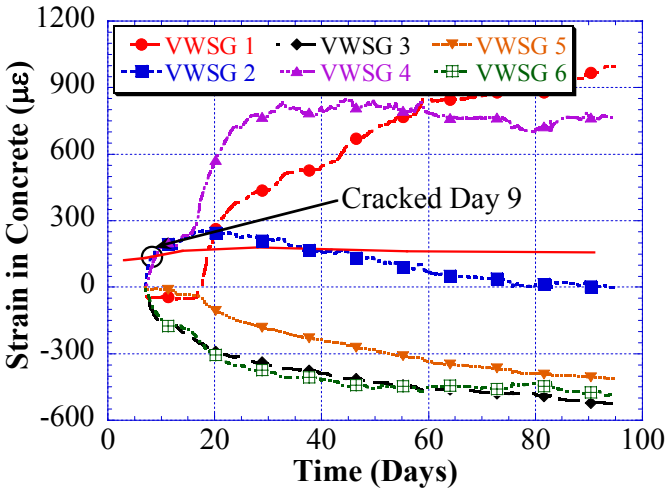

Figure 4.22. Concrete Strains for G3M1 Ring Specimen 2

Out of the 16 mixes considered only one mix experienced cracking that reached the inner steel ring. In the remaining mixes which cracked the cracks penetrated 1.5 to 2

inches towards the steel ring and stopped. The average crack widths for those types of cracks were between 0.01 mm and 0.04 mm. These cracks were located by the help of VWSG sensors which signaled the area of cracking locations. Figure 4.23 and Figure 4.24 illustrate the measured steel and concrete strains for mix G2M4, respectively. It can be seen that cracking was observed on day 16 and the strains in the VWSG sensor 5 continued to increase until day 30. Within this 14 day period the crack was observed to increase in width and also propagate towards the steel. After 30 days the strain rate decreased significantly and the crack stopped propagating and did not reach the steel. This is also evident in the steel strains which do not show any release of strain.

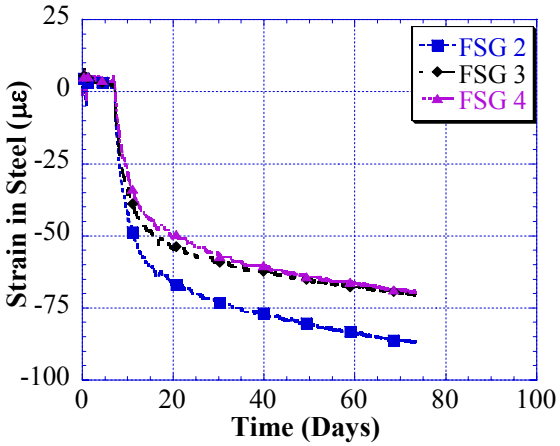

Figure 4.23. Steel Strains for G2M4 Ring Specimen 1

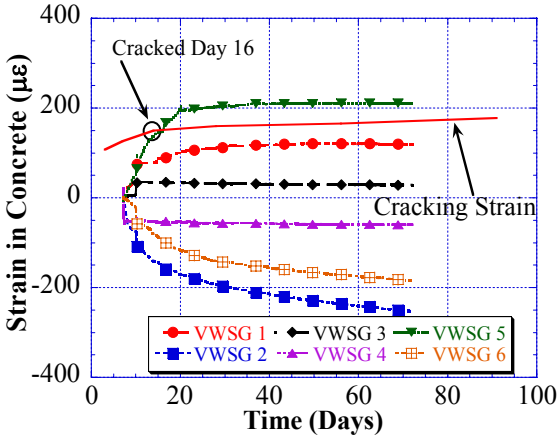

Figure 4.24. Concrete Strains for G2M4 Ring Specimen 1

Table 4.18 shows a summary of results for the restrained shrinkage testing. Cracking day (if the mix cracked) for both rings as well as the CA/FA ratio, total coarse aggregate content, and the total cementitious materials content is summarized in this table. It is observed that, with the exception of two mixes, all mixes which cracked had both rings cracked within 5 days of each other. The two mixes where the results are

inconclusive are currently being repeated to obtain more reliable data. Graphical illustrations of the steel and concrete strains, and crack drawings for these mixes can be found in Appendix A and Appendix B, respectively.

Table 4.18. Comparison of Cracked and Uncracked Mixes with Respect to Coarse Aggregate Content and CA/FA Ratio

Group	MIX	Cracking Day		CA/FA	CA Content (lbs/cu.yd)	Cement Content (lbs/cu.yd)
		Ring 1	Ring 2			
1	G1M1	8	10	1.33	1650	800
	G1M2	13	13	1.42	1700	658
	G1M3	Not Cracked	Not Cracked	1.57	1875	660
2	G2M1	47	44	1.42	1700	658
	G2M2	9	10	1.42	1700	658
	G2M3	Not Cracked	Not Cracked	1.48	1850	657
	G2M4	16	20	1.5	1850	658
	G2M5*	44	Not cracked	1.56	1825	661
	G2M6*	9	Not cracked	1.57	1811	683
3	G3M1	10	9	1.45	1725	735
	G3M2	Not Cracked	Not Cracked	1.37	1750	705
4	G4M1	Not Cracked	Not Cracked	1.48	1850	667
	G4M2	13	11	1.43	1700	658
	G4M3	Not Cracked	Not Cracked	1.48	1850	707
	G4M4	65	60	1.46	1800	690
* One ring specimen cracked only.						

4.4.3 Correlation of Cracking Potential under Restrained Shrinkage Conditions with Free Shrinkage Performance

Although restrained shrinkage is dependant on combination of free shrinkage and other mechanical properties of a given mix, the mechanism involving both are the same. Therefore, the magnitude and rate of free shrinkage could be a good indication of the performance of a concrete mixture in restrained shrinkage.

When restrained shrinkage and free shrinkage tests were analyzed, the strain relationship with time in the AASHTO setup was found to be proportional to the logarithm of time. When observed strains in free and restrained shrinkage were plotted against the logarithm of time, linear relationships were obtained. Using these linear relationships rates of free and restrained shrinkage can be determined. If a mix has cracked within 56-days, the rate at cracking age is used but if the mix did not crack before 56 days, the 56-day rate is used.

To understand the relationship between both rates, each group was analyzed separately, and the free as well as restrained shrinkage rates were compared. Figure 4.25a through Figure 4.25d show results for the free shrinkage strain, average steel strain, free shrinkage rate, and restrained shrinkage rate in Group 1 mixes. Among Group 1 mixes, G1M2 and G1M3 have different amounts of coarse aggregate and CA/FA aggregate ratios while G1M1 has higher cementitious content and lower aggregate content. Figure 4.25b shows that the steel strains are similar but the concrete strains in all mixes, as shown in Figure 4.25d, are different. Figure 4.25d shows that G1M3 used only 37% of its tensile capacity whereas G1M2 cracked at day 13. Also, mix G1M1, with the highest amount of cementitious content and the lowest coarse aggregate content, cracked

at 8 days. This difference is also noticed in their free shrinkage behavior depicted in Figure 4.25c. Moreover, Figure 4.25a shows that the free shrinkage strain of G1M3 is considerably less than that of G1M2 after 150 days due to the high aggregate content of mix G1M3.

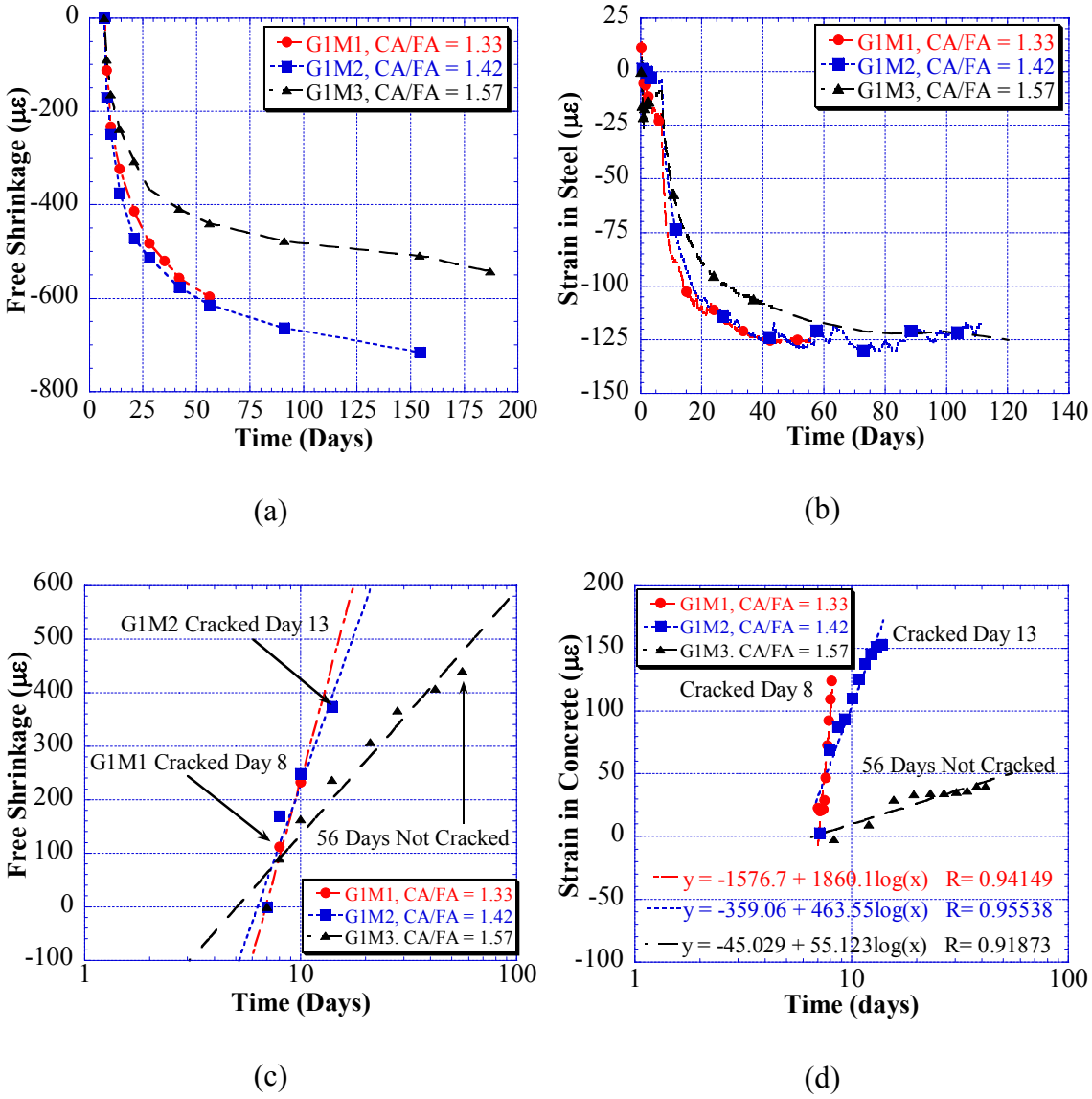

Figure 4.25. Group 1 Mixes Shrinkage Comparisons: a) Free Shrinkage, b) Steel Strains, c) Free Shrinkage Rate, and d) Restrained Shrinkage Rate

Figure 4.26a through Figure 4.26d illustrate the shrinkage comparisons for Group 2 mixes. A similar trend is also observed in Group 1 mixes, where mixes which had high free shrinkage values and rates had also showed high restrained shrinkage strains. Figure 4.26a shows that the two mixes (G2M1 and G2M2) which have the least coarse aggregate content experienced highest free shrinkage.

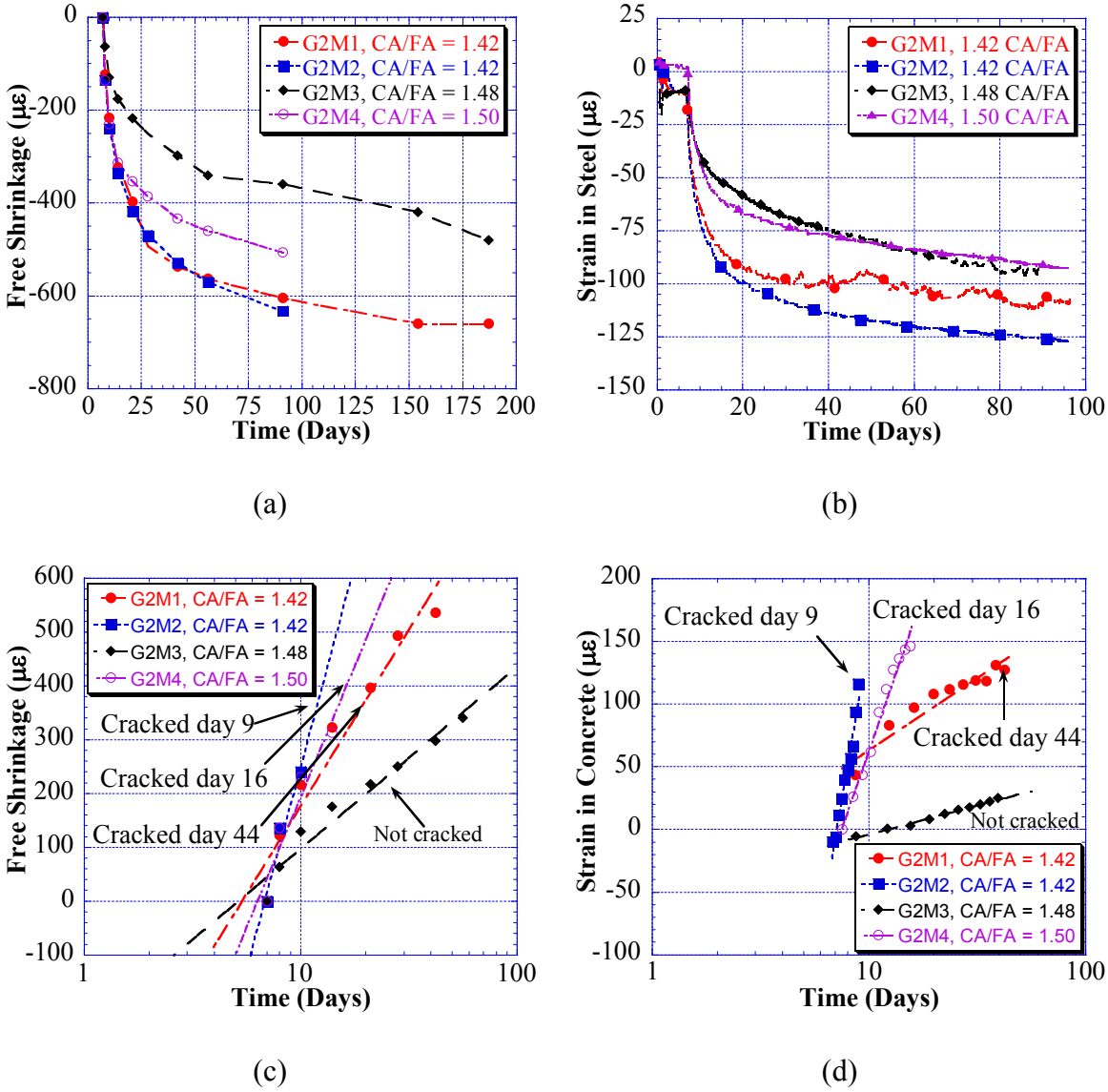

Figure 4.26. Group 2 Mixes Shrinkage Comparisons: a) Free Shrinkage, b) Steel Strains, c) Free Shrinkage Rate, and d) Restrained Shrinkage Rate

On the other hand mix G2M3 which has the highest coarse aggregate content of 1850 lbs/cu.yd has 45% less free shrinkage on day 56. This difference can also be observed in Figure 4.26b. The average measured steel strains for G2M1 and G2M2 are almost identical and higher than the strains observed in mix G2M3. Moreover, Figure 4.26c and Figure 4.26d show that rate of free shrinkage is similar to the rate of restrained shrinkage.

Figure 4.27a through Figure 4.27d illustrate the shrinkage comparisons for Group 3 mixes which are silica fume only mixes. Although silica fume only mixes are not currently allowed in the NJDOT Specifications it is important to test these mixes to verify their performance in terms of restrained shrinkage. The behavior observed in these two mixes is different from all other mixes. One of these reasons is, as mentioned before, the contaminated aggregate source of the G3M1 mix. Although this mix has same coarse aggregate content and higher CA/FA ratio than G3M2 it is observed that the mudstone contamination reduced the capacity of G3M1 considerably. Figure 4.27a shows that the free shrinkage for G3M1 is considerably higher than G3M2. Also, G3M1 was the only mix to experience a full depth crack which reached the inner steel ring. This can be observed in Figure 4.27b which shows a sudden decrease in the strain values signaling a crack has reached the steel, therefore allowing it to release the strain. Lastly, Figure 4.27c and Figure 4.27d illustrate the difference between the free shrinkage and restrained shrinkage rates. G3M2 which has not cracked is observed to have lower rates. However, it should be noted that mix G3M2 has experienced over 150 microstrains at day 91 utilizing more than 80% of its capacity. This is a confirmation that only silica fume mixes with high percentages of silica fume will have high cracking potentials.

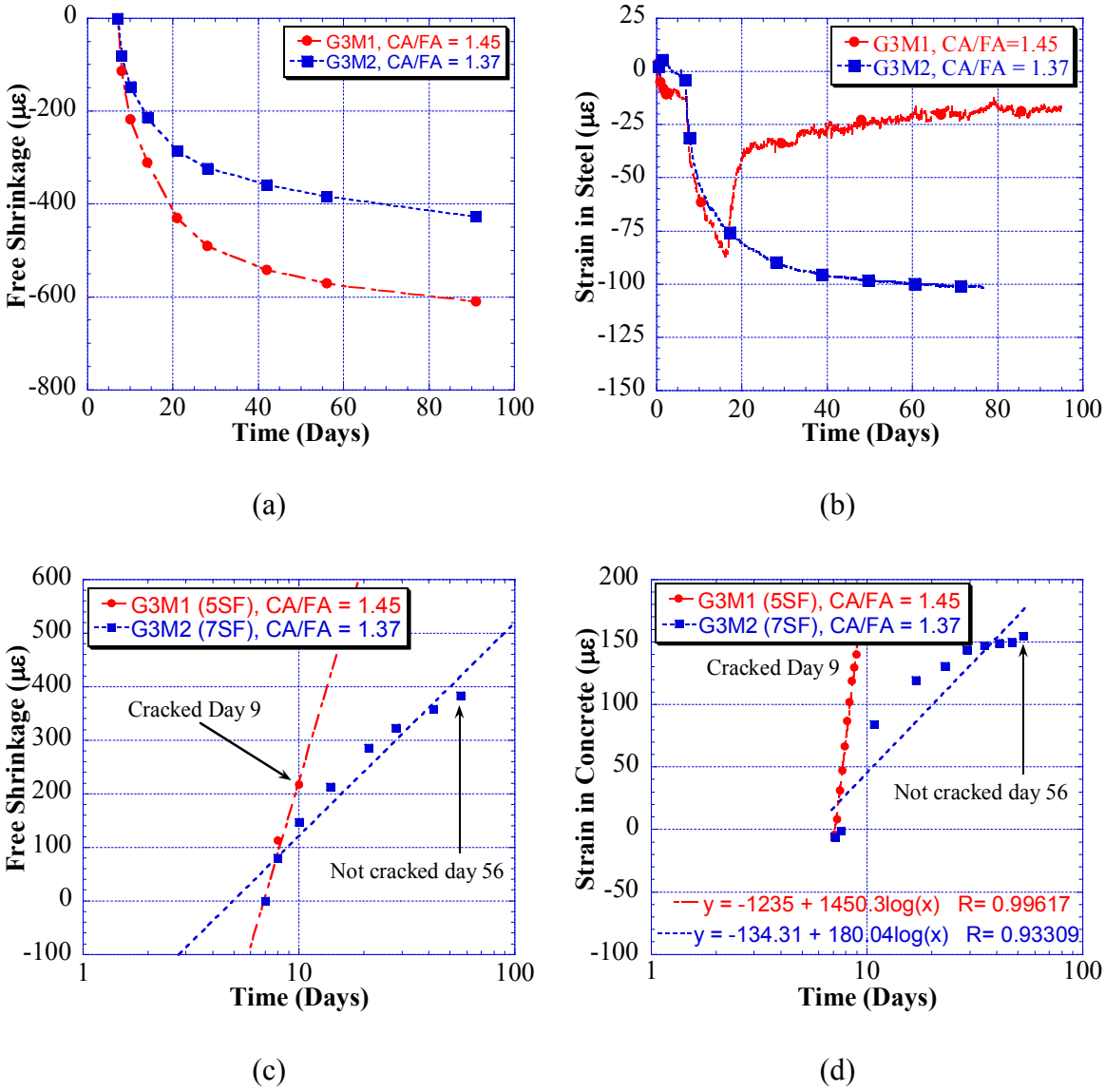

Figure 4.27. Group 3 Mixes Shrinkage Comparisons: a) Free Shrinkage, b) Steel Strains, c) Free Shrinkage Rate, and d) Restrained Shrinkage Rate

Finally, Group 4 mixes also follow the same trend. Figure 4.28c and Figure 4.28d show that the rate of free shrinkage correlates directly with the restrained shrinkage rate. G4M2 mix has the highest rate and it cracked at 11 days. Mix G4M4 has the second highest rate and it cracked at day 60. The remaining two mixes have the lowest restrained shrinkage rates and they did not experience any cracking for the period of

testing. The difference is also notice in free shrinkage values and measured steel strains. Figure 4.28a shows that G4M2 which cracked the earliest has the highest free shrinkage where as the other 3 mixes have considerably less values. Finally, Figure 4.28b shows that mixes G4M1 and G4M3 which did not crack experienced the least strains in the steel.

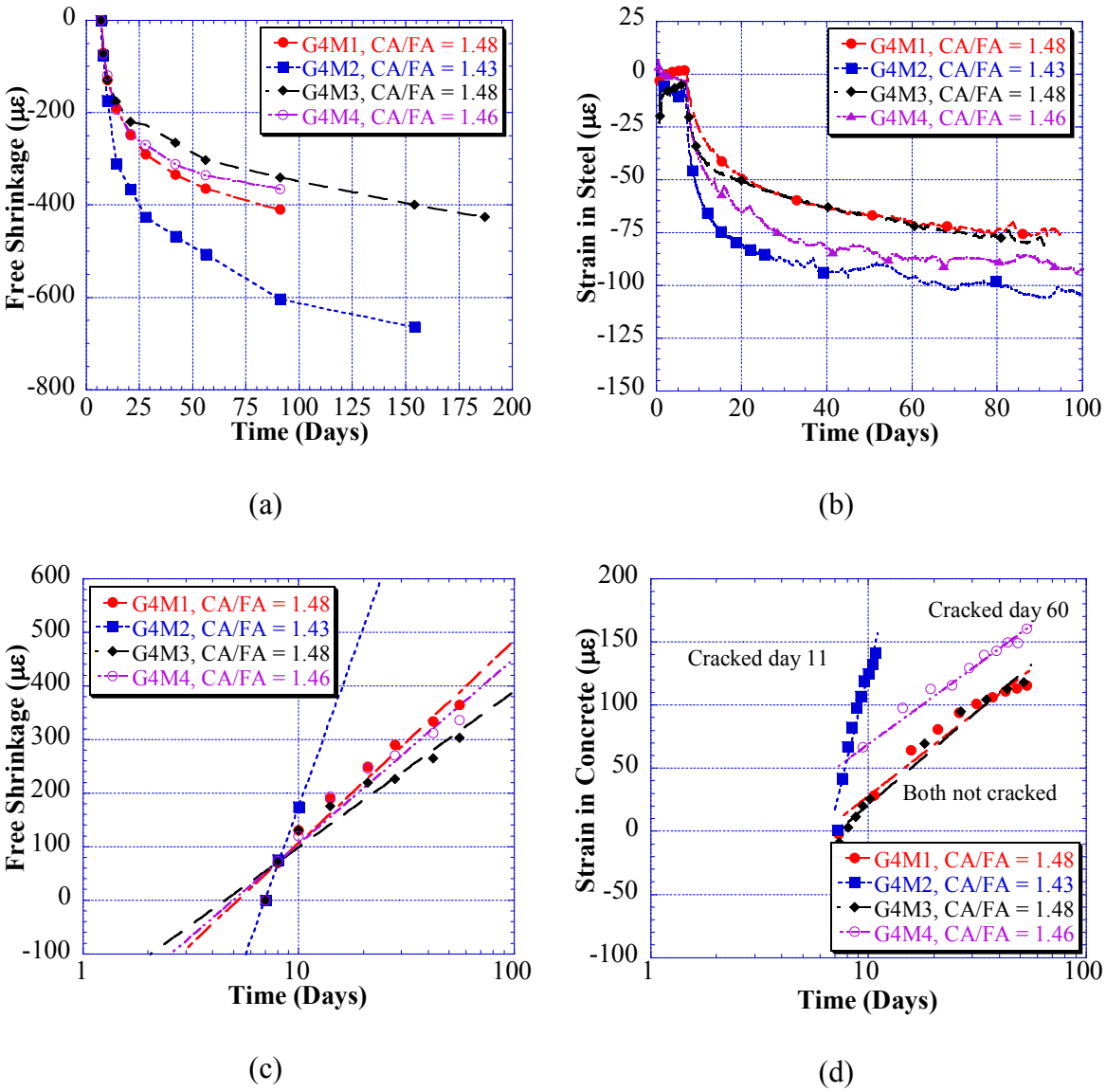

Figure 4.28. Group 4 Mixes Shrinkage Comparisons: a) Free Shrinkage, b) Steel Strains, c) Free Shrinkage Rate, and d) Restrained Shrinkage Rate

As mentioned before, the slope of the free shrinkage versus time and restrained shrinkage strain versus time graphs can be used as a rate of shrinkage to compare the mixes. Figure 4.29 illustrates the correlation of restrained and free shrinkage rates for all mixes. As expected, mixes with low free shrinkage rate have a low restrained shrinkage rate also. It was also observed that 5 mixes (out of 7) with the lowest free shrinkage rates and a measured free shrinkage strain lower than 450 micro-strains (i.e., mixes that are circled in Figure 4.29 and illustrated in Table 4.19) at 56 days did not exhibit any cracking during the testing period. The other two mixes exhibited cracking after all other mixes.

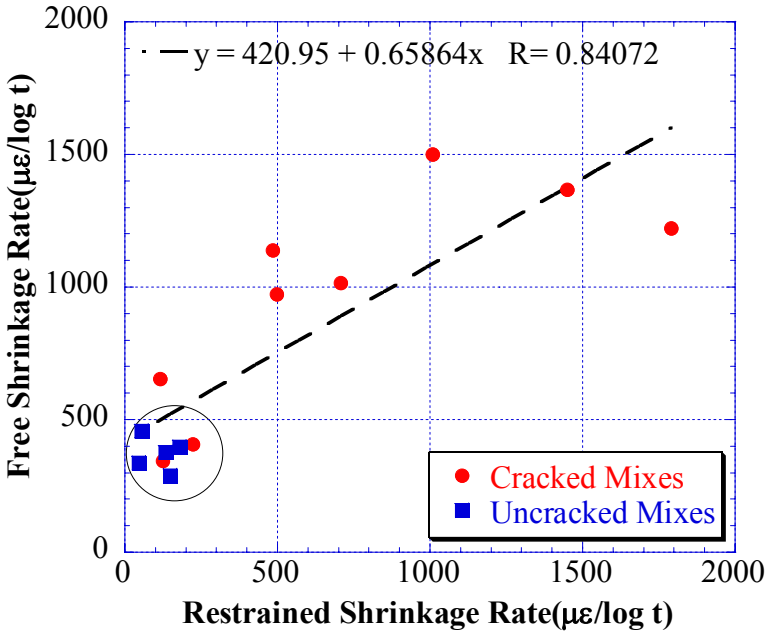

Figure 4.29. Comparison of Free Shrinkage Rate vs. Restrained Shrinkage Rate

Table 4.19. Mixes with Lowest Free and Restrained Shrinkage Rates

	G1M3	G2M3	G3M2	G4M1	G4M3	G4M4
Cracking Day	N/A	N/A	N/A	N/A	N/A	60
56 day Free Shrinkage (με)	-440	-340	-383	-365	-303	-336

A correlation was also made by comparing daily free shrinkage measurements until cracking (or 56 days) with the restrained shrinkage strains measured in the concrete ring. Figure 4.30 and Figure 4.31 illustrate this correlation between free and restrained shrinkages for all mixes (cracked and uncracked), respectively. In both figures, three zones are observed: 1) low slope for uncracked mixes, 2) midrange slope for uncracked mixes as well as mixes that cracked at a later age, and 3) high slope for mixes that cracked at early age. It is observed that uncracked mixes or those mixes that reached less than 60% of their cracking capacity, has a lower slope on the correlation lines. On the other hand, mixes which did not crack but attained more than 60% of their cracking capacity or in mixes which cracked at later ages had mid-range slope. Finally, mixes which cracked shortly after initiation of drying had the highest slopes.

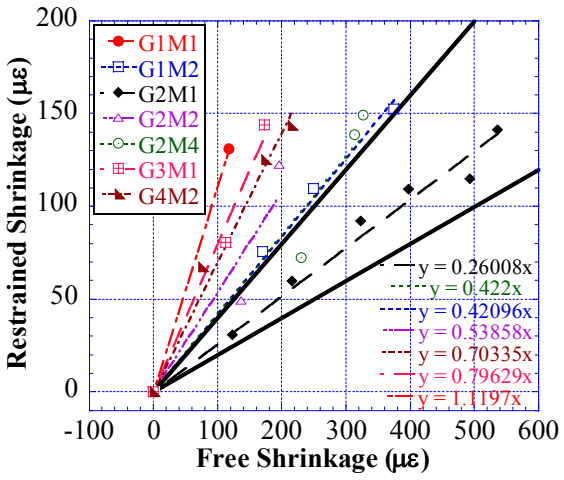

Figure 4.30. Restrained Shrinkage vs. Free Shrinkage for Cracked Mixes

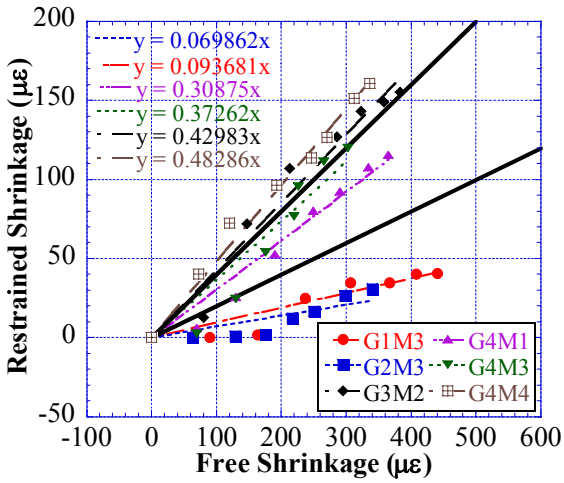

Figure 4.31. Restrained Shrinkage vs. Free Shrinkage for Uncracked Mixes

This suggests that the slope of the correlation functions, denoted as α (the correlation parameter for restrained and free shrinkage), can be used to correlate cracking

with other mechanical properties. As mentioned earlier, three zones were identified for the correlation parameter, α, in the mixes under consideration. A value for α between 0 to 0.2 was observed for mixes that did not crack, 0.2 and 0.4 for mixes which cracked late or which did not crack but had high concrete strains, and 0.4 or above for mixes that cracked shortly after initiation of drying.

Figure 4.32 shows the comparison of average daily free shrinkage rate to the correlation parameter, α. It can be seen that mixes which had a rate of 20 microstrains/day or less had a value for α of 0.4 or less. Two of the mixes which had correlation parameter value of less than 0.2 were observed to use less than 60% of their cracking capacities. This clearly demonstrates that this correlation parameter can be used in conjunction with the average daily free shrinkage rate of a mix in determining the likelihood of a mix to crack.

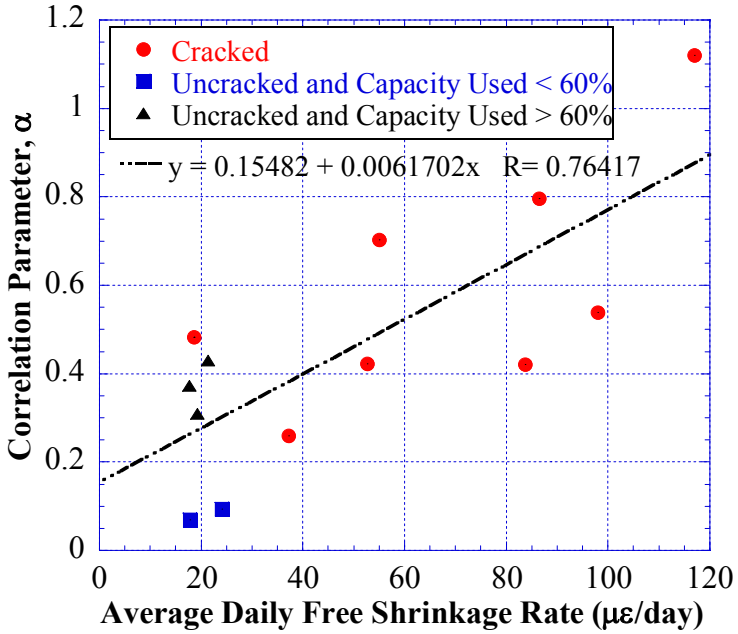

Figure 4.32. Correlation parameter, α, versus Average Daily Free Shrinkage Rate

4.4.4 Correlation of Cracking Potential with respect to Mix Proportions

When the mixes and the involved variables were investigated the only three variables that the effects could be identified were found to be coarse aggregate content, CA/FA ratio, and total cementitious content. It was not possible to investigate the effects of mix proportioning such as w/b ratio, percentage of pozzolanic materials used, chemical admixtures, and type of aggregates due to the limited amount of mixes under consideration.

4.4.4.1 Correlation of Cracking Potential with Aggregate Content and CA/FA Ratio

Table 4.18 shows a comparison between cracked and uncracked mixes to study the effect of coarse aggregate content and CA/FA ratio on cracking behavior. It can be seen that four out of the five uncracked mixes (highlighted in grey) have coarse aggregate content that is more than or equal 1850 lbs/cu.yd. Also, the CA/FA ratio for these four mixes is in the range of 1.48 to 1.57. The majority of the cracked mixes, however, have coarse aggregate contents less than or equal to 1725 lbs/cu.yd, and the CA/FA ratio for those mixes are all below 1.48. It is also observed that mix G1M1, which has the lowest coarse aggregate content, lowest CA/FA ratio, and the highest cementitious content cracked at the earliest time among all mixes. The results from mixes G2M5 and G2M6 are inconclusive since one ring specimen cracked only. Therefore, these mixes were not included in the correlations.

Figure 4.33 and Figure 4.34 show the comparison of the correlation parameter, α, with coarse aggregate content, and CA/FA ratio, respectively. It is clear that increasing the coarse aggregate content and the CA/FA ratio reduces the value of the correlation

parameter. It can be seen that the two mixes with the best performance had a total coarse aggregate amount of more than or equal to1850 lbs/cu.yd.

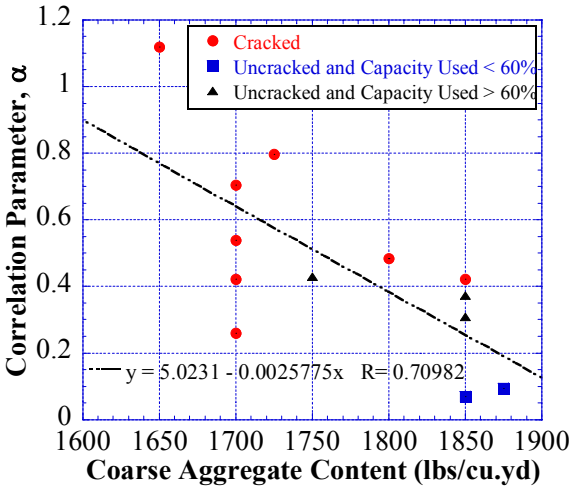

Figure 4.33. Comparison of Correlation Parameter, α, with Coarse Aggregate Content

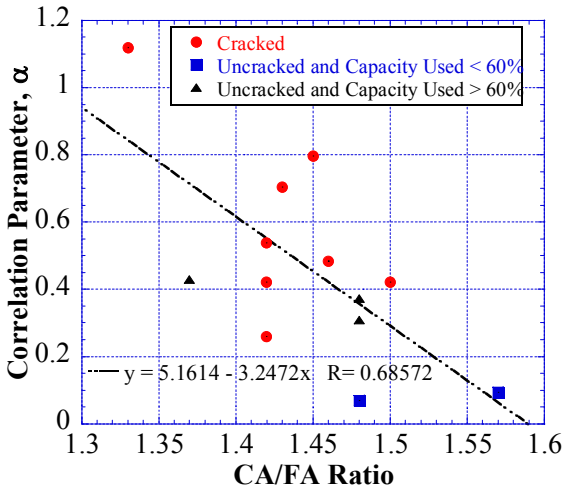

Figure 4.34. Comparison of Correlation Parameter, α, with CA/FA Ratio

Table 4.20 illustrates the percentages of cracked and uncracked mixes with respect to the amount of coarse aggregate used in their design and the CA/FA ratios. Seven out of the eight cracked mixes have CA/FA ratios lower than 1.48. Also, six of these mixes have less than 1725 lbs/cu.yd of coarse aggregate content in their design. The results are also numerically presented in Figure 4.35. By comparing these results it can concluded that the majority of the mixes that cracked have low aggregate content and the majority of the mixes that did not crack have high coarse aggregate contents.

Table 4.20. Percentage of Cracked or Uncracked Mixes with respect to Coarse Aggregate Content and CA/FA Ratio

	Number of Mixes	CA/FA Ratio	CA Content
Total Uncracked	5	80% equal to or greater than 1.48	80% equal to or higher than 1850 lbs/cu.yd
Total Cracked	8	88% less than 1.48	75% Less than 1725 lbs/cu.yd

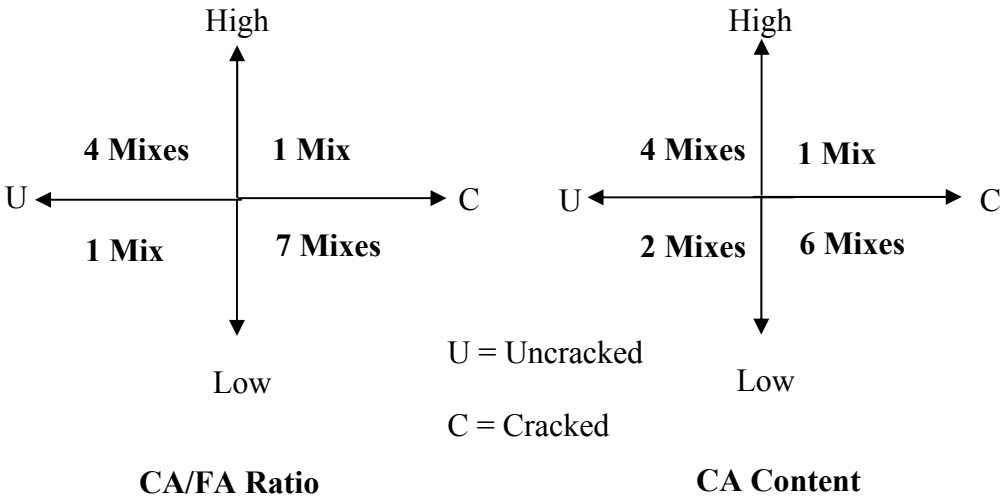

Figure 4.35. Number of Cracked or Uncracked Mixes with Respect to Coarse Aggregate Content and CA/FA Ratio

Another approach to compare the effect of coarse aggregate content and CA/FA ratio is to take mixes with similar compositions with only coarse aggregate content (therefore the CA/FA ratio) varying and comparing their shrinkage performances. Figure Figure 4.25a through Figure 4.25d in section 4.4.3 illustrate the shrinkage comparisons of Group 1 mixes. Mix G1M2 and G1M3 have same proportions except for their total coarse aggregate contents. Mix G1M3 having a higher coarse aggregate content is observed to experience less free shrinkage at the end of 91 days. Moreover, shrinkage

rates for G1M3 are considerably less than the rates observed in mix G1M2. It is also observed that mix G1M3 did not experience any cracking for the duration of testing but G1M2 cracked on day 13. All of these differences can be attributed to the coarse aggregate content since it is the only variable that is different for these two mixes.

Another example can be given from Group 2 mixes. If G2M2 and G2M4 are analyzed, their difference is in the coarse and fine aggregate amounts used. Mix G2M4 has a CA/FA ratio of 1.50 with a high coarse and fine aggregate content (1850 lbs/cu.yd coarse aggregate and 1230 lbs/cu.yd sand). On the other hand, mix G2M2 has a slightly lower CA/FA ratio of 1.42 (1700 lbs/cu.yd coarse aggregate and 1190 lbs/cu/yd sand). Figure 4.36 through Figure 4.39 illustrate the difference in shrinkage behavior of these mixes. As before, the mix with the higher CA/FA ratio experiences less free shrinkage and both free and restrained shrinkage rates are lower. Although both mixes cracked, the mix with the higher CA/FA ratio cracked 7 days later than the other mix.

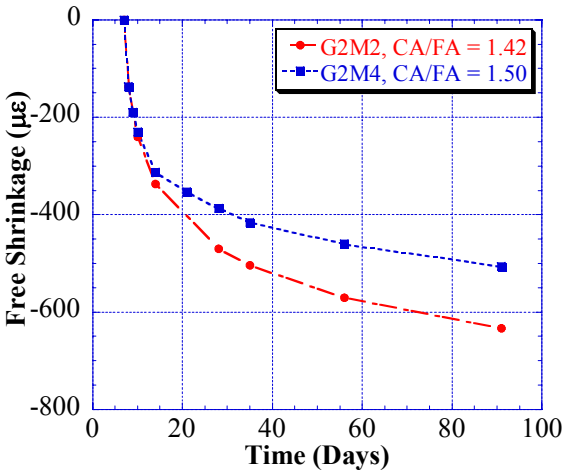

Figure 4.36. Comparison of Free Shrinkage Rate for G2M2 and G2M4

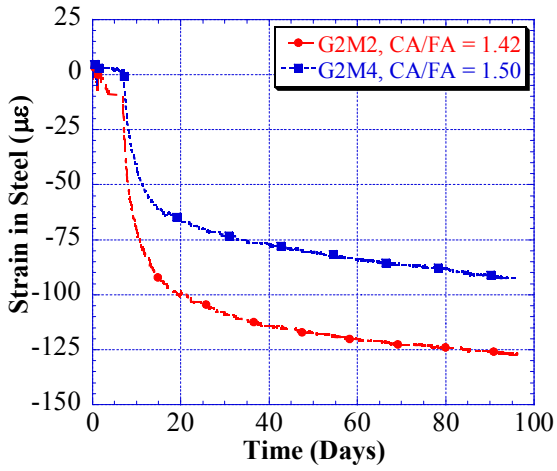

Figure 4.37. Steel Strain Comparison of G2M2 and G2M4

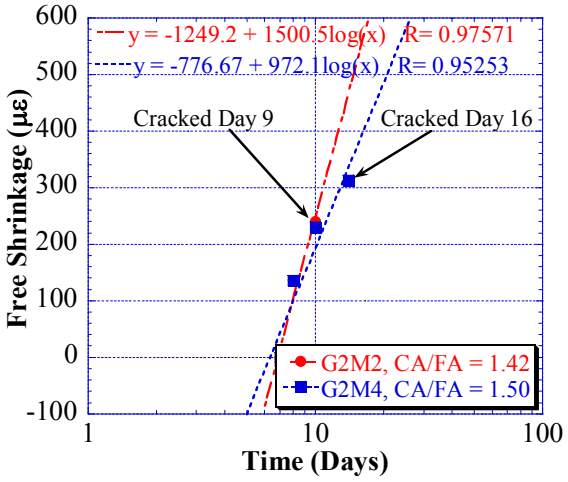

Figure 4.38. Comparison of Free Shrinkage Rate for G2M2 and G2M4

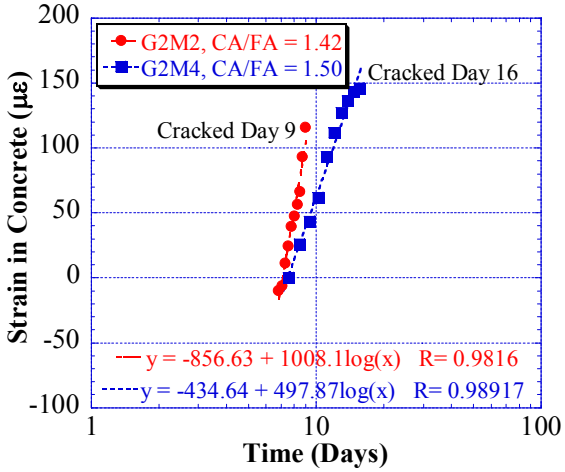

Figure 4.39. Comparison of Restrained Shrinkage Rate for G2M2 and G2M4

4.4.4.2 Correlation of Cracking Potential with Total Cementitious Content

Figure 4.40 illustrates the effect of total cementitious content on cracking performance. It can be seen that increasing the amount of total cementitious content will increase the value of the correlation parameter, α, suggesting a higher cracking potential. Except for one mix (G1M1) all mixes in this study have very similar cementitious contents (650 – 735 lbs/cu.yd). Concrete mixes with high cement contents are expected to experience higher shrinkage, and this was observed in mix G1M1 which cracked earliest among all mixes. For the remaining mixes shrinkage rate is affected by a combination of cement content, CA/FA ratio, w/c ratio, coarse aggregate content, and mechanical properties of concrete such as modulus of elasticity, and strength. This dependency is clear when shrinkage rates of mixes with 658 lbs/cu.yd cement content are analyzed. Although all of the mixes have the same cementitious content, the shrinkage rates vary tremendously de to the number of variables involved in their mix proportions.

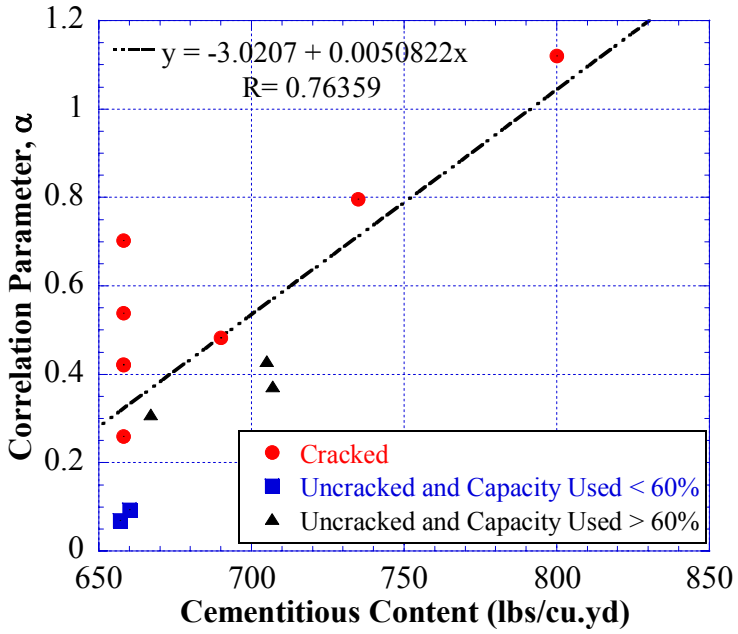

Figure 4.40. Comparison of Correlation Parameter, α, with Total Cementitious Content

4.4.5 Correlation of Cracking Potential with Mechanical Properties

Mechanical properties of concrete that is important in terms of affecting the cracking age is the tensile strength and elastic modulus. Higher tensile strength would provide more resistance to cracking by allowing concrete to sustain more load before cracking. Modulus of elasticity on the other hand can increase or decrease the cracking strain of a mix depending on its magnitude. The higher the elastic modulus the lower the cracking strain limit will be, and the sooner this limit will be reached by a given strain rate. When the relationship between tensile strength and elastic modulus was investigated, it was seen that the rate of increase in tensile strength was identical to rate of increase in elastic modulus. This provided more or less very similar cracking strains for all of the mixes. Therefore, the governing factor in cracking under restrained shrinkage was the rate at which these different mixes were shrinking. This is supported

by Figure 4.41 and Figure 4.42 where the relationship of modulus of elasticity and tensile strength with restrained shrinkage rate is shown to be identical. The relationship of these mechanical properties with the free shrinkage rate was also investigated. As shown in Figure 4.43 and Figure 4.44, this relationship is stronger for free shrinkage rate.

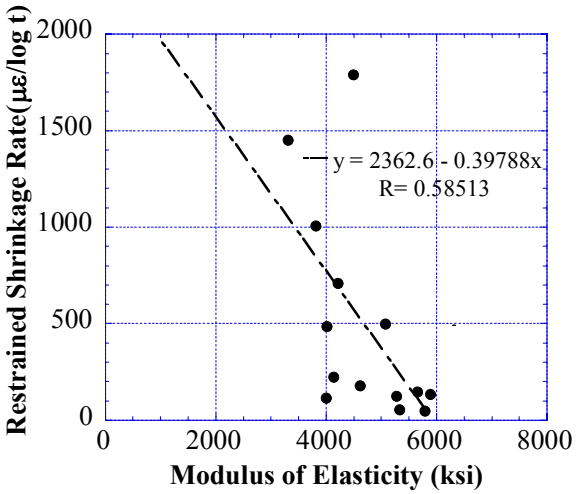

Figure 4.41. Restrained Shrinkage Rate versus Modulus of Elasticity

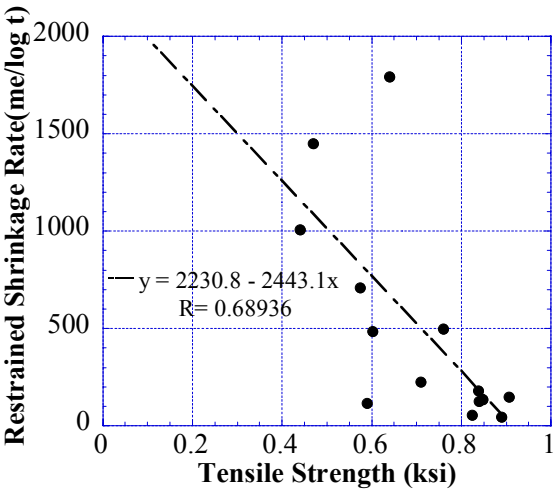

Figure 4.42. Restrained Shrinkage Rate versus Tensile Strength

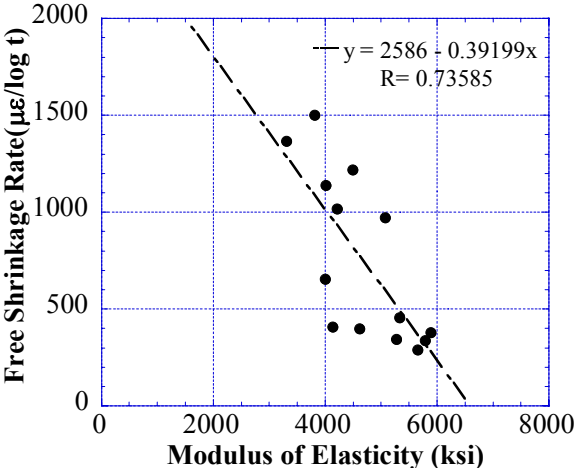

Figure 4.43. Free Shrinkage Rate versus Modulus of Elasticity

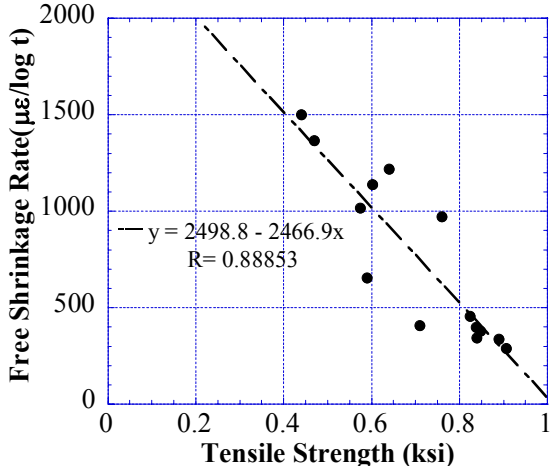

Figure 4.44. Free Shrinkage Rate versus Tensile Strength

4.4.6 Ranking of Mixes Based on Measured Concrete Strains

The results of the restrained shrinkage test can be used to comparatively rank mixes in terms of restrained shrinkage performance. Table 4.21 illustrates the ranking of the 15 mixes according to the measured concrete strains. If the mixes cracked before the end of testing the ranking is done by comparing the time to cracking from the time of pour. However, it should be noted that the ranking presented does not mean that the first and best mix in the list would not crack in field applications. Cracking in a real world applications depend on many factors like construction practices, the level of restraint in the structure, loads and etc. The list presented only compares the relative performance of the mixes in this study.

Table 4.21. Comparison of Restrained Shrinkage Performance Based on Measured Concrete Strains

		% of Cracking Strength			Cracking Day		
Mix Name	**Designation**	**Ring 1**	**Ring 2**	**Average**	**Ring 1**	**Ring 2**	**Average**
R200578S	G1M3	37%	NA	37%	NC	NC	NC
R309497	G2M3	58%	30%	44%	NC	NC	NC
R308278	G3M2	83%	68%	76%	NC	NC	NC
R309496	G4M3	86%	NA	86%	NC	NC	NC
R309495	G4M1	94%	NA	94%	NC	NC	NC
R408694	G4M4	100%	100%	100%	60	65	62.5
R408850	G2M1	100%	100%	100%	44	47	45.5
R310682	G2M4	100%	100%	100%	16	20	18
R408847	G1M2	100%	100%	100%	13	13	13
R408844	G4M2	100%	100%	100%	11	13	12
R409239	G2M2	100%	100%	100%	9	10	9.5
R308163	G3M1	100%	100%	100%	9	10	9.5
R311266	G1M1	100%	100%	100%	8	10	9

CHAPTER V

SUMMARY AND CONCLUSIONS

5.1 SUMMARY AND CONCLUSIONS

The primary purpose of this study is to define and compare the cracking potential of common HPC mixes used in bridge decks by New Jersey Department of Transportation (NJDOT). A total of 16 mix designs were obtained and mixed in the laboratory using same sources of materials. Four ASTM standard tests were performed to determine the mechanical properties of each mix. Modified AASHTO PP-34 restrained shrinkage test was used to compare the performances of each mix. The parameters investigated includes: (1) coarse aggregate content, (2) CA/FA ratio, (3) total cementitious content, and (4) rates of free and restrained shrinkage.

The following conclusions can be made from the results:

1) The modified method presented in this paper can be used to detect concrete cracking age as well as the cracking stresses.
2) The setup in AASHTO-PP34 method was found to be insufficient to detect cracking in the rings due to the cracking behavior observed.
3) Results show that the coarse aggregate content as well as the CA/FA ratio has the greatest effect on both free and restrained shrinkage. Mixes having high CA/FA ratios and relatively high coarse aggregate contents (e.g., 1800 lbs/cy)

experienced a significant reduction in free shrinkage compared to similar mixes with lower ratios and total coarse aggregate content. Also, all mixes that did not exhibit any cracking in the restrained shrinkage test had coarse aggregate contents of 1850 lbs/cu.yd or more which the CA/FA ratio was equal to or higher than 1.48.

4) As expected, the total cementitious content of a mix was also found to have a direct effect on shrinkage performance. Mixes with higher cementitious contents were observed to crack earlier than similar mixes having less cementitious materials. Therefore, it is suggested that the total cementitious materials amount in concrete deck mixes should not exceed 700lbs/cu.yd.
5) The potential of cracking in a HPC mix under restrained conditions can be reduced by increasing the coarse aggregate content (preferably higher than 1800 lbs/cu.yd) to give a high CA/FA ratio. This would help in reducing the ultimate shrinkage and also would reduce the rate at which shrinkage occurs.
6) Mixes that experienced more than 450 microstrains in free shrinkage at 56 days are not recommended, since all such mixes cracked under restrained ring test shortly after initiation of drying. In contrast, mixes that experienced less than 450 microstrains in free shrinkage at 56 days did not exhibit any cracking. It is recommended that a limit on the free shrinkage test of 450 microstrains be specified in order to indirectly control cracking under restrained conditions.

5.2 SCOPE FOR FUTURE RESEARCH

Future research is needed to investigate the effects of w/b ratio, percentage of cementitious materials, and cement type on restrained shrinkage performance of HPC

mixes. A parametric study to identify these effects would contribute in attaining mixes that are less likely to crack under restrained conditions. Using the experimental setup described in this study, the AASHTO test could be studied in more detail to make it more reliable in terms of detecting cracking of the mixes.

REFERENCES

1. Portland Cement Association, “Design and Control of Concrete Mixtures”, pp. 257 - 273
2. Annual Book of ASTM Standard, Volume 04.02, Concrete and Aggregate, 2006
3. P. –C. Aitcin, “The Art and Science of High-Performance Concrete”, Industria Italiana del Cemento, v 68, n 4, April, 1998, pp. 350-365
4. Holt, Erika E., “Early Autogenous Shrinkage of Concrete”, Vtt Publication 446, Technical Research Center of Finland, Espoo, 2001, 194 pages
5. ACI Committee 224, “Control of Cracking in Concrete Structures”, ACI 224R-01, 2001, 43 pages.
6. ACI Committee 224. “Causes, Evaluation, and Repair of Cracks in Concrete Structures”, ACI 224.1R-93, reapproved 1998, 22 pages
7. Hansen, Almudaiheem, “Ultimate Drying Shrinkage of Concrete – Influence of Major Parameters”, ACI Materials Journal, Vol. 84, pages 217-222, 1987
8. Picket, G., “Effect of Aggregate on Concrete Shrinkage and Hypothesis Concerning Shrinkage”, Journal of the American Concrete Institute, Vol. 27, No. 5, 1956, pp. 581-590
9. Krauss P., E. A. Rogalla, “Transverse Cracking in Newly Constructed Bridge Decks”, NCHRP Report 380, 1996
10. Chariton, T. and Weiss, W. J., “Using Acoustic Emission to Monitor Damage Development in Mortars Restrained from Volumetric Changes”, Concrete: Material Science to Application, A Tribute to Surendra P. Shah, ACI SP-206, 2002, pp. 205-218.
11. Paillere, A. M., Buil, M., Serrano, J. J., “Effect of Fibre Addition on the Autogeneous Shrinkage of Silica Fume Concrete”, ACI Materials Journal, Vol. 86 No. 2, March-April 1989, pp. 139-144
12. McDonald, J.E., “The Potential for Cracking of Silica-Fume Concrete.”, Concrete Construction, 1992
13. Gebler, S. H., Klieger, P., “Effect of Fly Ash on Physical Properties of Concrete,” ACI, SP-91, 1986, pp. 1 – 50.
14. Nasser, K. W., and Al-Manaseer, A. A., “Shrinkage and Creep of Concrete Containing 50 Percent Lignite Fly Ash at Different Stress-Strength Ratios,” ACI, SP-91, 1986, pp. 433 – 448.
15. Mladenka Saric-Coric, Pierre-Claude Aitcin, “Influence of Curing Conditions on Shrinkage of Blended Cements Containing Various Amounts of Slag”, ACI Materials Journal, Vol. 100, December-2003, pp. 477-483

16. Frank Collins, J.G. Sanjayan, “Cement and Concrete Research”, Vol. 30, 2000, pp. 791-798

17. Bisonnette B., J. Marchand, C. Martel, M. Pigeon, “Influence of Superplasticizer on the Volume Stability of Hydrating Cement Pastes at an Early Age”, Concrete: Material Science to Application, A Tribute to Surendra P. Shah, ACI SP-206, 2002, pp. 167-176

18. Neville, A. M., Properties of Concrete, Fourth Edition, 1996

19. Whiting, D., and Diezdzic, W., “Effects of Conventional and High-Range Water Reducers on Concrete Properties”, Research and Development Bulletin RD107, Portland Cement Association, 1992

20. R. W. Carlson, T. J. Reading, “Model Study of Shrinkage cracking in Concrete Building Walls”, ACI Structural Journal, Vol. 85. July-August 1988, pp. 395 – 404

21. Grzybowski M., Surendra P. Shah, “Shrinkage Cracking of Fiber Reinforced Concrete”, ACI Materials Journal, Vol. 87 March-April 1990, pp. 138 – 148

22. Wiegrink K., Marikunte S, and Surendra P. Shah, “Shrinkage Cracking of High-Strength Concrete”, ACI Materials Journal, Vol. 93 September-October 1996, pp. 409-415

23. Heather T. See, Emmanuel K. Attiogbe, and Matthew A. Miltenberger, “Shrinkage Cracking Characteristics of Concrete Using Ring Specimens”, ACI Materials Journal, Vol. 100 May-June 2003, pp. 239-245

24. Akhter B. Hossain, Jason Weiss, “Assessing Residual Stress Development and Stress Relaxation in Restrained Concrete Ring Specimens”, Cement & Concrete Composites, Vol. 26 July 2004, pp. 531 – 540

25. W. J. Weiss and S.P. Shah, “Restrained Shrinkage Cracking: the Role of Shrinkage Reducing Admixtures and Specimen Geometry”, Materials and Structures, Vol. 35 March 2002, pp. 85-91

26. Heather T. See, Emmanuel K. Attiogbe, and Matthew A. Miltenberger, “Potential for Restrained Shrinkage Cracking of Concrete and Mortar”, Cement, Concrete, and Aggregates, Vol. 26 December 2004, No. 2, pp. 123 – 130

27. Akhter B. Hossain, Jason Weiss, “The role of specimen geometry and boundary conditions on stress development and cracking in the restrained ring test”, Cement and Concrete Research, Vol. 36 2006, No. 1, pp. 189 – 199

28. Jae Heum Moon, F. Rajabipour, and W. J. Weiss, “Incorporating Moisture Diffusion in the Analysis of the Restrained Ring Test”, Presented at CONSEC (Concrete Under Severe Conditions—Environment and Loading), Seoul Korea, 2004, pp. 1973–1980

29. Jae Heum Moon, Jason Weiss, “Estimating residual stress in the restrained ring test under circumferential drying”, Cement and Concrete Composites, Vol. 28 2006, pp. 486 – 496

30. Z. P. Bazant, L. J. Najjar, “Drying of Concrete as a Nonlinear Diffusion Problem”, Cement and Concrete Research, Vol. 1 1971, pp. 461 – 473

31. Moon JH., “Shrinkage, residual stress, and cracking in heterogeneous materials”, PhD Thesis, Purdue University, 2006

APPENDIX A

PROPERTIES OF AGGREGATES

Specific Gravity and Absorption of Fine Aggregates

Source	Bulk Specific Gravity	Bulk Specific Gravity (SSD)	Apperant Specific Gravity	Absorption (%)
Clayton Jackson	2.54	2.56	2.61	1.03
Dunrite	2.49	2.50	2.52	0.52
Sahara	2.57	2.58	2.61	0.54
Tuckahoe	2.57	2.60	2.66	1.21
County	2.66	2.69	2.73	1.01
Amboy	2.54	2.57	2.60	0.97
Pierson	2.49	2.51	2.54	0.72

Sieve Analysis of Fine Aggregates

Source	Fineness Modulus
Clayton Jackson	2.5
Dunrite	2.78
Sahara	2.54
Tuckahoe	2.94
County	NA
Amboy	2.61
Pierson	2.69

Specific Gravity and Absorption of Coarse Aggregates

Source	Bulk Specific Gravity (SSD)	Absorption
Trap Rock	2.88	0.82
Tilcon Millington	2.84	1.94
Tilcon Oxford	2.89	0.61
Better Materials	2.67	1.20
Independence Materials	2.81	0.23
Fanwood	2.89	1.40
Stavola	2.90	1.34
Plumstead	2.69	0.94

APPENDIX B

RESTRAINED SHRINKAGE TEST RESULTS

GROUP 1 MIXES

G1M1 – R311266

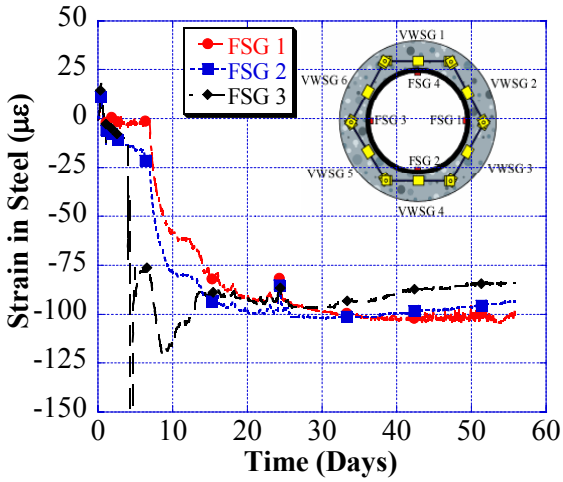

G1M1 – Specimen 1 – Steel Strains

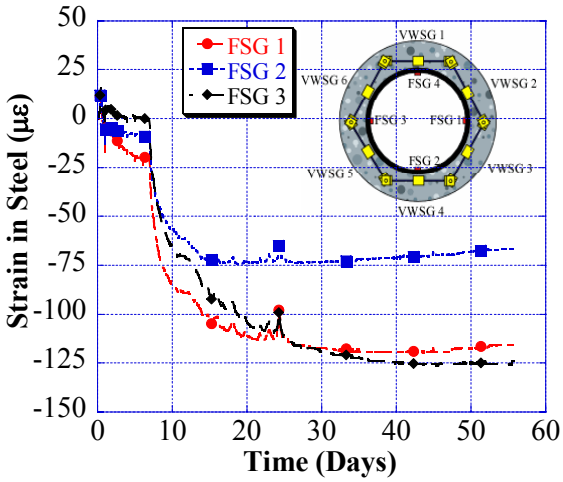

G1M1 – Specimen 2 – Steel Strains

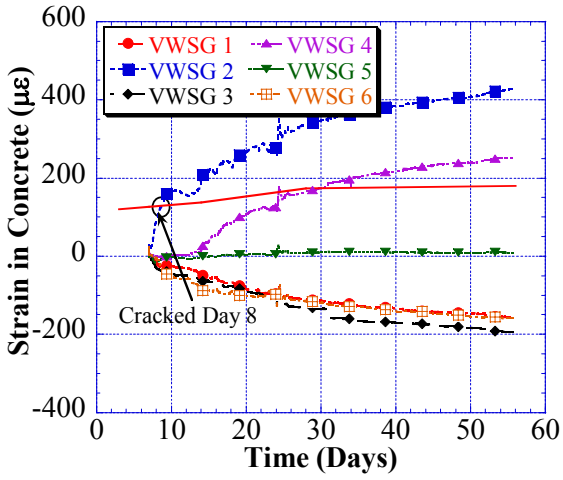

G1M1 – Specimen 1 – Concrete Strains

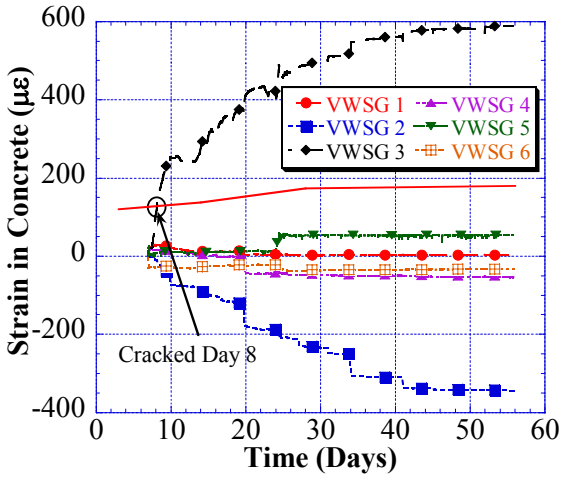

G1M1 – Specimen 2 – Concrete Strains

G1M2 – R408847

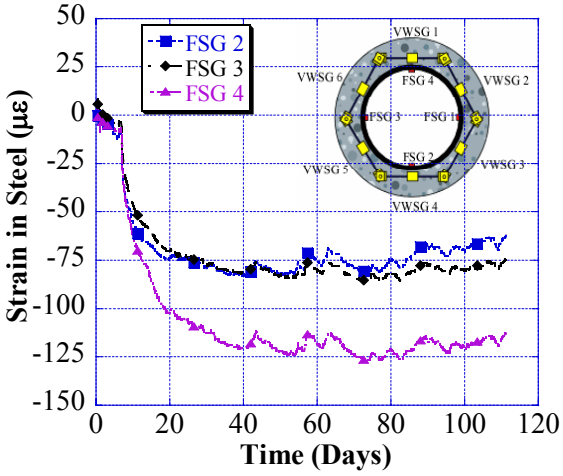

G1M2 – Specimen 1 – Steel Strains

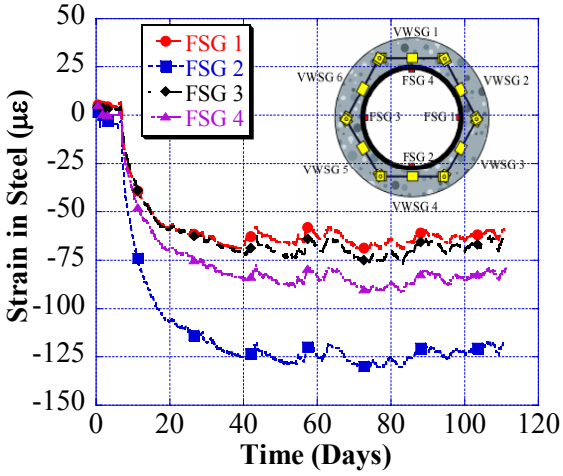

G1M2 – Specimen 2 – Steel Strains

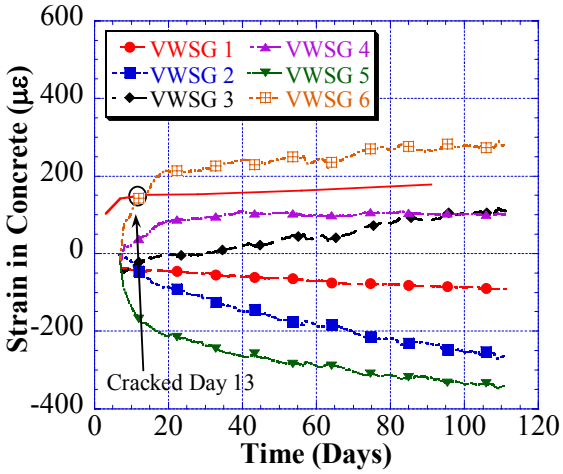

G1M2 – Specimen 1 – Concrete Strains

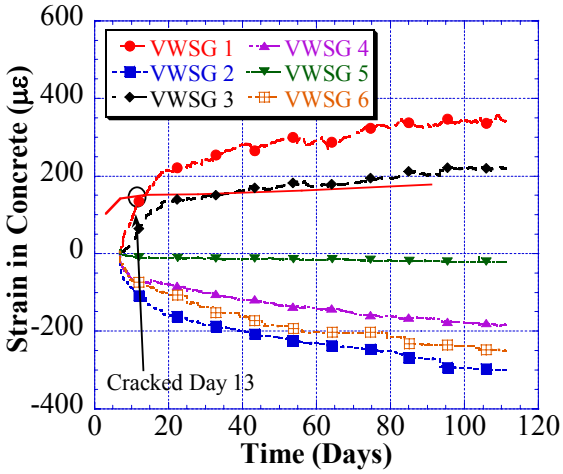

G1M2 – Specimen 2 – Concrete Strains

G1M3 – R200578S

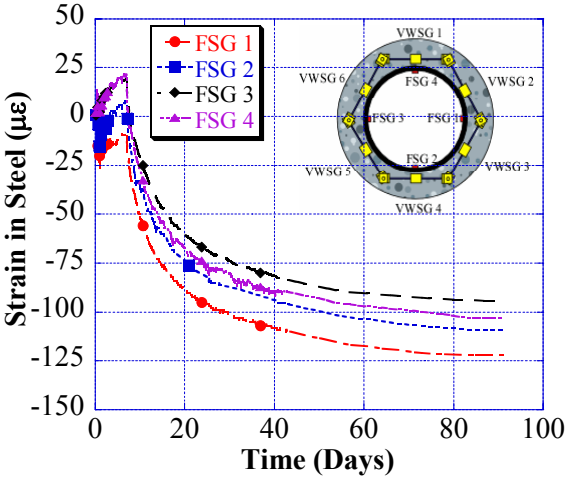

G1M3 – Specimen 1 – Steel Strains

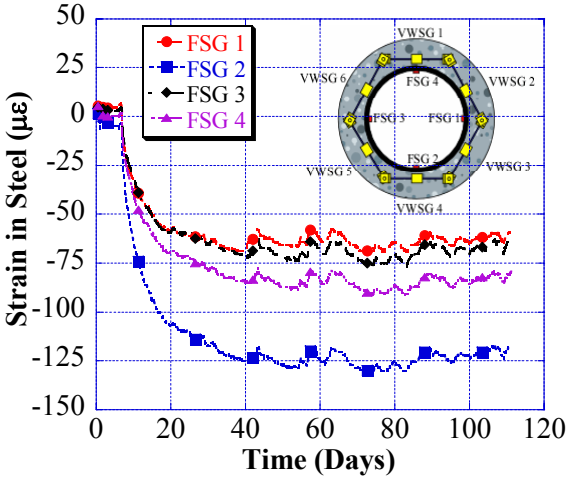

G1M3 – Specimen 2 – Steel Strains

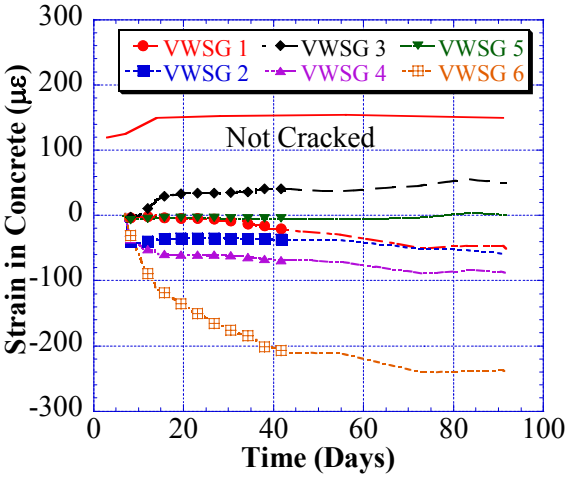

G1M3 – Specimen 1 – Concrete Strains

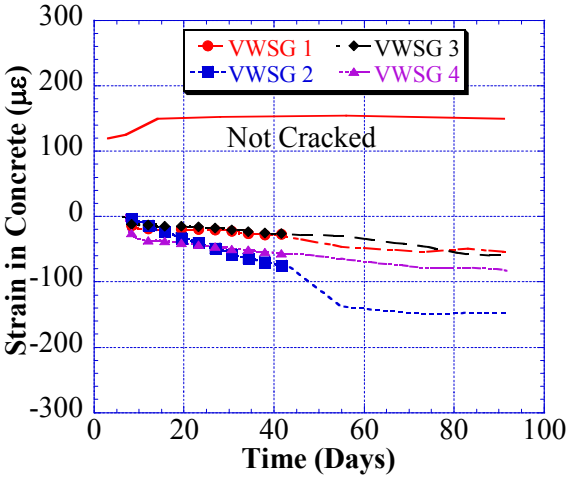

G1M3 – Specimen 2 – Concrete Strains

GROUP 2 MIXES

G2M1 – R408850

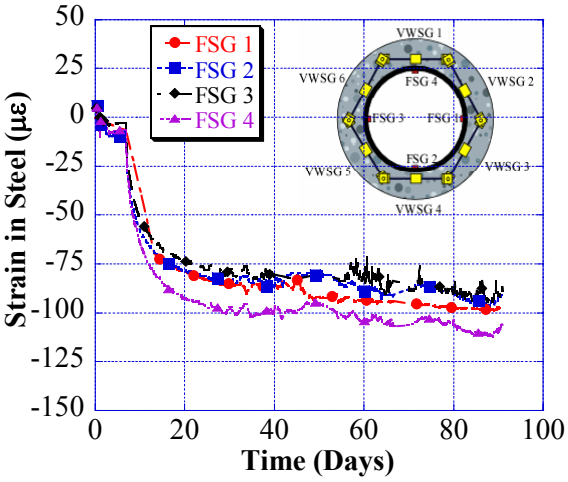

G2M1 – Specimen 1 – Steel Strains

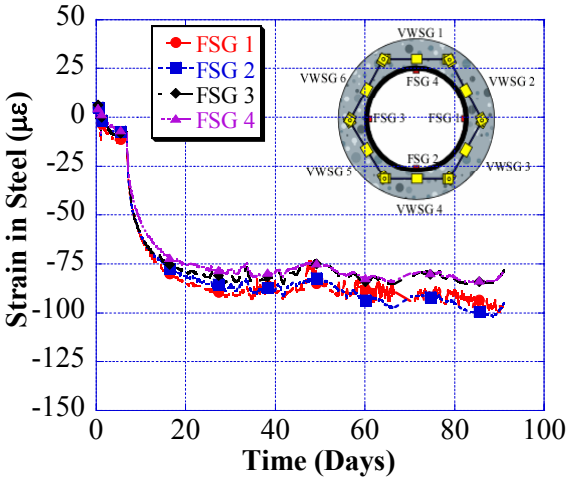

G2M1 – Specimen 2 – Steel Strains

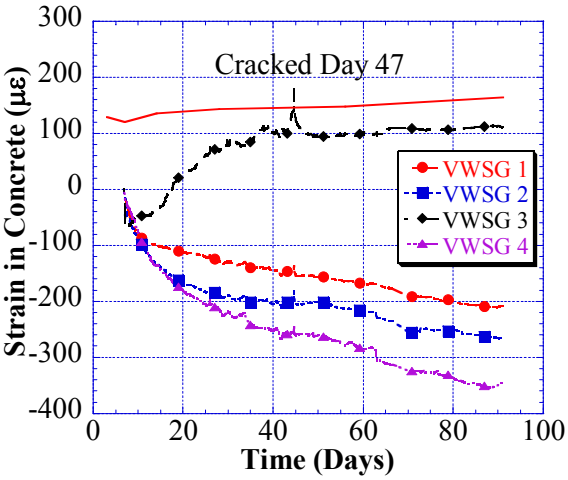

G2M1 – Specimen 1 – Concrete Strains

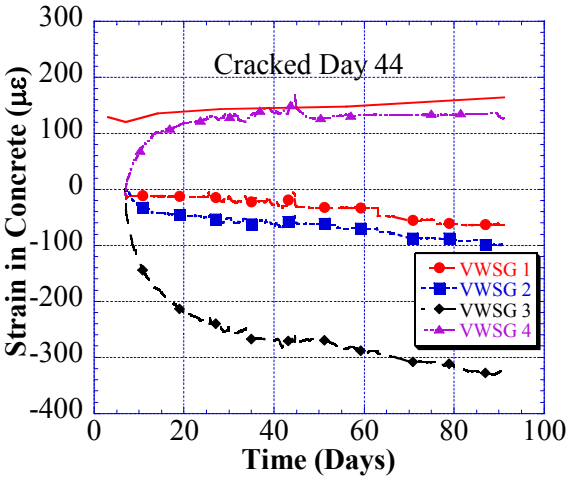

G2M1 – Specimen 2 – Concrete Strains

G2M2 – R409239

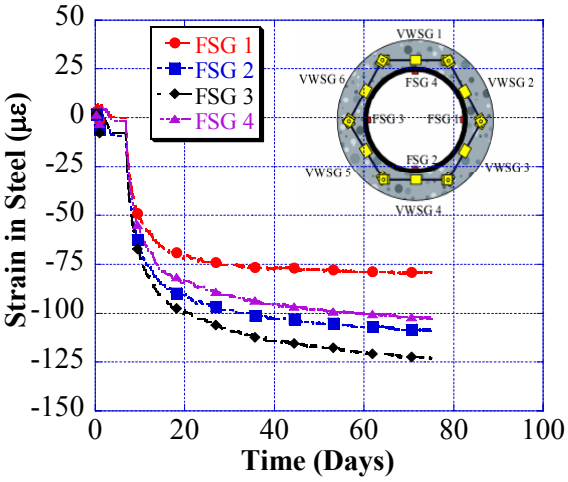

G2M2 – Specimen 1 – Steel Strains

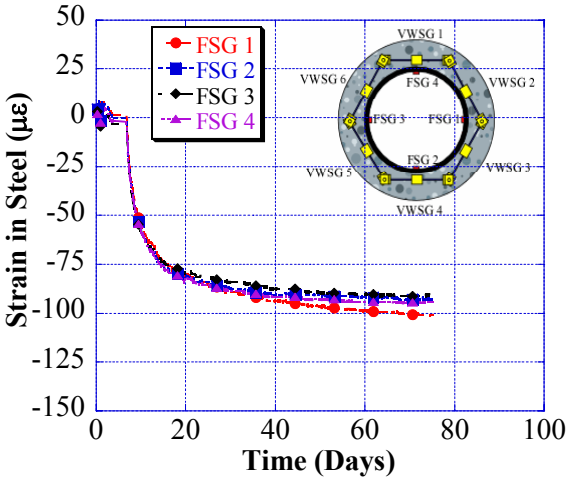

G2M2 – Specimen 2 – Steel Strains

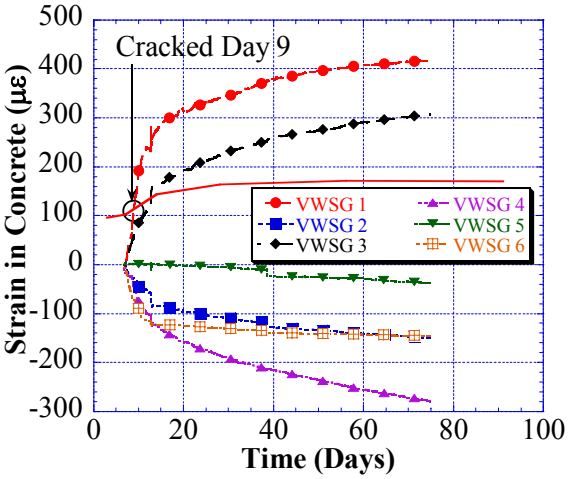

G2M2 – Specimen 1 – Concrete Strains

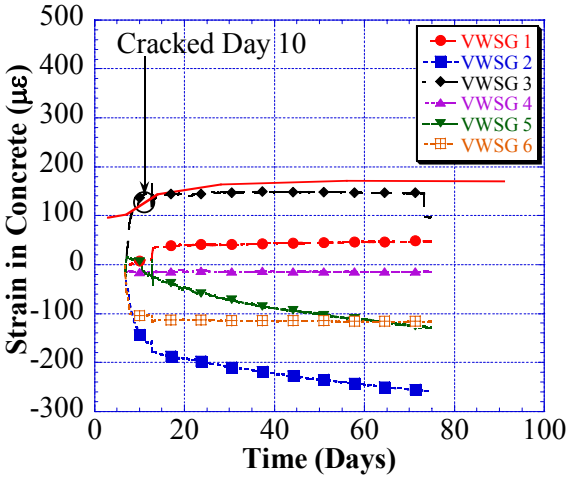

G2M2 – Specimen 2 – Concrete Strains

G2M3 – R309497

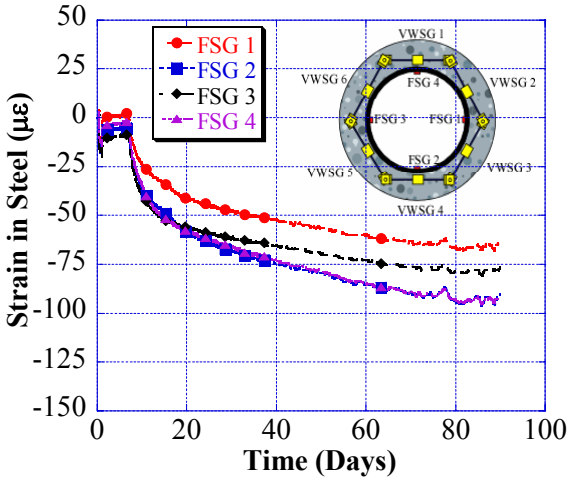

G2M3 – Specimen 1 – Steel Strains

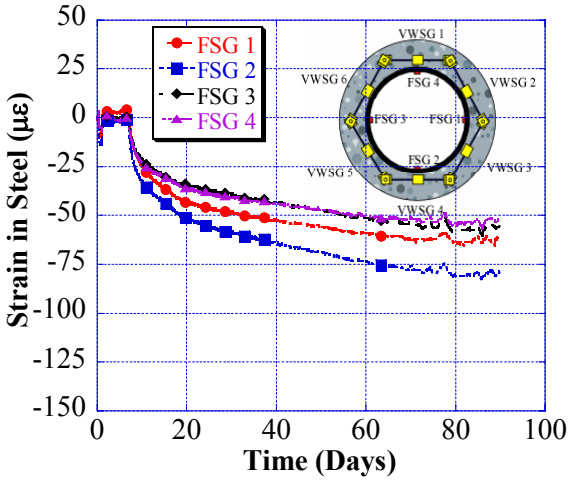

G2M3 – Specimen 2 – Steel Strains

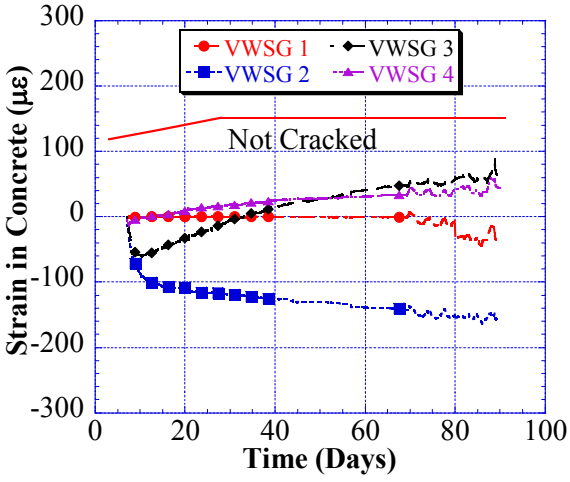

G2M3 – Specimen 1 – Concrete Strains

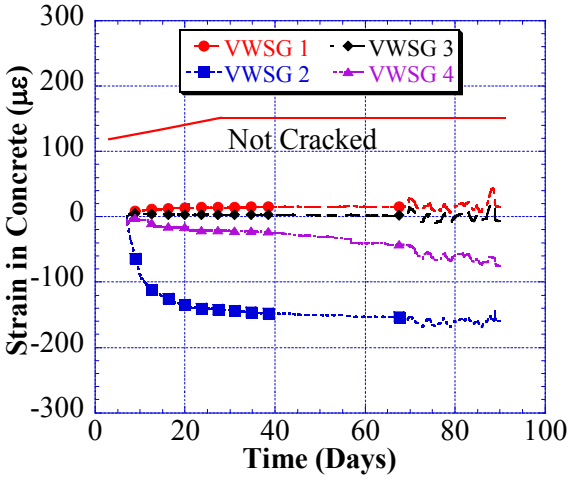

G2M3 – Specimen 2 – Concrete Strains

G2M4 – R310682

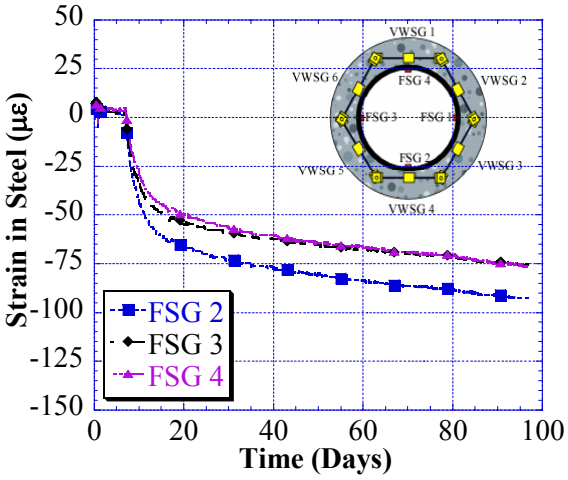

G2M4 – Specimen 1 – Steel Strains

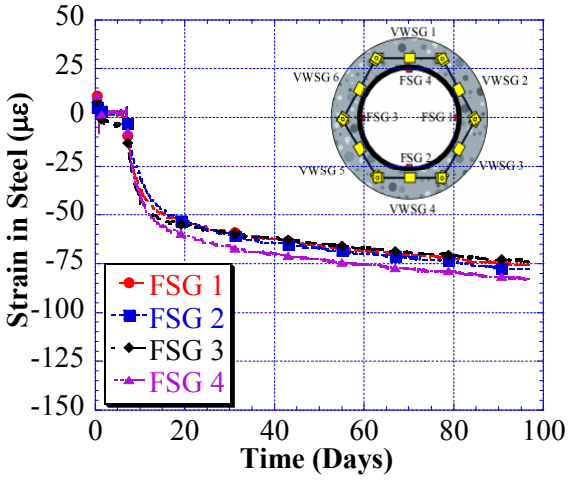

G2M4 – Specimen 2 – Steel Strains

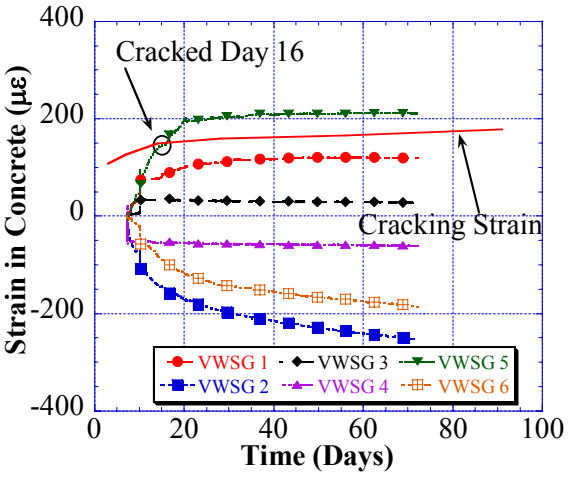

G2M4 – Specimen 1 – Concrete Strains

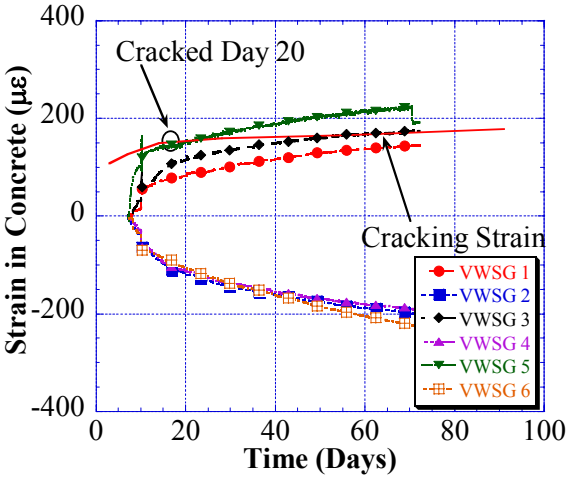

G2M4 – Specimen 2 – Concrete Strains

G2M5 – R200626S

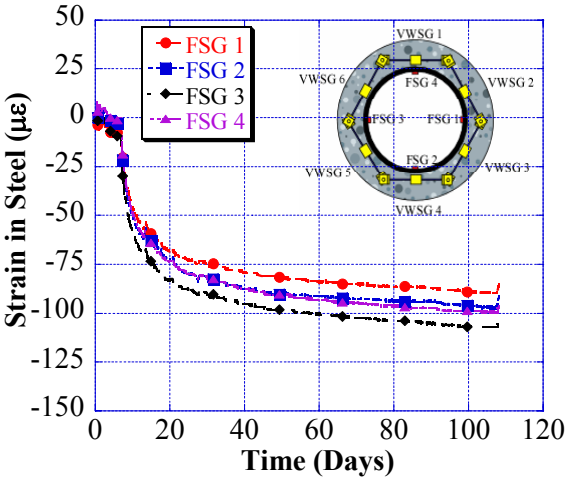

G2M5 – Specimen 1 – Steel Strains

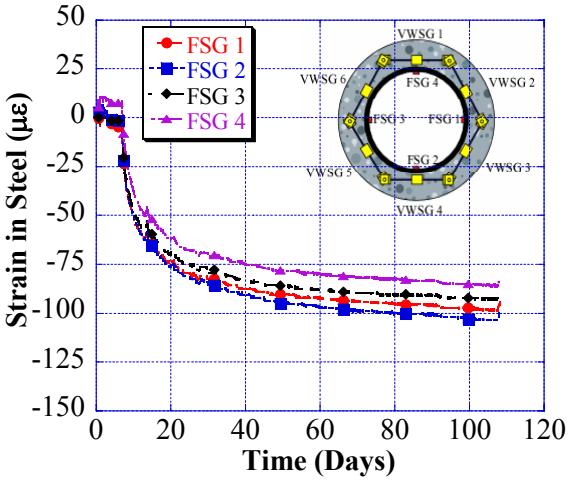

G2M5 – Specimen 2 – Steel Strains

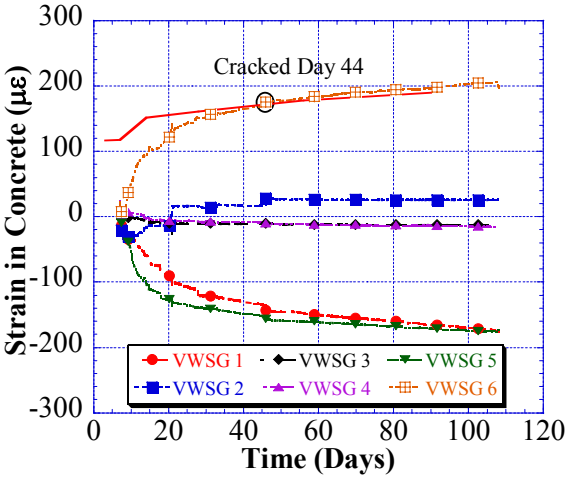

G2M5 – Specimen 1 – Concrete Strains

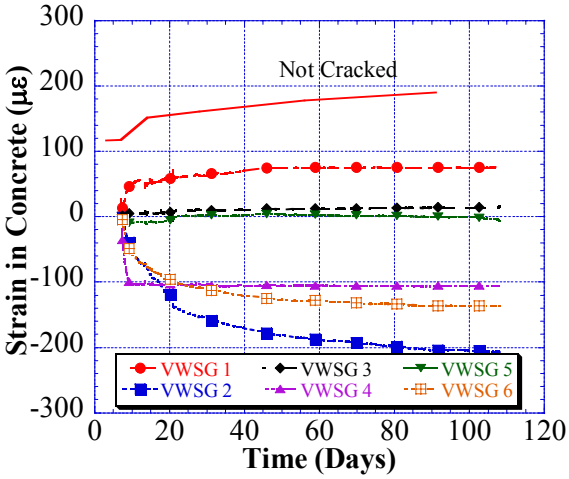

G2M5 – Specimen 2 – Concrete Strains

G2M6 – R200633S

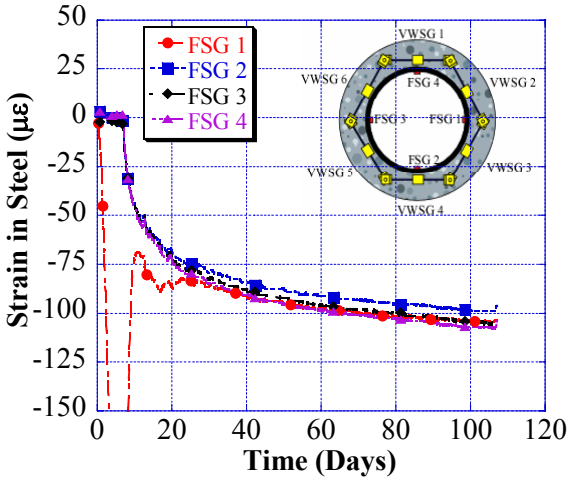

G2M6 – Specimen 1 – Steel Strains

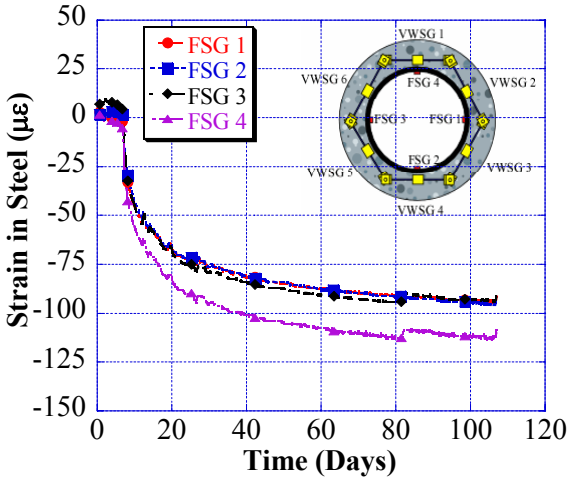

G2M6 – Specimen 2 – Steel Strains

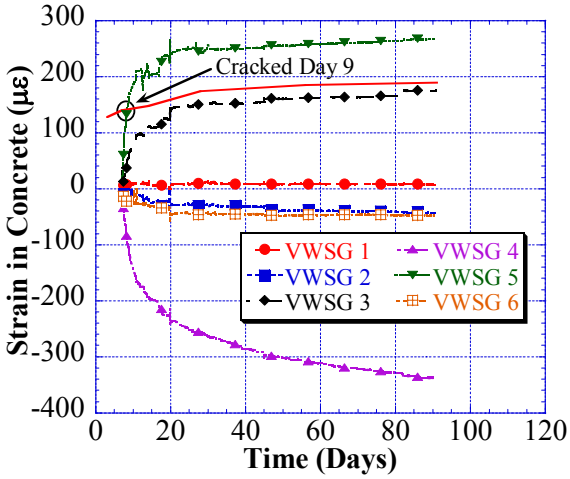

G2M6 – Specimen 1 – Concrete Strains

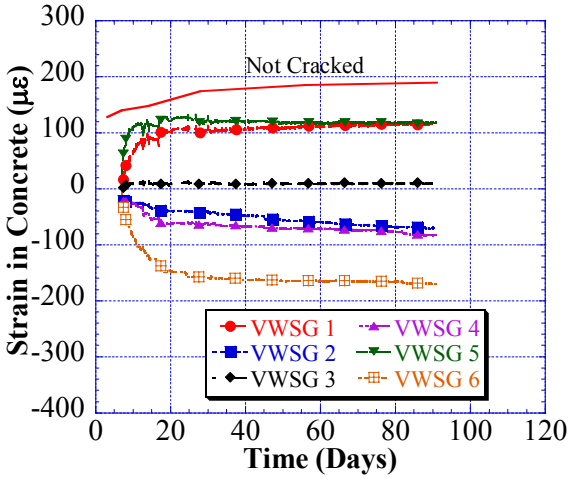

G2M6 – Specimen 2 – Concrete Strains

GROUP 3 MIXES

G3M1 – R308163

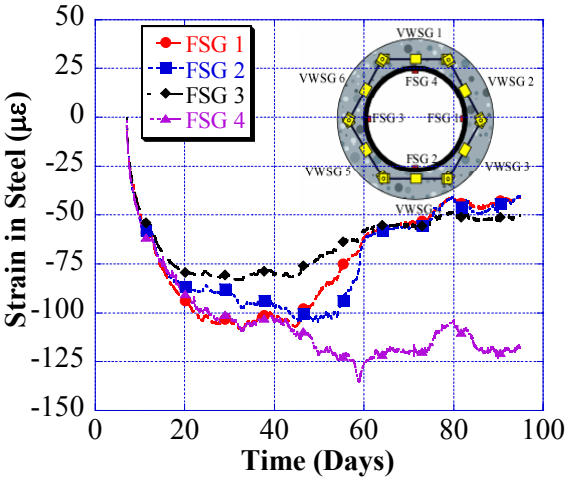

G3M1 – Specimen 1 – Steel Strains

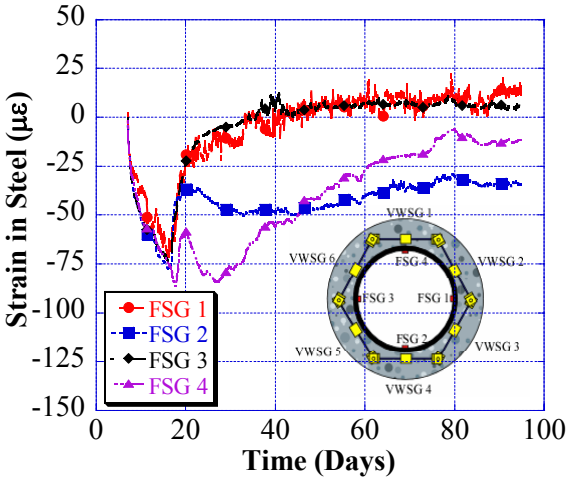

G3M1 – Specimen 2 – Steel Strains

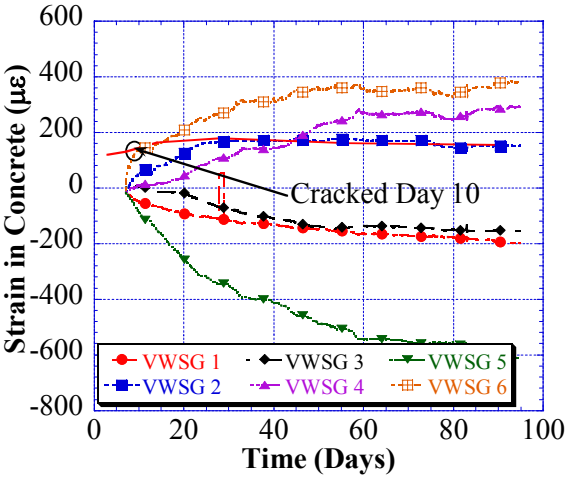

G3M1 – Specimen 1 – Concrete Strains

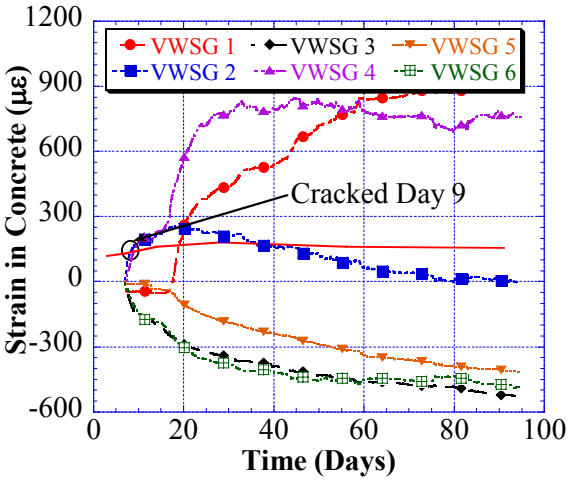

G3M1 – Specimen 2 – Concrete Strains

G3M2 – R308278

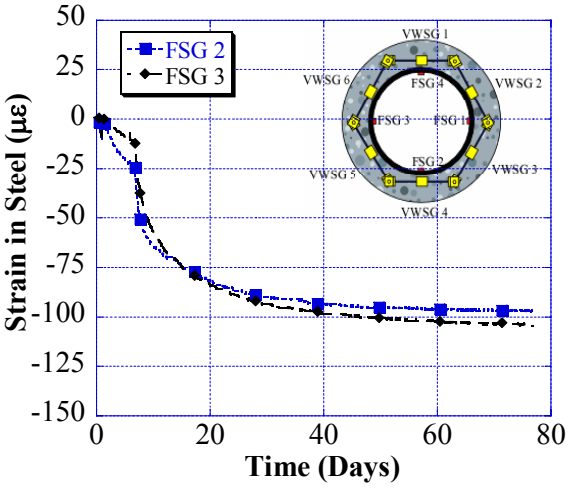

G3M2 – Specimen 1 – Steel Strains

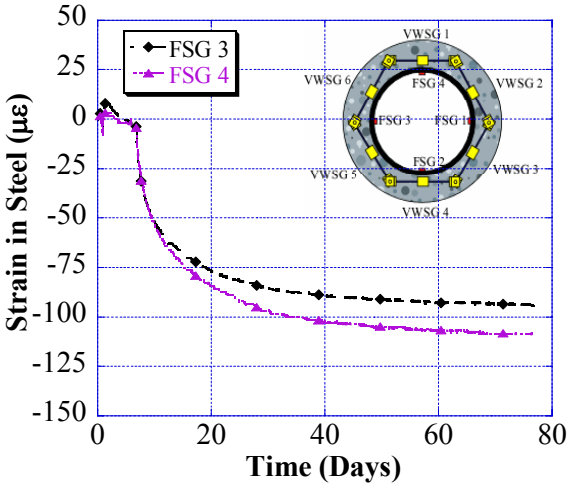

G3M2 – Specimen 2 – Steel Strains

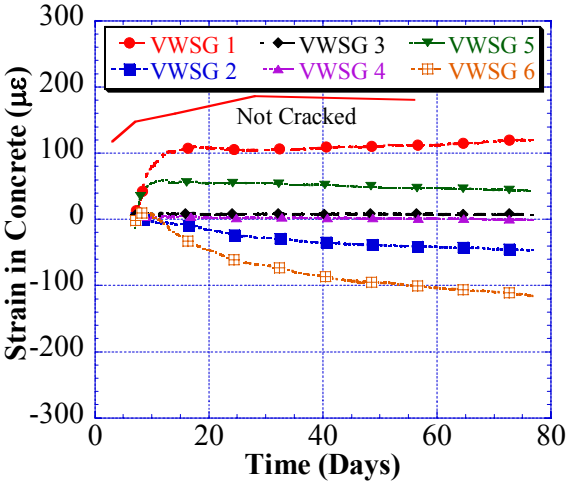

G3M2 – Specimen 1 – Concrete Strains

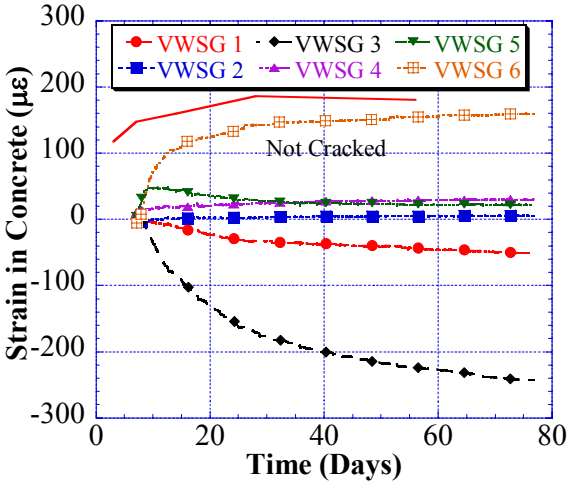

G3M2 – Specimen 2 – Concrete Strains

GROUP 4 MIXES

G4M1 – R309495

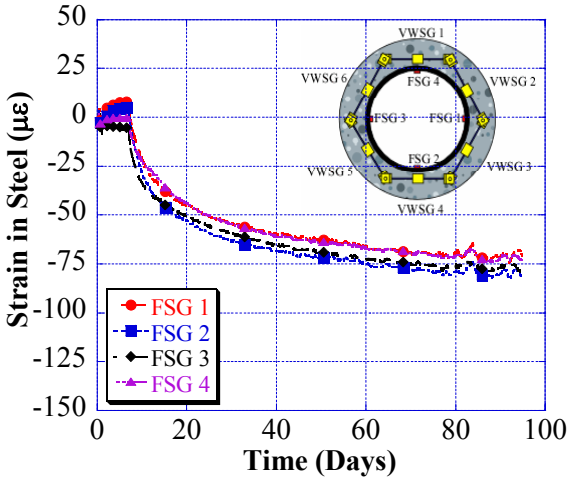

G4M1 – Specimen 1 – Steel Strains

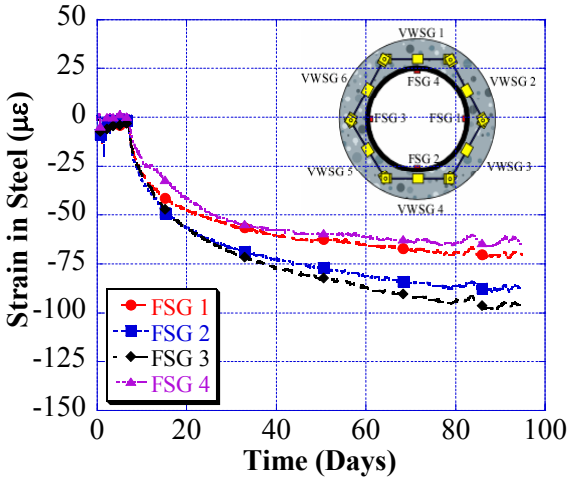

G4M1 – Specimen 2 – Steel Strains

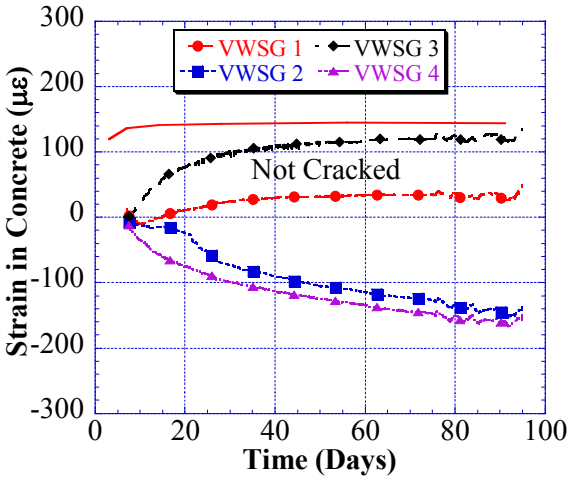

G4M1 – Specimen 1 – Concrete Strains

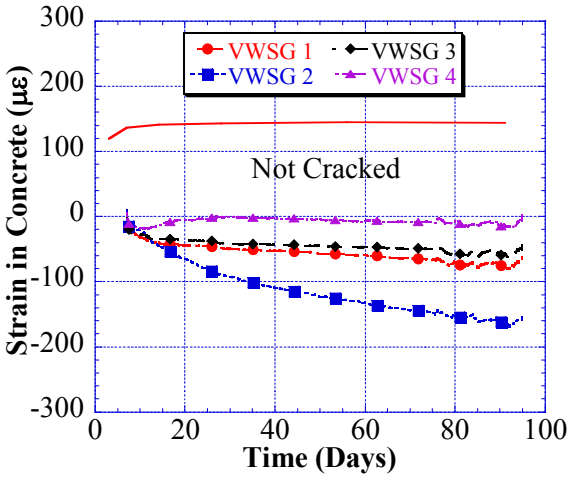

G4M1 – Specimen 2 – Concrete Strains

G4M2 – R408844

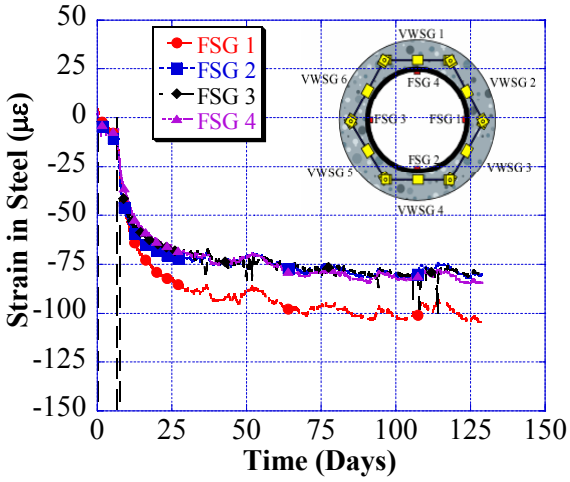

G4M2 – Specimen 1 – Steel Strains

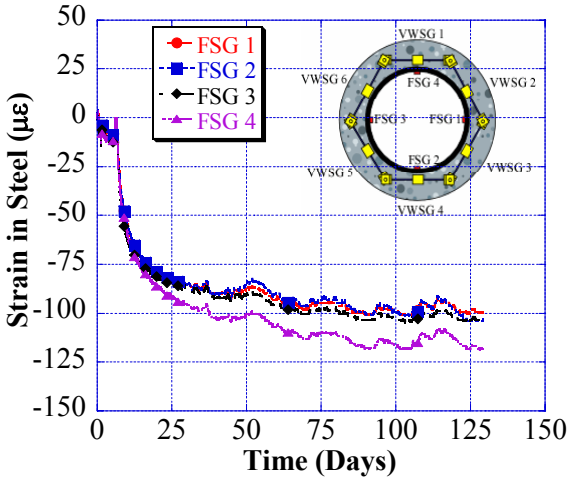

G4M2 – Specimen 2 – Steel Strains

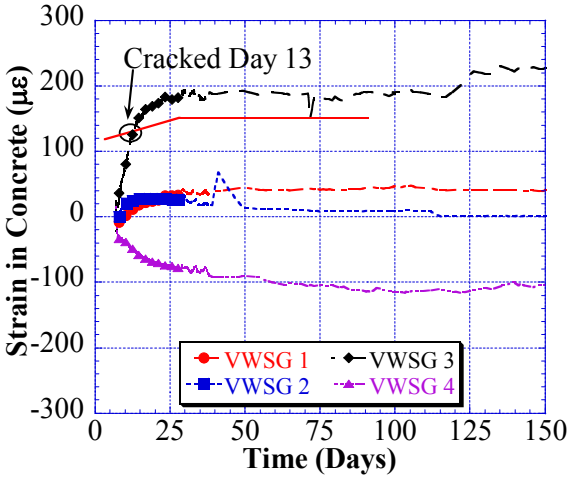

G4M2 – Specimen 1 – Concrete Strains

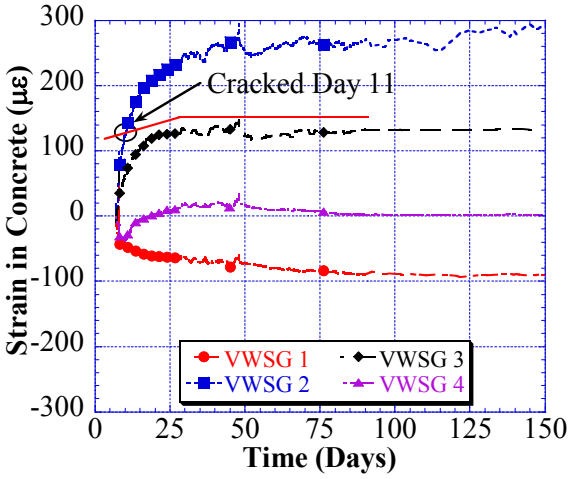

G4M2 – Specimen 2 – Concrete Strains

G4M3 – R309496

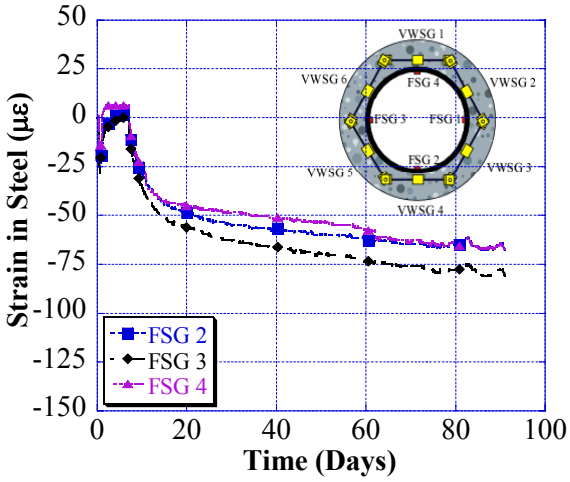

G4M3 – Specimen 1 – Steel Strains

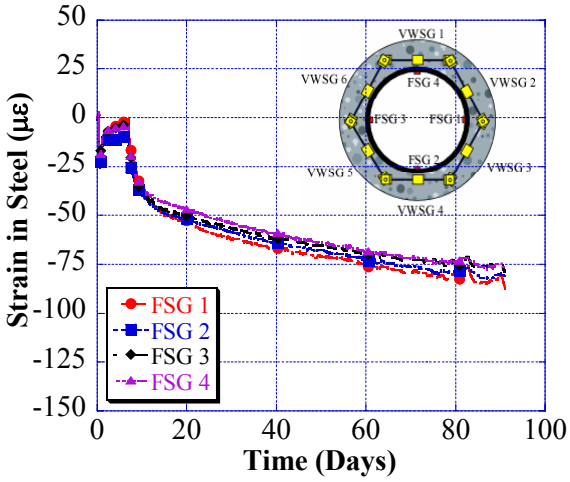

G4M3 – Specimen 2 – Steel Strains

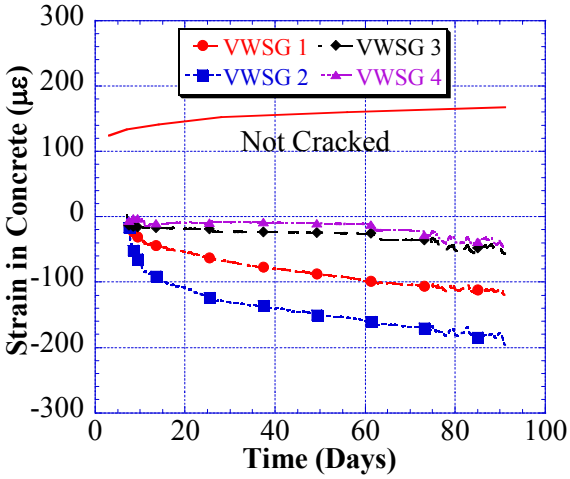

G4M3 – Specimen 1 – Concrete Strains

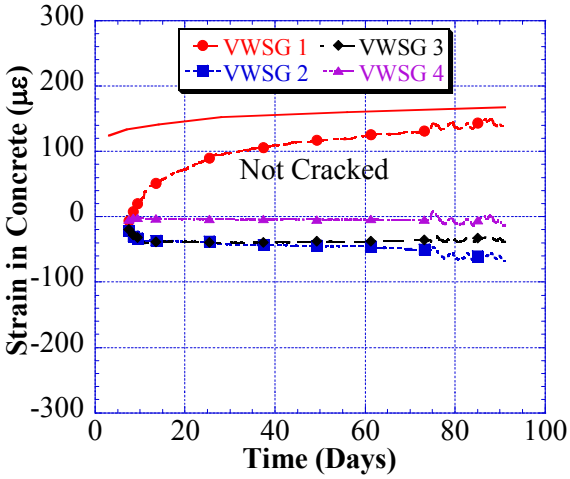

G4M3 – Specimen 2 – Concrete Strains

G4M4 – R408694

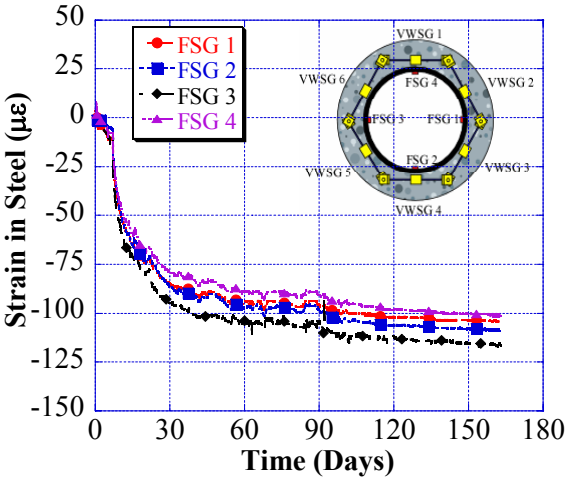

G4M4 – Specimen 1 – Steel Strains

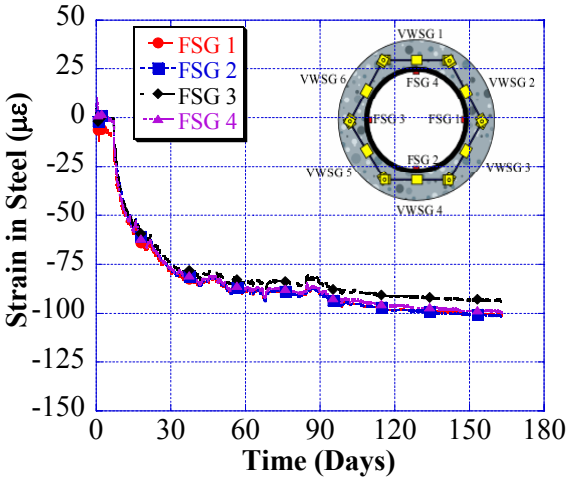

G4M4 – Specimen 2 – Steel Strains

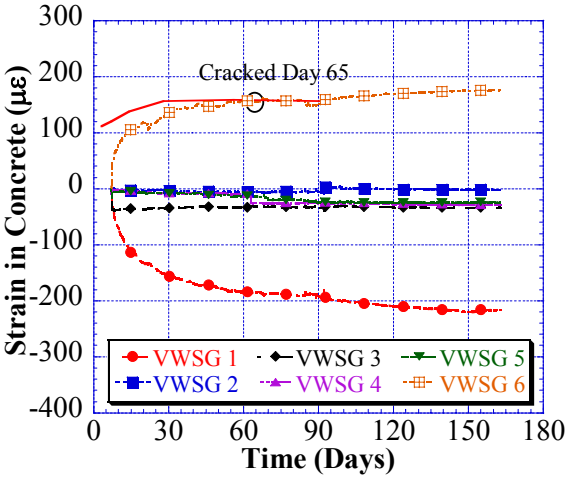

G4M4 – Specimen 1 – Concrete Strains

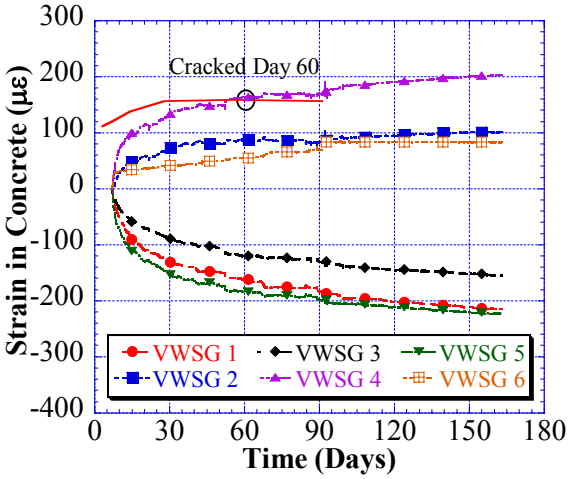

G4M4 – Specimen 2 – Concrete Strains

APPENDIX C

RING CRACK DRAWINGS

GROUP 1 MIXES

G1M1 – R311266

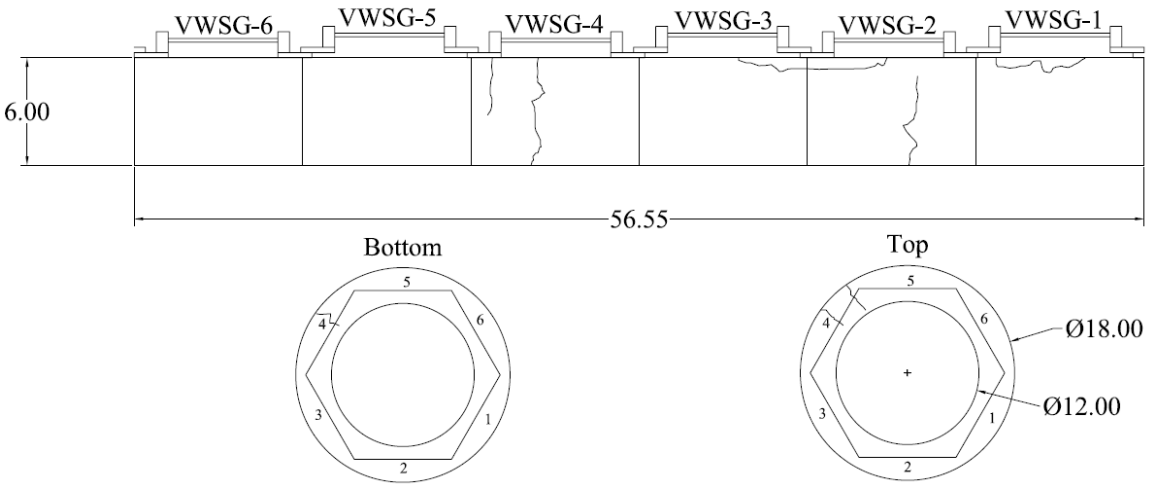

G1M1 – Ring Specimen 1 – Crack Drawings

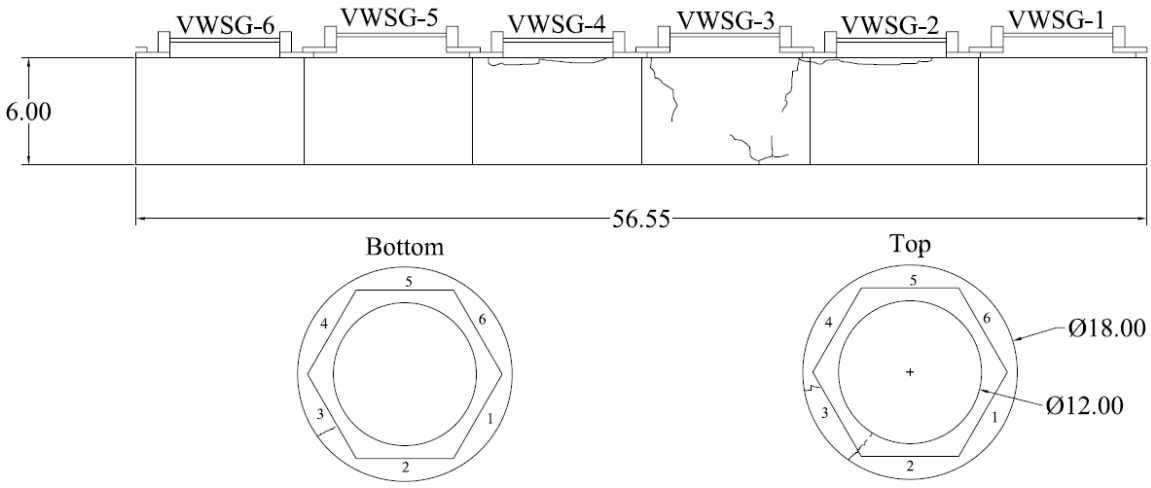

G1M1 – Ring Specimen 2 – Crack Drawings

G1M2 – R408847

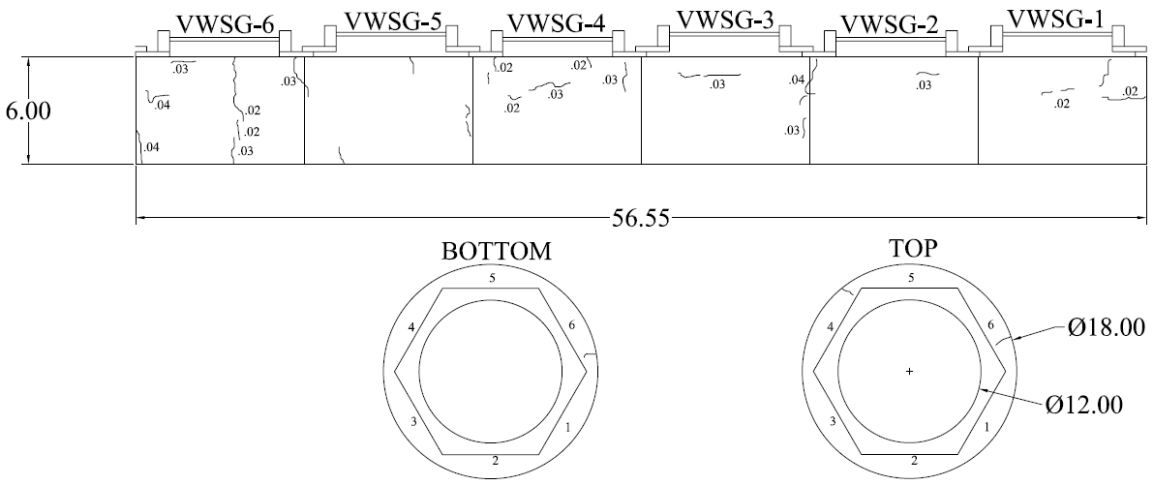

G1M2 – Ring Specimen 1 – Crack Drawings

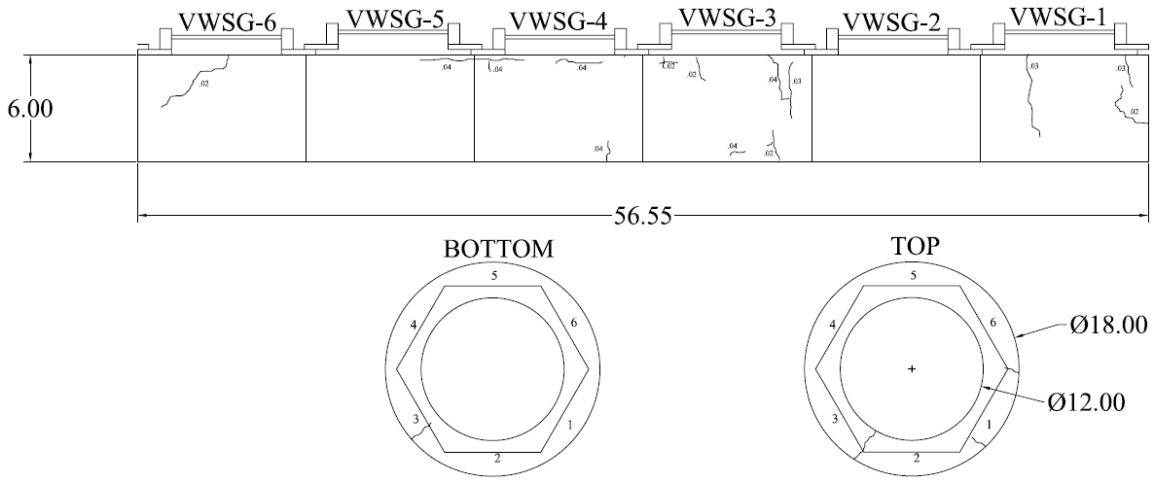

G1M2 – Ring Specimen 2 – Crack Drawings

G1M3 – R200578S

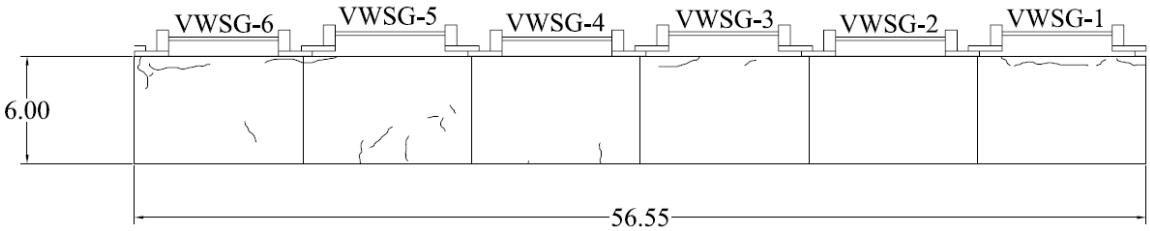

G1M3 – Ring Specimen 1 – Crack Drawings

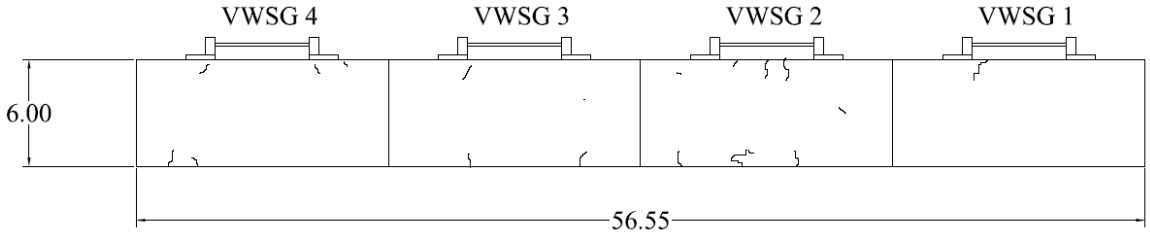

G1M3 – Ring Specimen 2 – Crack Drawings

GROUP 2 MIXES

G2M1 – R408850

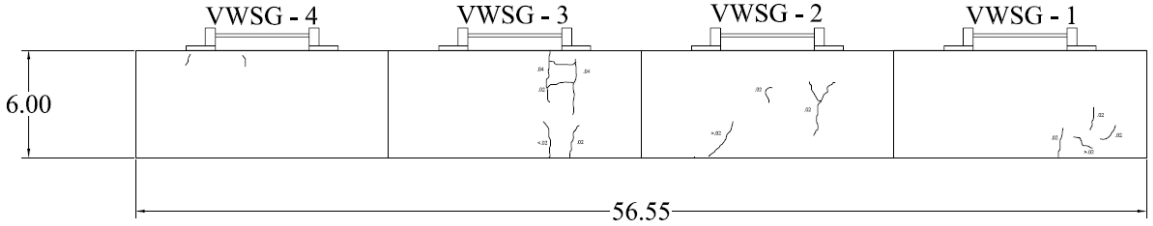

G2M1 – Ring Specimen 1 – Crack Drawings

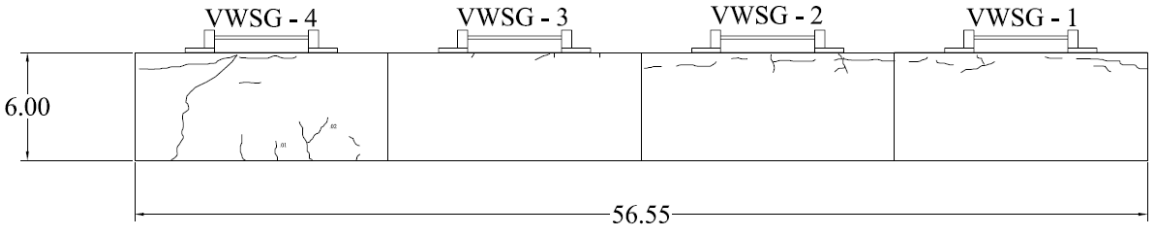

G2M1 – Ring Specimen 2 – Crack Drawings

G2M2 – R409239

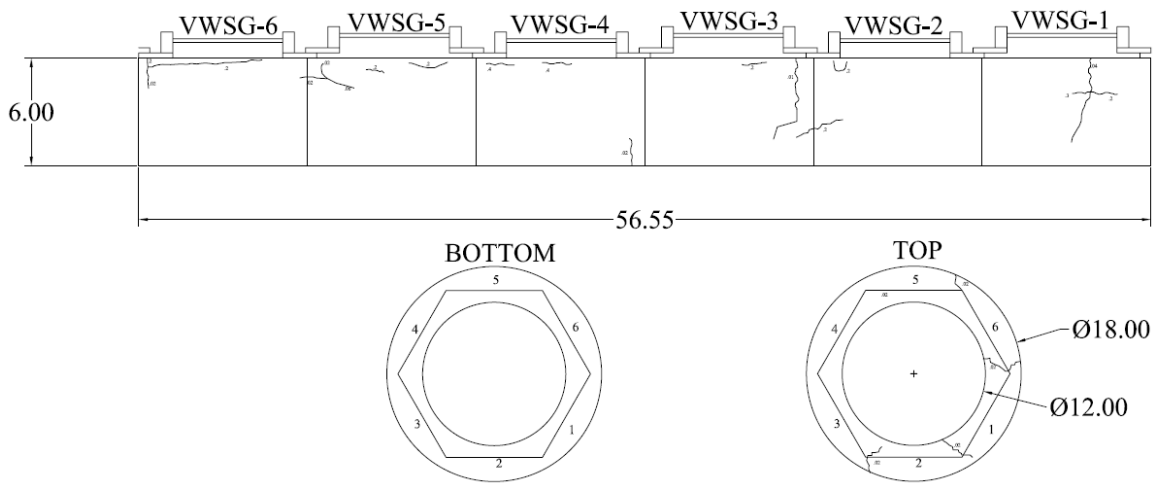

G2M2 – Ring Specimen 1 – Crack Drawings

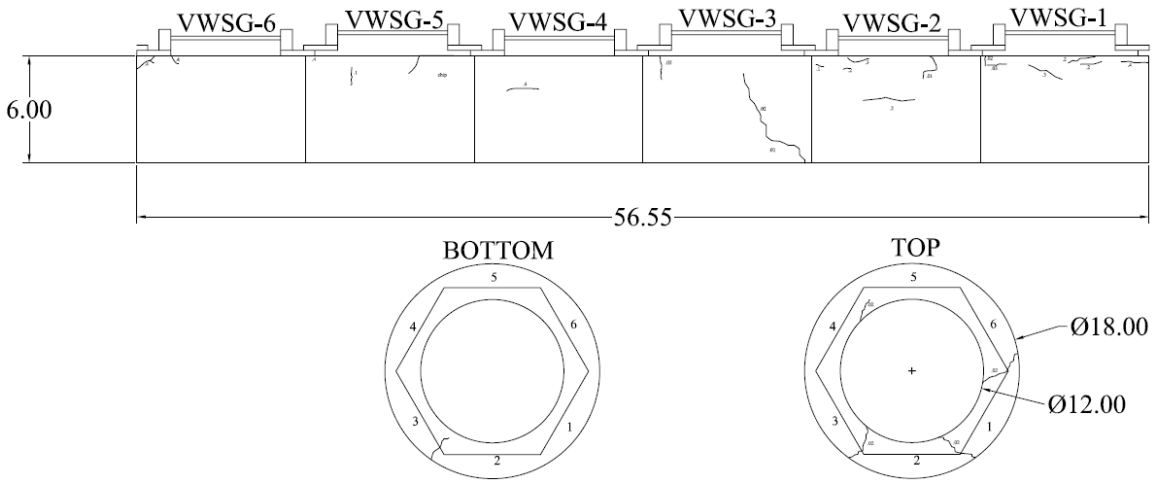

G2M2 – Ring Specimen 2 – Crack Drawings

G2M3 – R309497

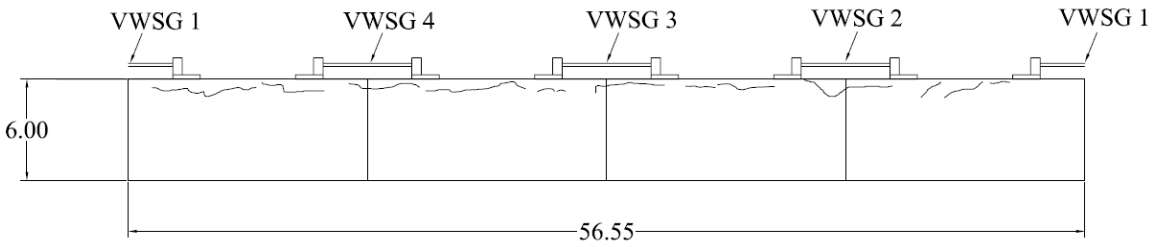

G2M3 – Ring Specimen 1 – Crack Drawings

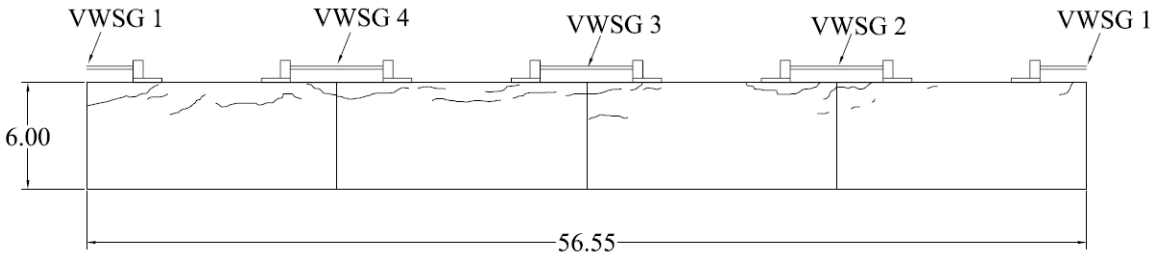

G2M3 – Ring Specimen 2 – Crack Drawings

G2M4 – R310682

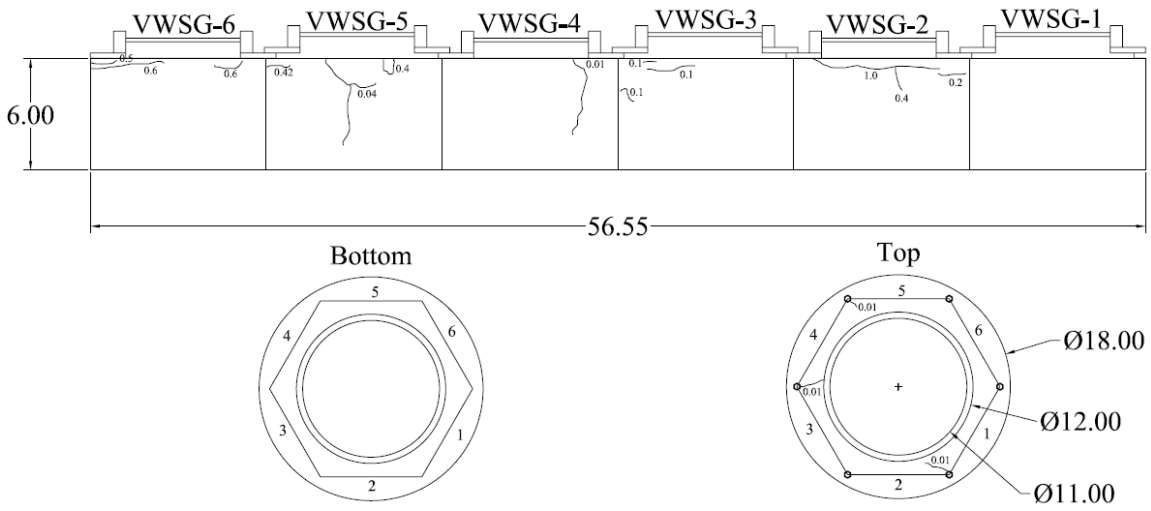

G2M4 – Ring Specimen 1 – Crack Drawings

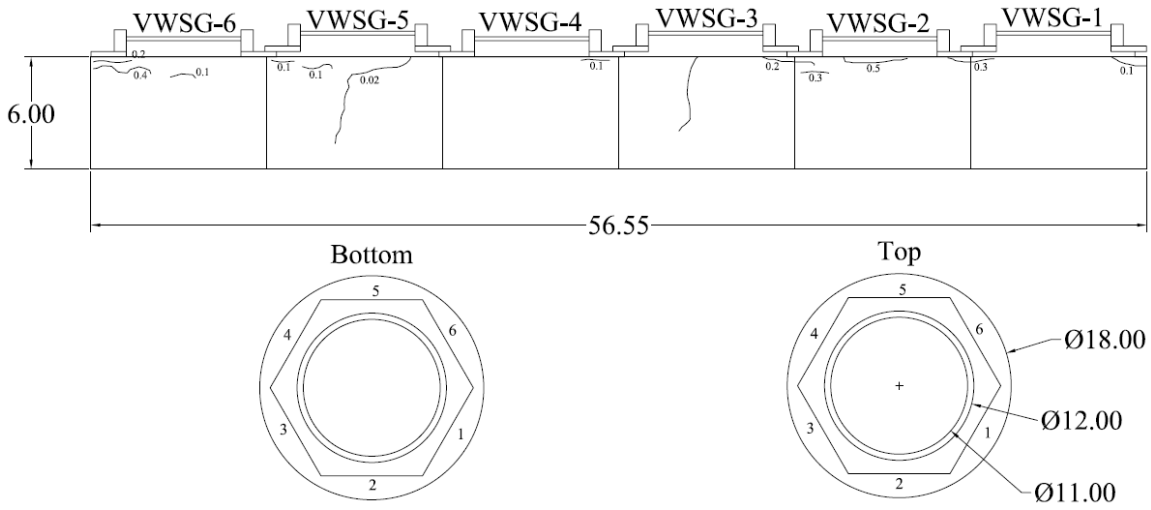

G2M4 – Ring Specimen 2 – Crack Drawings

G2M5 – R200626S

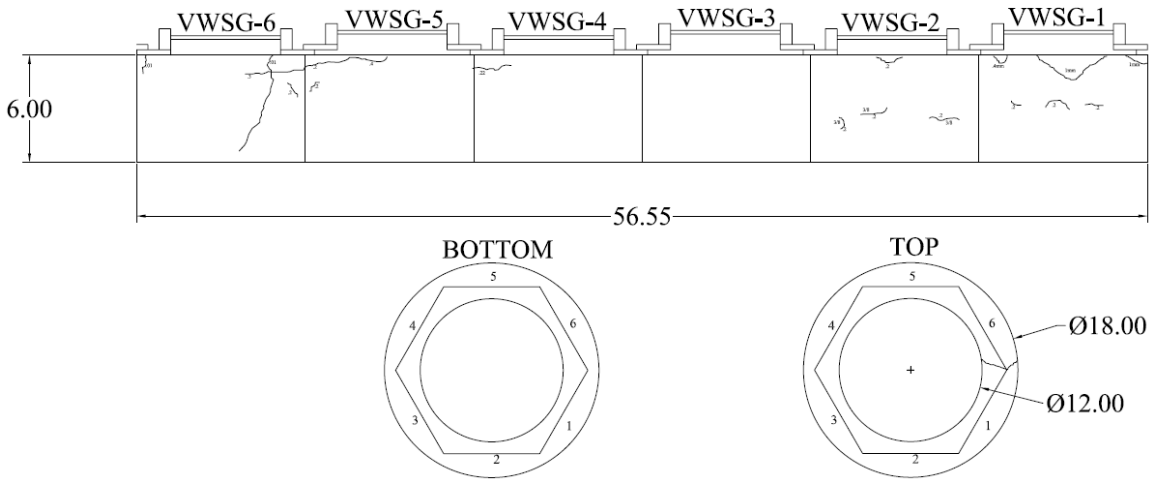

G2M5 – Ring Specimen 1 – Crack Drawings

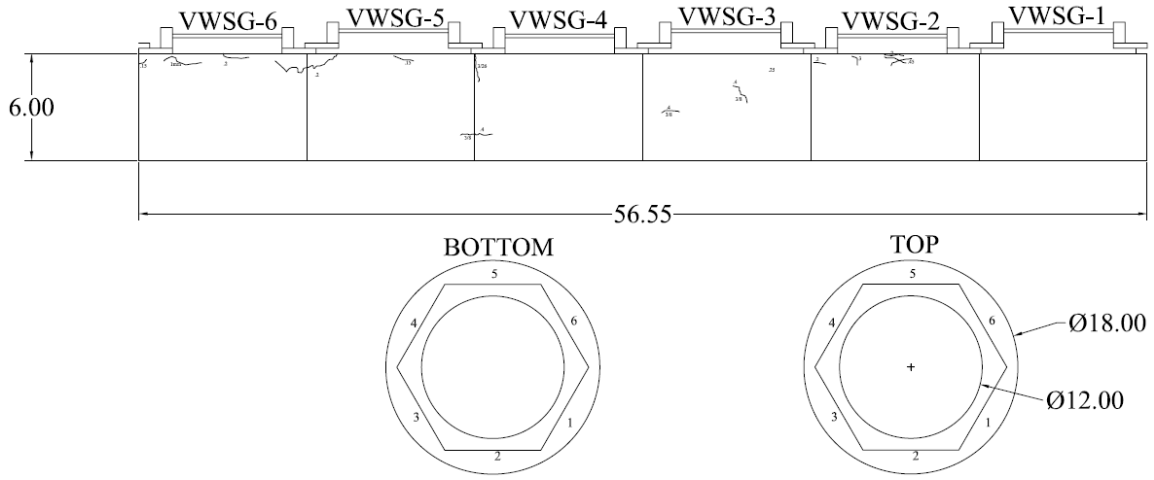

G2M5 – Ring Specimen 2 – Crack Drawings

G2M6 – R200633S

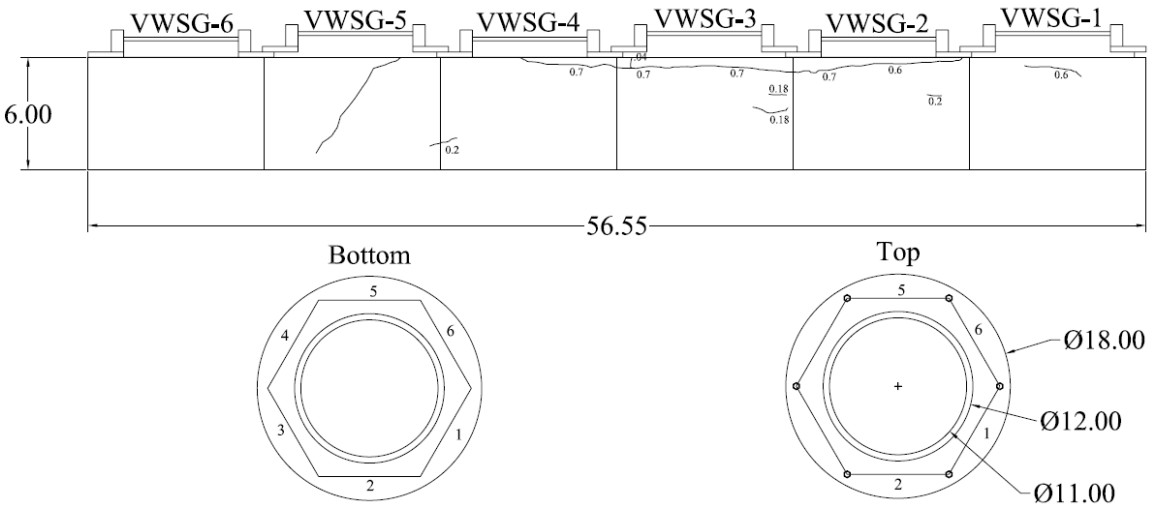

G2M6 – Ring Specimen 1 – Crack Drawings

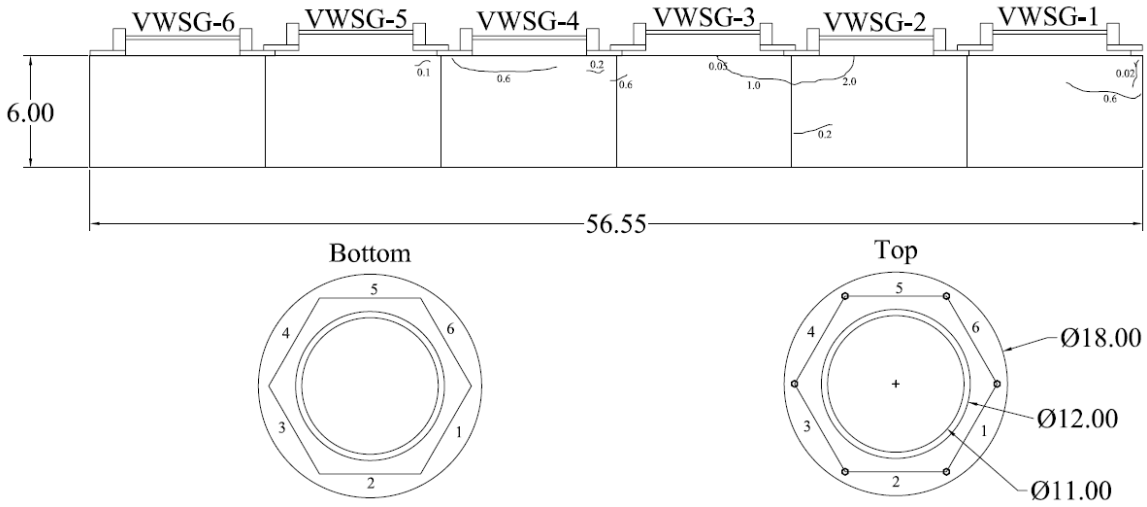

G2M6 – Ring Specimen 2 – Crack Drawings

GROUP 3 MIXES

G3M1 – R308163

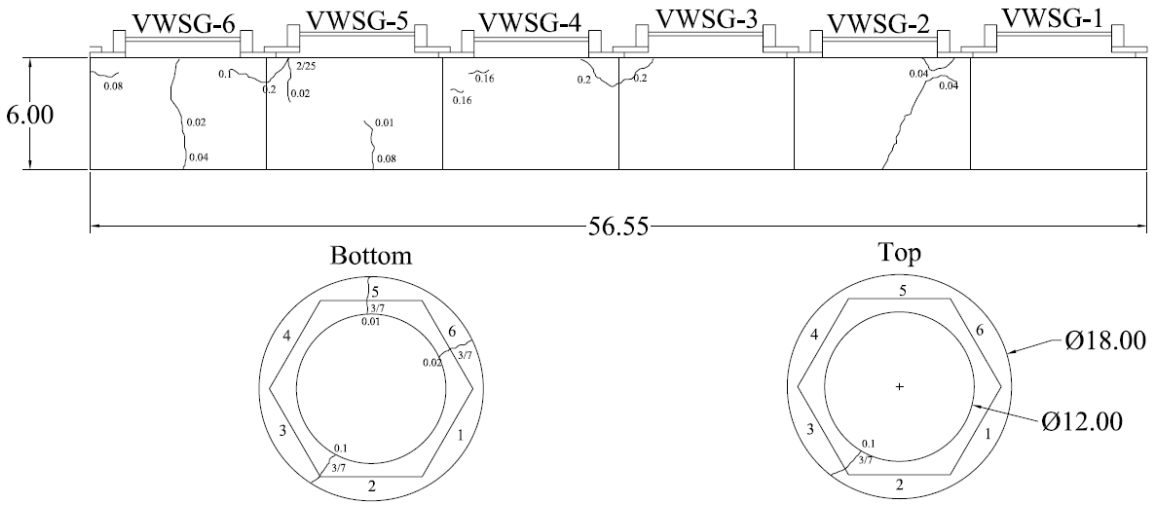

G3M1 – Ring Specimen 1 – Crack Drawings

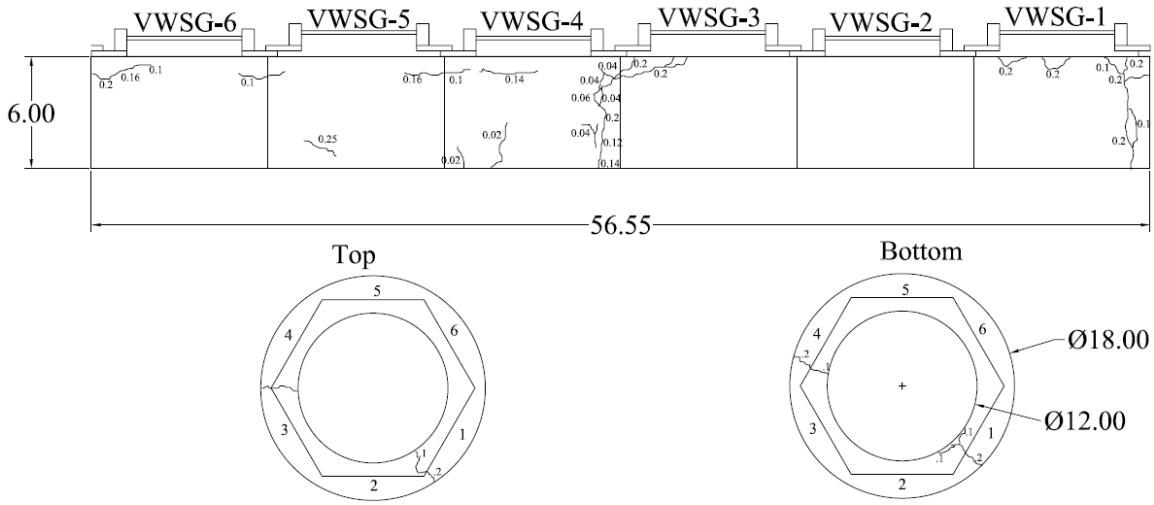

G3M1 – Ring Specimen 2 – Crack Drawings

G3M2 – R308278

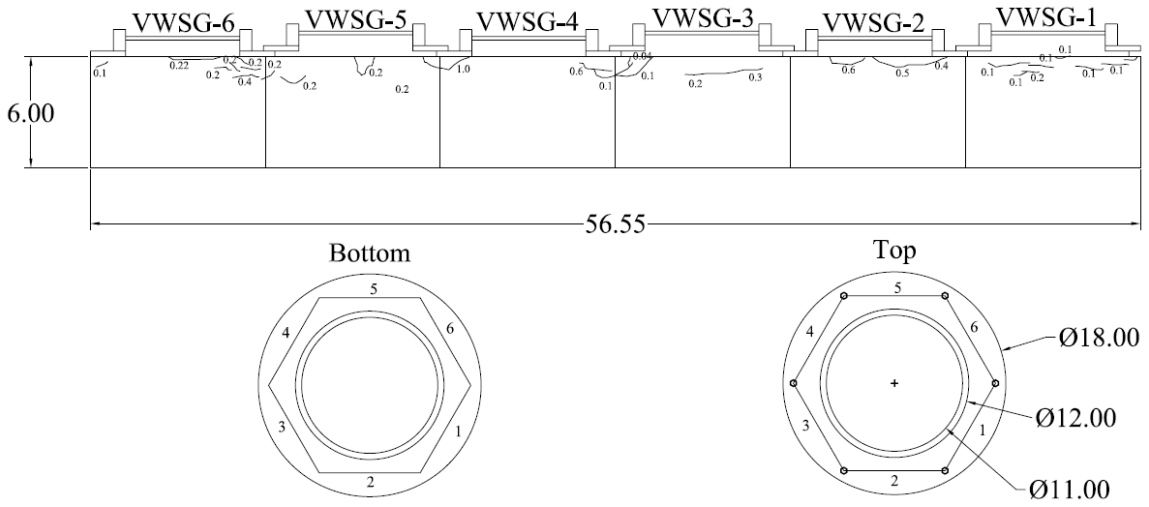

G3M2 – Ring Specimen 1 – Crack Drawings

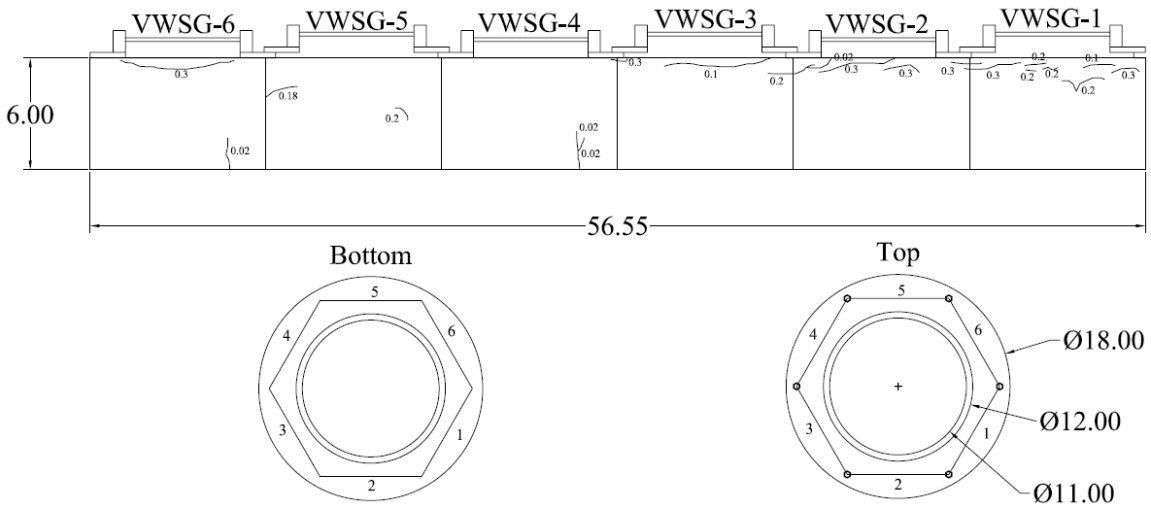

G3M2 – Ring Specimen 2 – Crack Drawings

GROUP 4 MIXES

G4M1 – R309495

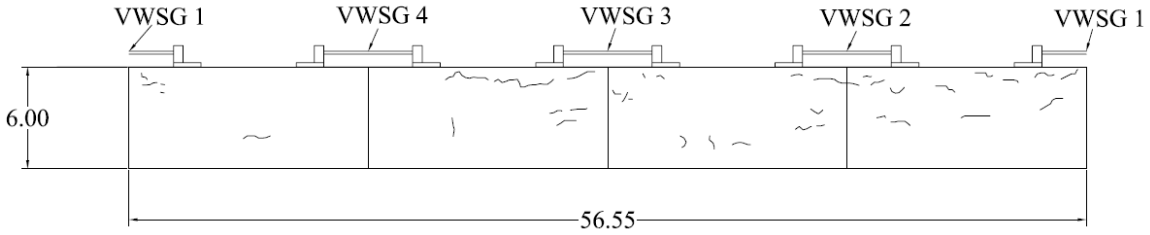

G4M1 – Ring Specimen 1 – Crack Drawings

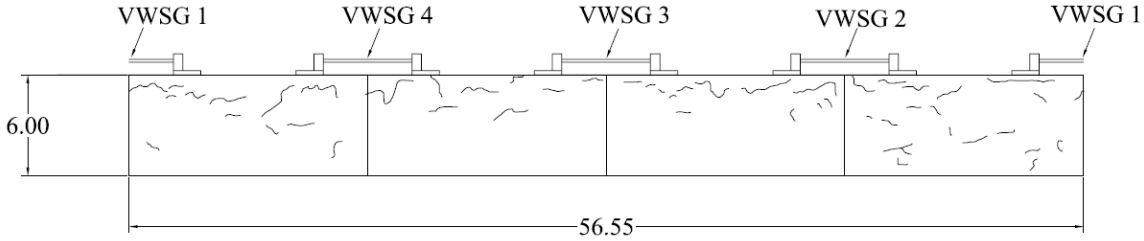

G4M1 – Ring Specimen 2 – Crack Drawings

G4M2 – R408844

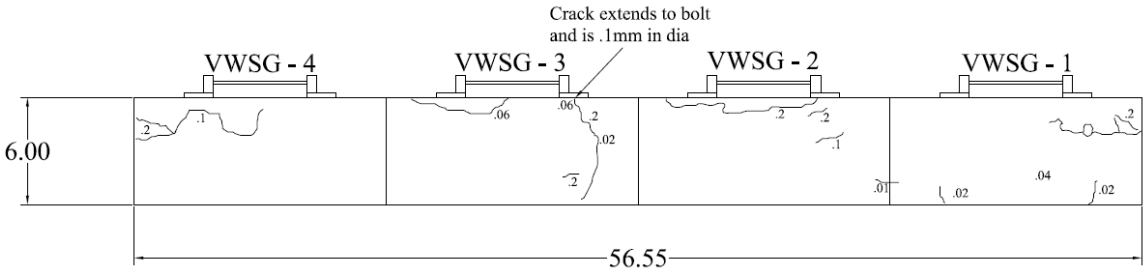

G4M2 – Ring Specimen 1 – Crack Drawings

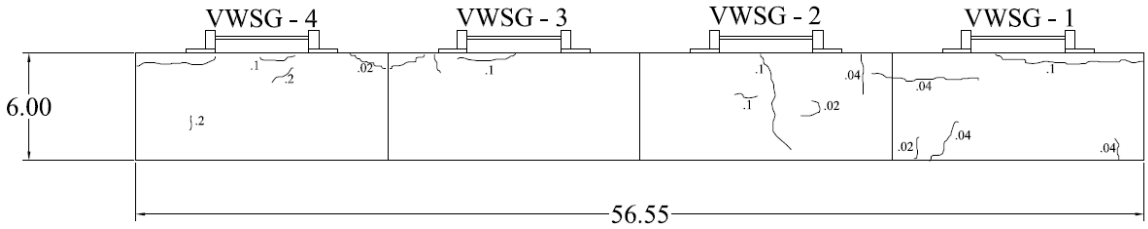

G4M2 – Ring Specimen 2 – Crack Drawings

G4M3 – R309496

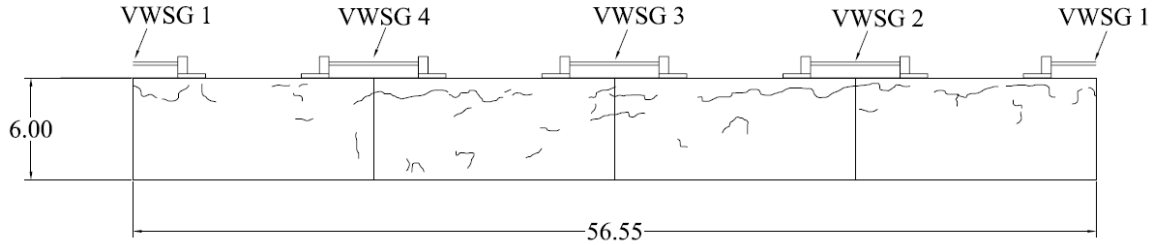

G4M3 – Ring Specimen 1 – Crack Drawings

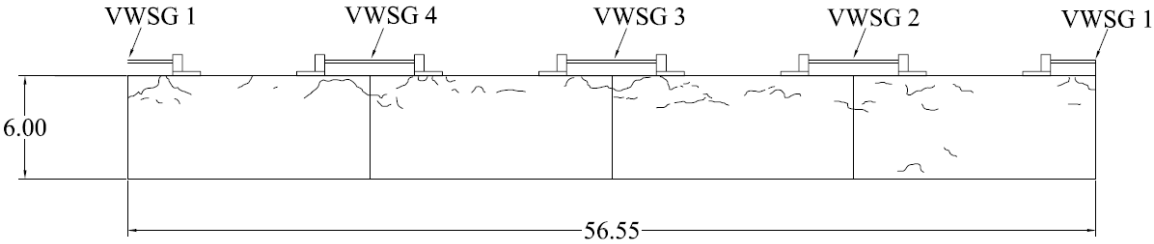

G4M3 – Ring Specimen 2 – Crack Drawings

G4M4 – R408694

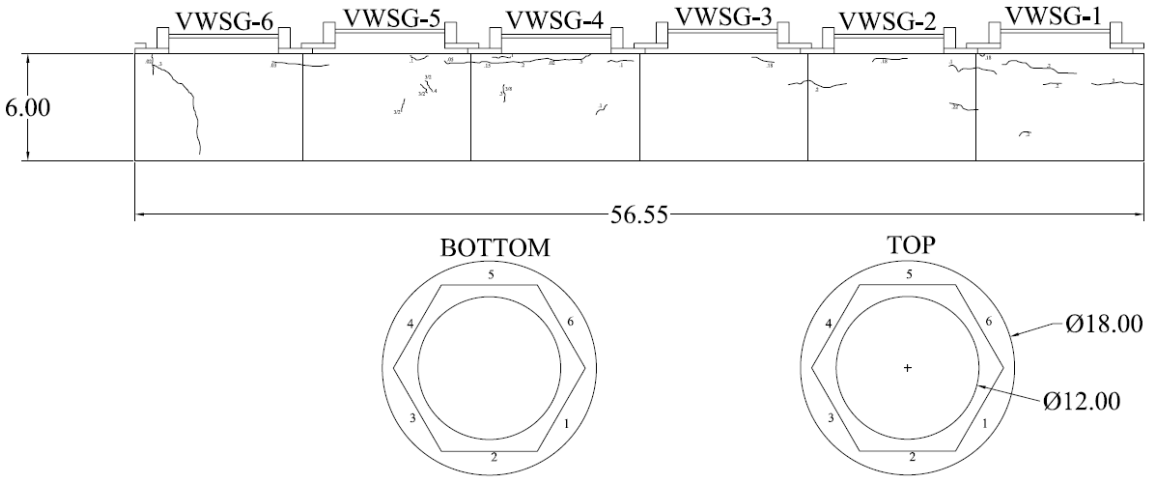

G4M4 – Ring Specimen 1 – Crack Drawings

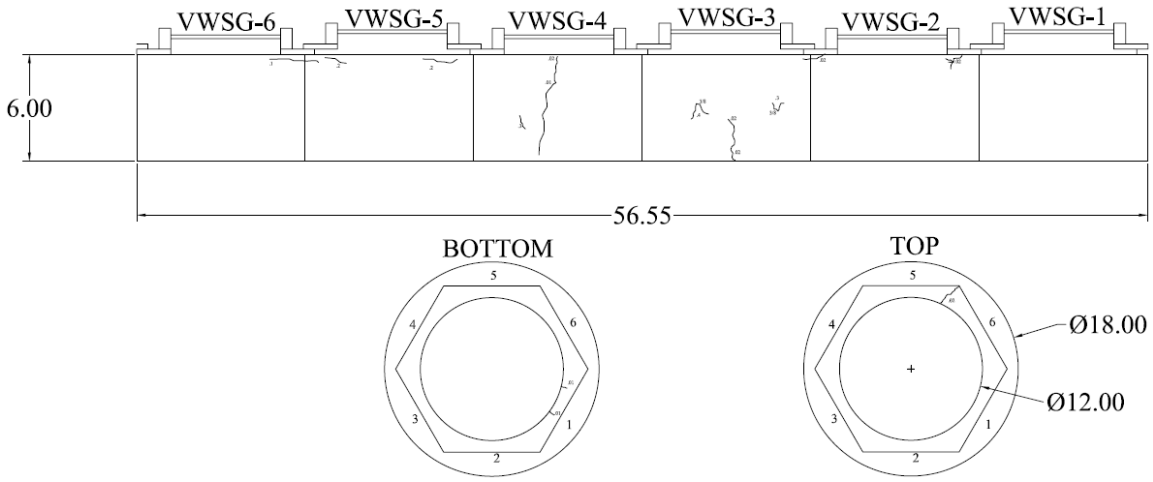

G4M4 – Ring Specimen 2 – Crack Drawings